

CURRENT DRIVEN INSTABILITIES AND
NON-LINEARITIES IN MAGNETIC SYSTEMS

JOREN S. HARMS

CURRENT DRIVEN INSTABILITIES AND
NON-LINEARITIES IN MAGNETIC SYSTEMS

**Door stroom aangedreven instabiliteiten en niet-lineariteiten
in magnetische systemen**
(met een samenvatting in Nederlands)

Proefschrift

ter verkrijging van de graad van doctor aan de
Universiteit Utrecht
op gezag van de
rector magnificus, prof. dr. H.R.B.M. Kummeling,
ingevolge het besluit van het college voor promoties
in het openbaar te verdedigen op

vrijdag 10 november 2023 des middags te 12.15 uur

door

Joren Stan Harms

geboren op 14 Augustus 1994
te Groningen

Promotor:

Prof.dr. R.A. Duine

Copromotor:

Dr. D. Schuricht

Beoordelingscommissie:

Prof. dr. T.W. Grimm

Prof. dr. L.R.M. Maas

Prof. dr. M.V. Mostovoy

Prof. dr. T. van der Sar

Prof. dr. ir. H.T.C. Stoof

Dit proefschrift werd mede mogelijk gemaakt met financiële steun van de Nederlandse organisatie voor wetenschappelijk onderzoek (NWO).

PUBLICATIONS

This Thesis is based on the following publications

- Part of Chapter 1 is based on J. S. Harms, H. Y. Yuan, and R. A. Duine, “Antimagnonics,” arXiv:2210.16698 (2022).
- Chapter 2 is based on J. S. Harms, A. Rückriegel, and R. A. Duine, “Dynamically stable negative-energy states induced by spin-transfer torques,” *Physical Review B* **103**, 144408 (2021).
- Chapter 3 is based on J. S. Harms and R. A. Duine, “Theory of the dipole-exchange spin wave spectrum in ferromagnetic films with in-plane magnetization revisited,” *Journal of Magnetism and Magnetic Materials* **557**, 169426 (2022).
- Chapter 4 is based on J. S. Harms, H. Y. Yuan, and R. A. Duine, “Enhanced magnon spin current using the bosonic Klein paradox,” *Physical Review Applied* **18**, 064026 (2022).
- Chapter 5 is based on R. A. Duine, V. Errani, and J. S. Harms, “Non-linear dynamics near exceptional points of synthetic antiferromagnetic spin-torque oscillators,” *Phys. Rev. B* **108**, 054428 (2023).
- Chapter 6 is based on unpublished work by J. S. Harms and R. A. Duine, *in preparation*.

Other publication to which the author has contributed

- P. M. Gunnink, J. S. Harms, R. A. Duine, and A. Mook, “Zero-frequency chiral magnonic edge states protected by nonequilibrium topology,” *Phys. Rev. Lett.* **131**, 126601 (2023).

CONTENTS

1	Introduction	1
1.1	The ferromagnetic phase transition	6
1.2	Low energy $T \ll T_c$ dynamics of magnetism	8
1.2.1	Non dissipative dynamics and the Landau Lifshitz equation	8
1.2.2	Dissipation of magnetic energy and damped precession	12
1.3	Heisenberg model and the Curie temperature	13
1.3.1	The Curie temperature in terms of the exchange coupling	14
1.3.2	Magnetization dynamics and the total magnetization at low temperatures	16
1.4	Spin injection	20
1.4.1	Spin transfer torques in a magnetic continuum	20
1.4.2	Spin orbit torques	22
1.5	Low energy excitations on magnetically stable and magnetically unstable ground states	24
1.5.1	Preliminaries	25
1.5.2	Symmetries and the conserved norm of the equation of motion	28
1.5.3	Spin waves, again	29
1.5.4	Spin-wave excitations around an inverted ground state	30
1.5.5	Canonical quantization	32
1.5.6	Quantization from the microscopic Hamiltonian using the Holstein-Primakoff transformation	33
1.5.7	Representations of magnons and antimagnons	34
1.6	This Thesis	40

I	Dipole-exchange spin waves	
2	Dynamically stable negative-energy states induced by spin-transfer torques	45
2.1	Introduction	46
2.2	Metallic thin film ferromagnet	48
2.2.1	Model and set-up	48
2.2.2	Dipole-exchange spin wave modes	50
2.3	Energetic and dynamical spin wave instabilities	52
2.4	Discussion and Outlook	58
2.A	Critical thickness of energetic instabilities at zero current	59
2.B	Approximate dipole-exchange mode in thin films	60
3	Theory of the dipole-exchange spin wave spectrum in ferromagnetic films with in-plane magnetization revisited	63
3.1	Introduction	63
3.2	Thin-film ferromagnet	65
3.2.1	Model and set-up	65
3.2.2	Bulk dipole-exchange spin-waves and it's boundary conditions	67
3.3	Dipole-exchange dispersion relation	70
3.3.1	General derivation	70
3.3.2	Thick thin-film approximation for the lowest exchange mode	75
3.3.3	Thin film approximation for the lowest energy mode	76
3.3.4	Comparison with Kalinikos and Slavin [83, 84]	78
3.4	Discussion and conclusions	80
II	Applications of negative energy modes and non-linear dynamics	
4	Enhanced magnon spin current using the bosonic Klein paradox	85
4.1	Introduction	86
4.2	Physical model	87
4.2.1	Set-up and magnonic and antimagnonic excitations	87
4.2.2	Exchange coupling at the interface	91
4.3	Scattering off the interface	92

4.4	Numerical verification	95
4.5	Discussions and conclusions	98
4.A	Detailed comparison between the original and the magnon Klein paradox	99
4.B	Parameter specification in numerical simulations	99
4.C	Correlations of incident, reflected, and transmitted magnon spin current	101
5	Non-linear dynamics near exceptional points of synthetic antiferro- magnetic spin-torque oscillators	105
5.1	Introduction	105
5.2	Linear Analysis	107
5.3	Non-linear dynamics	110
5.4	Numerical Results	113
5.5	Discussion and Conclusions	115
5.A	Second type of limit cycles for $J_{\perp}^2 < K^2$ for $J_z \rightarrow 0$	116
5.B	Stability requirements for limit cycles with $\eta = 0$	119
5.C	Stability requirements for limit cycles with $\eta \neq 0$	119
5.D	Phase diagram for $K < 0$ with $J_z \rightarrow 0$	120
6	Single-mode spin-wave laser driven by spin-orbit torque	123
6.1	Introduction	123
6.2	Model	125
6.3	Non-linear analyses of the spin-wave lasing mode	129
6.4	Current interval for a stable one-mode laser	131
6.5	Conclusion, discussion and outlook	133
7	Conclusion and outlook	135
	Bibliography	141

INTRODUCTION

Let us begin by asking ourselves the following question “Which of my activities today involved some form of digital computing?” For most of us in the western world, the answer will be along the lines of “A lot.” We probably have checked our email before we ended up here. If we, for example, drive a modern car, the navigation and many other “smart” features rely on integrated circuits (ICs). Also, many devices like our televisions are equipped with ICs. Besides the energy consumption of the integrated circuits in the device itself, it also request computational power in data centres elsewhere. For instance, every online search and video you watch require computational power of data centres. It is estimated that the total information and communications technology (ICT) ecosystem is responsible for 2 – 4% of global carbon emissions [7–10]. Moreover, it is very likely that this percentage will keep increasing in the coming ten years [7–10].

To avoid the possible catastrophic consequences of climate change to the habitability of our planet, all sectors of the global economy, including the ICT sector should aim to reduce their carbon footprint. Without drastic changes in legislation, the demand for computational tasks is expected to increase strongly [7]. Given this fact, we should aim to lower, or at least cease the increase, of carbon emission of the ICT sector by developing more efficient technology.

Although large efforts are being made to make integrated circuits more efficient, current technologies are approaching fundamental constraints limiting its further development [11]. A major problem in making these integrated

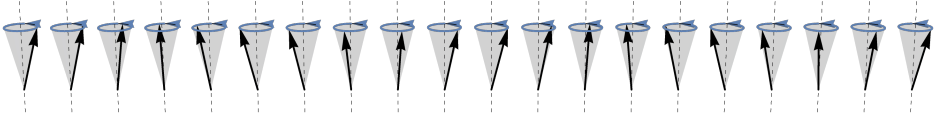


Figure 1.1: Figure of a spin wave. It corresponds to the collective precession of spins in which their phase difference is determined by the wavelength of the spin wave.

circuits more energy efficient is that electric currents induce joule-heating, which converts part of the electric current into heat. This is an unwanted byproduct that can be reduced but never completely circumvented. Historically, integrated circuits became more energy efficient by increasing the density of transistors. Currently, however, the size of these electronic devices can not simply be reduced much further and is plateauing [11] and hence their energy consumption is. A possible way around this problem is to consider devices that are fundamentally different from current devices and are thus not susceptible to the same fundamental constraints.

One of the candidates for such a new generation of devices are spintronic and magnonic devices [12, 13]. Here, spin waves rather than electrons are used as information carriers. These spin waves, and their quanta called magnons, are collective excitations that occur in ordered magnets, as shown in Fig. 1.1. As information carriers, magnons have the advantages of low power-consumption and efficient parallel data processing, as they do not give rise to Joule heating. Moreover, they are useful for both classical information processing, which includes logic gates [14, 15], transistors [16–19] and diodes [20], and for quantum science and technologies, including single-magnon states, squeezed states and entanglement with other quantum platforms [21–25].

A hurdle towards realizing magnon-based technology is the dissipation of magnons which results from interactions of magnons with their environment, such as conduction electrons, phonons and impurities. These interactions dissipate the amplitude and coherence of magnon currents and are detrimental for efficient application of magnons in nanoscale spintronic devices. Therefore, a central challenge in magnonics is to counteract the effect of

magnon dissipation and to find reliable knobs to sustain the magnon current for long-distance transport.

Furthermore, in order to combine magnonics with electronics the ability to efficiently inject, detect and control magnons using electrical currents is crucial. Coherent excitation of magnons typically uses alternating currents (AC) — using for instance antennas —, while direct currents (DC) are usually used to excite magnons diffusively using the spin Hall effect (SHE) to create a local spin accumulation. Although excitation of coherent magnons with AC currents is relatively straightforward, excitation of coherent magnons using DC currents is usually more complex and relies on injection of angular momentum with either spin-transfer-torque (STT) or spin-orbit-torque (SOT). Since efficient excitation of magnons by electrical current is crucial to combine magnonic devices with electronic devices, the ability to inject coherent magnons with DC currents is significant towards the technological use of magnonics.

In this Thesis, we put forward new ideas to address these two central questions. Namely, how does one extend the lifetime of, or amplify, magnons and how can one coherently excite magnons using DC currents? Perhaps surprisingly, most of the ideas developed in this Thesis draw inspiration from the field of analogue gravity [26–29] — which tries to mimic quantum field theories (QFTs) in curved spacetimes in the lab, with special attention to analogue black-hole (BH) horizons. This is a vast field of research and we will not try to capture all or even most of its details. Let us nonetheless try to give some of the essentials for this Thesis.

There are a variety of physical systems in which their quasiparticles act as if they live in a curved spacetime [26, 31–38]. In most of these systems, but not necessarily all, this curvature stems from some form of flowing background which Doppler shifts the dispersion of the excitations of the system. Since the velocity profile — of for instance flowing water — is easily tunable, artificial background curvatures such as the Schwarzschild metric near the horizon can be achieved, see Fig. 1.2. And as a consequence, these analogue horizons should also spontaneously emit pairs of particles, which, — with a bit of a stretch of the word — in analogy to astronomical black holes can be called Hawking radiation. The chance of measuring Hawking radiation in experiments with

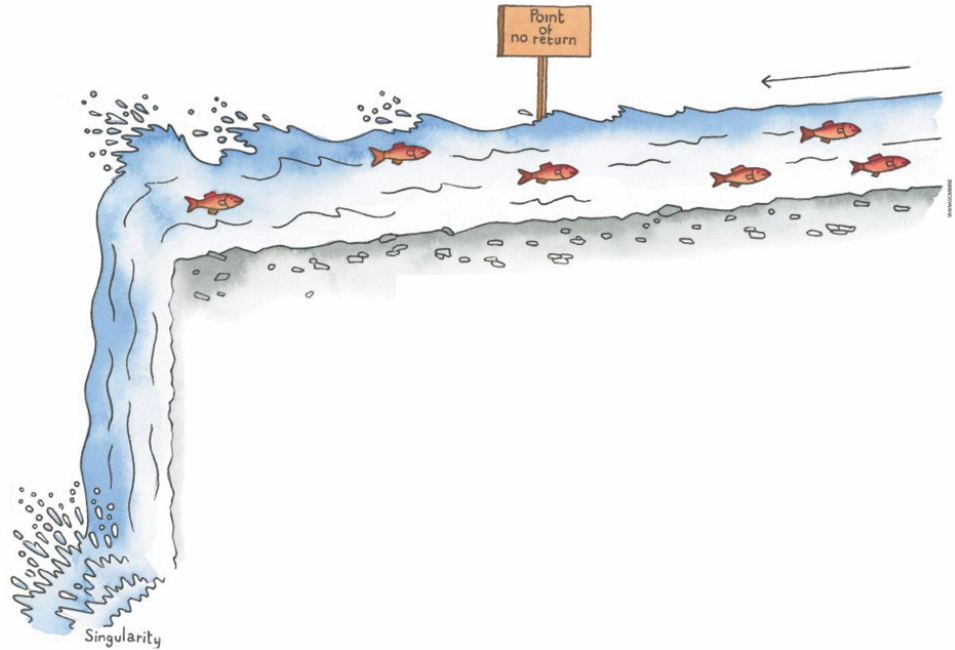


Figure 1.2: An illustration of an analogue event horizon for fish in flowing water. The water close to the waterfall flows much faster than the water far to the right of the waterfall. Let us suppose the fish have a maximal speed at which they are able to swim, which is slower than the flow velocity of the water close to the waterfall, but faster than the flow of water far to the right of the waterfall. Then there exists a point of no return for the fish. Once the fish has passed this point it is never able to swim further upstream and hence has crossed the analogue event horizon. In physical systems the fish are replaced by quasi particles. For dispersive systems we abstract even further and define the analogue event horizon as the point beyond which negative energy excitations exist. This illustration was taken from L. Susskind, “Black holes and the information paradox,” *Scientific American* (1997).

water however is rather small, since its Hawking temperature is approximately 3×10^{-7} Kelvin, which according to Unruh [26] “is a rather low temperature, and is probably undetectable in the presence of turbulent instabilities, etc., which would arise in trying to drive the fluid transsonically through a small nozzle. It is, however, a much simpler experimental task than creating a 10^{-8} -cm black hole.” Recently, a direct measurement of Hawking radiation has been claimed in flowing Bose-Einstein condensates [32].

Let us consider an observer of an astronomical black hole infinitely far from the horizon. From this point of view, particles inside the horizon carry negative energy, and one is thus unable to define a global vacuum state [39]. As a consequence, quantum fluctuations create a thermal spectrum of spontaneous emitted pairs of particles from the horizon — Hawking radiation — even if nothing is moving towards the horizon. From the perspective of this Thesis, this is the most essential ingredient for application of the ideas developed within the analogue gravity community. Namely, that the non-existence of a vacuum state and thus the existence of a region with energetically unstable excitations, gives rise to novel phenomena. For instance, breaking local Lorentz invariance, i.e. considering a non-linear dispersion, gives a non-thermal spectrum of spontaneously emitted particles, but still gives spontaneous emission. Throughout this Thesis, we further abstract the meaning of analogue gravity in the sense that we disregard Lorentz invariance and hence have no background metric to refer to. We do however rely on the existence of negative energy excitations and their consequences, for instance superradiant scattering [40]. As a final remark about analogue gravity, we like to mention the idea, put forward by Corley and Jacobson [41], that a combination of event horizons can be used as a laser. While they have shown that a slight superluminal dispersion does not effect the Hawking spectrum of an analogue BH horizon much [42], the inclusion a second analogue white-hole (WH) horizon — the time reverse of a black hole horizon — changes this conclusion drastically. When considering a bosonic theory, the negative energy excitations between the horizons form closed orbits of specific frequencies and becomes self amplified [41, 43, 44]. The title of their paper was “Black hole lasers”, and forms the inspiration for Chapters 5 and 6.

Since the contents of this Thesis, as you might have guessed, center around the use of magnetic negative energy excitations to answer the questions, “how does one extend the lifetime or amplify spin waves and how can one coherently excite them using DC currents?”, we first need to get an understanding of what spin waves are, what we precisely mean with magnetically ordered materials, and how one can create long lived excitations that carry negative magnetic energy.

1.1 THE FERROMAGNETIC PHASE TRANSITION

Throughout this Thesis, we work mostly on coherent spin transport in the ferromagnetic state. Hence, a good starting point would be to question “what characterises the ferromagnetic state?” Furthermore, we could take a step back and ask the question, “what characterizes a magnetic state?” The answer would be along the lines, “a material with a magnetic response.” This means that the magnetic susceptibility is nonvanishing, i.e. $\partial\mathbf{M}/\partial\mathbf{H} \neq 0$, with \mathbf{M} the magnetization of the material and \mathbf{H} an external magnetic field. The ferromagnetic state is a special magnetic state in the sense that it, below a critical temperature T_c — which is the Curie temperature —, acquires a non-zero permanent magnetization which is not induced by an external magnetic field. As a consequence, ferromagnets feel an attractive force in the neighborhood of most other magnetic materials. From our experience in day to day life this is also the most well known magnetic effect, of which a common example is the refrigerator magnet.

The dominant mechanism responsible for magnetic structure is the exchange interaction. There are a variety of exchange mechanisms which lead to a macroscopic magnetic structure, but we will not go into the different mechanisms here. What is important to know, however, is that, as a consequence of the exchange interaction the magnitude of the magnetization at each unit cell — this can be an atom or a group of atoms — is a conserved quantity and it can furthermore create a non-vanishing macroscopic magnetization at sufficiently low temperatures at zero field. Or to state it the other way around, in a magnet the magnetization in each unit cell is conserved, which

on the microscopic level stems from an exchange interaction. Hence, as we will see later, the magnitude of the magnetization is set by strength of the exchange interaction. In order to describe the ferromagnetic phase transition, let us denote $F_L[\mathbf{M}]$ the equilibrium free energy of the magnet in the absence of an external magnetic field \mathbf{H} . Since F_L denotes the equilibrium free energy it should be invariant under time reversal symmetry, i.e. $F_L[-\mathbf{M}] = F_L[\mathbf{M}]$ — if we include an external magnetic field, invariance under time reversal implies $F_L[-\mathbf{M}, -\mathbf{H}] = F_L[\mathbf{M}, \mathbf{H}]$. Furthermore, since the atomic exchange interaction is largely independent of the total magnetic moment with respect to the crystalline lattice, we assume the free energy to be independent of the overall direction of the magnetization, i.e. $F_L[\overset{\leftrightarrow}{R}\mathbf{M}] = F_L[\mathbf{M}]$, with $\overset{\leftrightarrow}{R}$ a rotation matrix. By assuming $|\mathbf{M}|$ and its gradients to be small around the critical temperature, the Landau expansion of the free energy becomes [45, 46]

$$F_L[\mathbf{M}] = \int dV \bar{A}(T)(\partial_i M_j)(\partial_i M_j) + a(T)\mathbf{M}^2 + b(T)\mathbf{M}^4, \quad (1.1)$$

where $\bar{A}(T)$, $a(T)$ and $b(T)$ are the Landau parameters that depend on temperature T . These constants stem from the microscopic exchange interaction, in which $\bar{A}(T)$ characterizes the non-uniform energetic contribution. Above the Curie temperature T_c the magnetization should vanish, while below T_c the ferromagnetic phase acquires a finite magnetization. Furthermore, we assume the ferromagnetic phase transition to be of second order. Since the free energy should be minimized in thermal equilibrium and we expect the magnetization to be uniform, we conclude $a > 0$ for $T > T_c$ and $a < 0$ for $T < T_c$. Thus, above the Curie temperature the average magnetization vanishes $\mathbf{M} = 0$. Below the Curie temperature, minimization of the free energy on the other hand gives

$$|\mathbf{M}| = \sqrt{a(T - T_c)/2b(T_c)}. \quad (1.2)$$

Hence, the Landau mean field theory predicts a square root decrease of the magnetization as we approach the Curie temperature. In reality fluctuations of the magnetization become strong around the magnetic phase

transition and should thus be taken into account close to the critical temperature. Self consistency implies that the above theory is valid if fluctuations of the magnetization are smaller than the average value of the magnetization, i.e. $\langle \mathbf{M}(\mathbf{x})\mathbf{M}(\mathbf{x}') \rangle \ll \langle \mathbf{M} \rangle$. This is the Levanyuk-Ginzburg criterion which states that the Landau theory is applicable for temperatures satisfying $|T - T_c|/T_c \ll 4b^2/aA^3$ [45, 47, 48]. When approaching the critical temperature past the Ginzburg criterion a renormalization group analysis is necessary, which is beyond the scope of this Thesis.

1.2 LOW ENERGY $T \ll T_c$ DYNAMICS OF MAGNETISM

In this section we are interested in weak excitations of the ferromagnetic state. As mentioned before, these excitations are called spin waves, which at the semi-classical level, describe precessing spins with a phase difference corresponding to their wavelength. If the wavenumber \mathbf{k} of the spin wave is much larger than the lattice spacing, the spin wave dispersion $\omega(\mathbf{k})$ may be expressed in the phenomenological parameters that occur in the macroscopic equations of the magnetic moments.

1.2.1 *Non dissipative dynamics and the Landau Lifshitz equation*

As it turns out, the minima in the free energy (1.1) are not unique. This is the case, since the free energy is unchanged under rotations of the magnetic moment. The free energy namely has an $O(3)$ symmetry which is spontaneously broken by the finite magnetization $|\mathbf{M}| \neq 0$ below the Curie temperature. Hence, according to Goldstone's theorem, spontaneous symmetry breaking leads to gapless excitations for fluctuations in the direction of the spontaneously broken symmetry group.

Thus, for temperatures far below the Curie temperature $T \ll T_c$ we expect the low energy dynamics to be dominated by these Goldstone modes, and

hence the low energy equation of motion of the magnetic moment \mathbf{M} should conserve $|\mathbf{M}|$. We may thus write

$$\partial\mathbf{M}/\partial t = \boldsymbol{\Omega} \times \mathbf{M}, \quad (1.3)$$

where $\boldsymbol{\Omega}$ is the angular velocity of the precessing magnetization. Additionally, the above equation of motion depends crucially on the assumption that the timescale in which the magnetization relaxes back to thermal equilibrium is much larger than the intrinsic timescale of precession of the magnetic moment.

Our next task is to find what the angular velocity $\boldsymbol{\Omega}$ would be. We proceed as follows, up to lowest order in the dynamics, we ignore the dissipation of energy relaxing the magnetization back to its equilibrium value. This dissipation of energy of the precessing magnetization, or the work W needed to bring the system in the out of equilibrium state, can be expressed as follows

$$\partial E/\partial t = -\partial W/\partial t = -\partial F/\partial t. \quad (1.4)$$

Where the derivative of the free energy can be given by taking the functional derivative w.r.t. the magnetization, i.e.

$$-\partial F/\partial t = \int dV \mathbf{H}_{\text{eff}} \cdot (\partial\mathbf{M}/\partial t) = \int dV \mathbf{H}_{\text{eff}} \cdot (\boldsymbol{\Omega} \times \mathbf{M}), \quad (1.5)$$

with $\mathbf{H}_{\text{eff}} = -\delta F/\delta\mathbf{M}$ the effective field. Note, that the field \mathbf{H}_{eff} is only nonvanishing out of equilibrium. Since we assume dissipation towards equilibrium to be absent, we put $\partial F/\partial t = 0$, which implies $\boldsymbol{\Omega} \propto \mathbf{H}_{\text{eff}}$. Thus the equation of motion, governing the magnetization precession becomes

$$\partial\mathbf{M}/\partial t = \text{constant} \times \mathbf{H}_{\text{eff}} \times \mathbf{M}. \quad (1.6)$$

This describes a precession of the magnetic moment around the effective magnetic field \mathbf{H}_{eff} where the precise angular velocity is still unknown.

In order to fix the remaining constant, we consider how the magnetization precesses in the presence of an external magnetic field strength \mathbf{H} . We incorporate this in the following way. If we apply an external magnetic field

to an macroscopic medium, the change in free energy will be given by [45, 49] $dF = -SdT + \int dV \mathbf{H} \cdot d\mathbf{B}$, with S the entropy, T the temperature, B the magnetic induction and V the volume of the ferromagnet. Since we want to consider an ensemble in which \mathbf{H} is fixed rather than \mathbf{B} , we need to perform a Legendre transformation such that $\tilde{F} = F - \int dV \mathbf{H} \cdot \mathbf{B}$. Hence, the free energy density of \tilde{F} should satisfy $d\tilde{F}/d\mathbf{H} = -\mathbf{B}$. If we furthermore note that $\mathbf{B} = \mu_0(\mathbf{H} + \mathbf{M})$ in a macroscopic medium, we find the free energy containing \mathbf{H} to be

$$\tilde{F} = F_0 - \int dV \mu_0 \mathbf{H} \cdot \mathbf{M} - \mu_0 \mathbf{H}^2/2, \quad (1.7)$$

with F_0 the free energy defined in Eq. (1.1). Note, that the prescense of an external magnetic field \mathbf{H} in principle breaks the $O(3)$ symmetry in \tilde{F} which allows us to conserve $|\mathbf{M}|$. On the other hand, we assume that the exchange energy is the dominant energy scale of this problem and hence $|\mathbf{M}|$ is still conserved by the low energy excitations and the above arguments still apply. If we now consider the uniform precession of the magnetization in a static external magnetic field we get

$$\partial \mathbf{M} / \partial t = \text{constant} \times \mu_0 \mathbf{H} \times \mathbf{M}. \quad (1.8)$$

Since the above equation of motion should reduce to the precession of a magnetic moment in an external magnetic field, the constant in the equation of motion should be given by the gyromagnetic ratio $\gamma = g\mu_B/\hbar = g|e|/2m$, with μ_B the Bohr magneton, \hbar Planck's constant, e the electron charge, m the electron mass and g the g-factor of the ferromagnet. The final equation of motion that describes the precession of the magnetization is called the Landau-Lifshitz equation (LL) and is given by [50]

$$\partial \mathbf{M} / \partial t = \gamma \mathbf{H}_{\text{eff}} \times \mathbf{M}. \quad (1.9)$$

To conclude, the LL equation gives the precession of the magnetization around the effective magnetic field in the absence of dissipation for temperatures far below the Curie temperature.

Furthermore, in order to completely describe the dynamics of the magnetization its magnetic dipole moment should also be taken into account. Thus,

the magnetization dynamics should also satisfy the Maxwell equations. Since the frequency of spin waves is typically small compared to the speed of light times the wavenumber of spin waves $\omega \ll ck$, the dynamic components of the Maxwell equations can be ignored and only the magnetostatic Maxwell equations are important to form a complete set of equations describing spin waves [49]

$$\nabla \times \mathbf{H} = 0, \quad \nabla \cdot \mathbf{B} = \mu_0 \nabla \cdot (\mathbf{H} + \mathbf{M}) = 0. \quad (1.10)$$

For both chapters in Part i we will consider both the LL equation and the magnetostatic Maxwell equations. In Part ii, we will only take the static contribution of the magnetostatic Maxwell equations into account. This typically gives a shape anisotropy on the magnetization that can effectively be incorporated in the free energy.

Let us finish this section by discussing the spectrum of low energy excitations of the magnetization in ferromagnets, which are called spin waves. The spectrum of spin waves in a macroscopic medium is described by small fluctuations of the magnetization around the symmetry broken thermal equilibrium state. The spin wave spectrum that is obtained by linearizing the LL equation becomes

$$\omega(\mathbf{k}) = 2\gamma\bar{A}(T)|\mathbf{M}|\mathbf{k}^2 + \gamma\mu_0|\mathbf{H}|. \quad (1.11)$$

We thus find a quadratic dispersion with a gap set by the external magnetic field. The latter is expected, since spin waves are predicted to be gapless in the absence of an external magnetic field by Goldstone's theorem. The inclusion of the magnetostatic Maxwell equations leads to a geometry dependent spin wave spectrum. We would like to refer the reader interested in the spin wave spectrum with the inclusion of the magnetostatic Maxwell equation to Chapters 2 and 3, in which we discuss the dipole-exchange spectrum in ferromagnetic thin films. Next, we consider how the dissipation of energy effects the LL equation.

1.2.2 Dissipation of magnetic energy and damped precession

To phenomenologically include dissipation to the LL equation we follow the argument presented by Gilbert [51]. In his 1955 article Gilbert argues that the dissipation of energy can be implemented in a Lagrangian formulation of the magnetization dynamics using the canonical form of the Rayleigh dissipation functional. The Euler Lagrange equations of motion in the absence of Rayleigh dissipation are given by

$$\delta L[\mathbf{M}, \dot{\mathbf{M}}]/\delta \mathbf{M} = 0. \quad (1.12)$$

Here, the Lagrangian that describes the magnetization precession in Eq. (1.9) is given by

$$L = \int dV \mathbf{A}(\mathbf{M}) \cdot \partial \mathbf{M} / \partial t - \tilde{F}, \quad (1.13)$$

where \mathbf{A} is a vector potential defined by $\nabla_{\mathbf{M}} \times \mathbf{A}(\mathbf{M}) = \mathbf{M}/\gamma$. Note that this vector potential is not unique since it has a gauge degree of freedom, meaning that one can add the divergence of a scalar function and obtain the same equation of motion, i.e. $\mathbf{A}(\mathbf{M}) \rightarrow \mathbf{A}(\mathbf{M}) - \nabla_{\mathbf{M}} \Lambda(\mathbf{M})$ with Λ a scalar function. The canonical way of including dissipation in the equation of motion is by using a Rayleigh dissipation functional proportional to the square of the velocity $\dot{\mathbf{M}}$ of the field, i.e.

$$\mathcal{R} = \frac{\alpha}{2\gamma|\mathbf{M}|} \int dV |\partial \mathbf{M} / \partial t|^2, \quad (1.14)$$

where α is the dimensionless Gilbert damping parameter. Additionally, the Euler Lagrange equations of motion including Rayleigh dissipation are given by

$$\frac{\delta L[\mathbf{M}, \dot{\mathbf{M}}]}{\delta \mathbf{M}} + \frac{\delta \mathcal{R}[\dot{\mathbf{M}}]}{\delta \dot{\mathbf{M}}} = 0. \quad (1.15)$$

Hence, the equation that describes the precession of the magnetization which dissipatively relaxes back to thermal equilibrium is called the Landau-Lifshitz-Gilbert (LLG) equation and is according to Eq. (1.15) given by

$$\frac{\partial \mathbf{M}}{\partial t} = \gamma \mathbf{H}_{\text{eff}} \times \mathbf{M} + \frac{\alpha}{|\mathbf{M}|} \mathbf{M} \times \frac{\partial \mathbf{M}}{\partial t}. \quad (1.16)$$

This is the most important dynamical equation for the purpose of this Thesis and will be used in each chapter.

As a final comment we would like to stress that the Rayleigh dissipation function is a direct measure of the dissipation of energy of the magnetic system. This can be seen as follows, the dissipation of energy according to Eqs. (1.15) and (1.16) is given by

$$-d\tilde{F}/dt = \int dV \dot{\mathbf{M}} \cdot (\delta\mathcal{R}[\dot{\mathbf{M}}]/\delta\dot{\mathbf{M}}) = 2\mathcal{R}[\dot{\mathbf{M}}]. \quad (1.17)$$

Thus the dissipation function directly relates to the dissipation of energy for quadratic velocities, which by the second law of thermodynamics should be positive, i.e. $\alpha/\gamma > 0$.

The use of the Lagrangian formalism with Rayleigh dissipation is equivalent to the LLG equation and will appear once more in Chapter 6, since it is more convenient to change coordinates in the Lagrangian formulation.

So far we have been discussing classical magnetization dynamics at the phenomenological level. In the next section we discuss a widely used microscopic model to describe magnetic ordering.

1.3 HEISENBERG MODEL AND THE CURIE TEMPERATURE

At low energies, excitations of electrons into higher electron shells are less relevant and the electrons can be integrated out to give an effective Hamiltonian in terms of only the total spin of the atoms — or group of atoms [52–55]. Here, we take into account exchange interactions, which gives the ground state total spin at each lattice site, but also gives an interaction between the relative orientations of the spins. We furthermore consider the interaction of the magnetic dipole of the spin with an external magnetic field. We will thus consider the Hamiltonian

$$\mathcal{H} = - \sum_{i,j} J_{ij} \hat{\mathbf{S}}_i \cdot \hat{\mathbf{S}}_j - \sum_i \gamma \mu_0 \mathbf{H} \cdot \hat{\mathbf{S}}_i, \quad (1.18)$$

where J_{ij} is the exchange integral, $\hat{\mathbf{S}}_i$ the spin operator at lattice site i and \mathbf{H} the external magnetic field. The Hamiltonian presented in Eq. (1.18) is called

the Heisenberg Hamiltonian and gives an effective microscopic low energy description of magnetic ordering. In principle we should also include the energetic contribution of the dipole-dipole interaction between the spins, but we ignore them for the moment — claiming that the exchange is the dominant energy scale to determine for instance the Curie temperature. Additionally, the exchange interaction between spins drops of quite rapidly and hence considering the exchange integral as a local interaction is reasonable. We thus consider the exchange integral to be local and isotropic, which means that we consider the sum in Eq. (1.18) to only sum over nearest neighbours with an exchange integral of magnitude J . The isotropic assumption is also well justified since the exchange interaction is rotationally invariant up to lowest order in spin-orbit coupling. Under these assumptions, this model shows ferromagnetic order if $J > 0$ and antiferromagnetic order for $J < 0$.

Before we discuss the Curie temperature and the elementary excitations of this model, let us briefly consider the Heisenberg equation of motion for the uniform spin mode, expressed in its magnetic moment $\hat{\mathbf{M}} = -n\gamma\hat{\mathbf{S}}$. Here, n is the atomic density, $\gamma = g\mu_B/\hbar = g|e|/2m$ the gyromagnetic ratio, g the g-factor and μ_B the Bohr magneton. The Heisenberg equation of motion expressed in terms of the magnetic moment becomes

$$\frac{\partial\hat{\mathbf{M}}}{\partial t} = \frac{1}{i\hbar} \left[\hat{\mathbf{M}}, \mathcal{H} \right] = \gamma\mu_0\mathbf{H} \times \hat{\mathbf{M}}, \quad (1.19)$$

which has the operator form of the phenomenologically derived LL equation in Eq. (1.9).

1.3.1 *The Curie temperature in terms of the exchange coupling*

Below we approximate the Curie temperature of this model in terms of the exchange integral J_{ij} . Since the Curie temperature is defined at vanishing external field we disregard the external magnetic field \mathbf{H} and solely consider the exchange interaction. Again, we assume the exchange integral is isotropic, thus invariant under global spin rotations and invariant under translations of the lattice. Furthermore, we take into account only the nearest neighbour

interactions between the spins. We thus consider the following Heisenberg Hamiltonian

$$\hat{\mathcal{H}} = -J \sum_{\langle i,j \rangle} \hat{\mathbf{S}}_i \cdot \hat{\mathbf{S}}_j, \quad (1.20)$$

with $J > 0$ and $\langle i, j \rangle$ displays the sum over nearest neighbours.

We proceed by simplifying Eq. (1.20) using the mean field approximation $\hat{\mathbf{S}}_i \cdot \hat{\mathbf{S}}_j \simeq \hat{\mathbf{S}}_i \cdot \langle \hat{\mathbf{S}}_j \rangle + \langle \hat{\mathbf{S}}_i \rangle \cdot \hat{\mathbf{S}}_j - \langle \hat{\mathbf{S}}_i \rangle \cdot \langle \hat{\mathbf{S}}_j \rangle$. As we have seen in Section 1.1, the Curie temperature is determined by the constants $a(T)$ and $b(T)$ in Eq. (1.1), which both characterise uniform configurations of the magnetization. Hence, only the zero wavevector mode in the Fourier transformation of the spin is of interest to determine the Curie temperature. We may thus assume

$$\langle \hat{\mathbf{S}}_i \rangle \simeq \langle \mathbf{S}_0 \rangle. \quad (1.21)$$

Note that we should include nonzero wavevectors if we want describe nonuniform excitations in the magnet and thus find $\bar{A}(T)$. In this mean field approximation the Hamiltonian becomes

$$\mathcal{H}_{\text{MF}} = (JzV/2)\langle \mathbf{S}_0 \rangle^2 - Jz \sum_i \langle \mathbf{S}_0 \rangle \cdot \hat{\mathbf{S}}_i, \quad (1.22)$$

with z the amount of nearest neighbours and V is the volume of the magnet. The partition function corresponding to mean field Hamiltonian (1.22) becomes

$$Z = \text{Tr} \exp \left(-\frac{\beta JzV}{2} \langle \mathbf{S}_0 \rangle^2 + \beta Jz \sum_i \langle \mathbf{S}_0 \rangle \cdot \hat{\mathbf{S}}_i \right), \quad (1.23)$$

in which $\beta = 1/k_B T$, with k_B Boltzmann's constant and T the temperature. The trace in the above partition function runs over the spin eigenstates with spin S and quantization axis $\langle \mathbf{S}_0 \rangle$. The free energy of this model can now be expressed in terms of the partition function via $F = -\beta^{-1} \log Z$, which gives

$$F = F_0 + JzV \langle \mathbf{S}_0 \rangle^2 / 2 - \beta^{-1} V \log Z_0(\langle \mathbf{S}_0 \rangle), \quad (1.24)$$

with F_0 the spin independent part of the free energy and $Z_0(\langle \mathbf{S}_0 \rangle) = \sum_{S^z=-S}^S \exp(-\beta Jz \langle S_0 \rangle \hbar S^z)$, the single spin partition function. This is

a geometric series for which the solution, for general spin S , is given by $Z_0(\langle \mathbf{S}_0 \rangle) = \sinh(\beta J z \hbar \langle S_0 \rangle (S + 1/2)) / \sinh(\beta J z \hbar \langle S_0 \rangle / 2)$. We may re-express the averaged spin in terms of its magnetic moment $\mathbf{M} = -n\gamma \langle \mathbf{S}_0 \rangle$ and assume the magnetic moment to be small $|\mathbf{M}| \ll 1$ near the phase transition. Henceforth the approximate free energy density becomes

$$F/V = F_0/V + \frac{Jz}{6n^2\gamma^2} \left(3 - S(S+1)\beta Jz\hbar^2 \right) \mathbf{M}^2 + \mathcal{O}(\mathbf{M}^4). \quad (1.25)$$

We thus find $a(T) \propto 3 - \beta S(S+1)Jz\hbar^2$ in terms of the Landau free energy parameters, and as a result, the corresponding Curie temperature is

$$T_c = S(S+1)Jz\hbar^2/3k_B. \quad (1.26)$$

In conclusion, we approximated the Curie temperature of the microscopic Heisenberg model using mean field theory. We found this temperature to scale proportional to the zero temperature exchange interaction between neighbouring spins. In principle one can derive the free energy functional from the ground up using microscopic models. Throughout this Thesis, however, we use a more phenomenological approach and take the parameters in the free energy as material parameters which are given by experiment.

1.3.2 Magnetization dynamics and the total magnetization at low temperatures

In this section we discuss the low energy excitations of the ferromagnetic Heisenberg model in Eq. (1.18). These excitations are magnons which are the quanta of spin waves. But, let us begin by describing the ground state of the Heisenberg model. In order to do so it is convenient to rewrite the Heisenberg Hamiltonian in terms of the spin raising and lowering operators $\hat{S}^\pm = \hat{S}^x \pm i\hat{S}^y$, which satisfy the following commutations relations

$$\left[\hat{S}^z, \hat{S}^\pm \right] = \pm \hbar \hat{S}^\pm, \quad \left[\hat{S}^+, \hat{S}^- \right] = -2\hbar \hat{S}^z. \quad (1.27)$$

As a result, S^+ raises the spin by \hbar on the z axis, while S^- lowers the spin by \hbar along the z axis, i.e. $\hat{S}^z |S^z\rangle = \hbar S^z |S^z\rangle$, $\hat{S}^\pm |S^z\rangle = \hbar \sqrt{S(S+1) - S^z(S^z \pm 1)} |S^z \pm$

$1\rangle$, with $|S^z\rangle$ shorthand for $|S, S^z\rangle$ where S is the total spin at each lattice site and S^z the eigenvalue of the z axis projection of the spin operator. When we express the Heisenberg Hamiltonian in the raising and lowering operators we find

$$\mathcal{H} = -\frac{J}{2} \sum_{\langle i,j \rangle} 2\hat{S}_i^z \hat{S}_j^z + \hat{S}_i^+ \hat{S}_j^- + \hat{S}_i^- \hat{S}_j^+ - \sum_i \gamma \mu_0 H \hat{S}_i^z \quad (1.28)$$

The ground state $|0\rangle$ of this Hamiltonian will thus be the state with the maximal spin projection of $\hbar SN$ in the z direction, with $N = V/a^3$ the total number of spins, V the volume of the magnet and a^3 the volume of one unit cell. This state has a ground state energy given by $\hbar\omega_0 = -Jz\hbar^2 S^2 N - \gamma\mu_0 H \hbar SN$, with z the number of nearest neighbours.

We expect the low energy excitations to lower the total spin of the projection along z of the ground state by \hbar , such that total spin projection of this state becomes $\hbar(SN - 1)$. Furthermore, if we find an operator such that its commutation relation with the Hamiltonian satisfies

$$\left(\hat{\mathcal{H}} - \hbar\omega_0\right) \hat{S}^- |0\rangle \equiv \left[\hat{\mathcal{H}}, \hat{S}^-\right] |0\rangle = \hbar\omega \hat{S}^- |0\rangle, \quad (1.29)$$

then $\hat{S}^- |0\rangle$ would be an eigenstate of $\hat{\mathcal{H}}$. This state should furthermore satisfy $\sum_i \hat{S}_i^z \hat{S}^- |0\rangle = \hbar(SN - 1)$ since it creates an excitation with spin \hbar . We will thus search for an operator that satisfies condition (1.29) and lowers the spin projection in the z direction by \hbar . This operator can not be \hat{S}_i^- , since the Heisenberg Hamiltonian is translationally invariant. We thus consider its Fourier transform as ansatz

$$\hat{\Psi}_{\mathbf{k}}^\dagger |0\rangle \equiv \hbar^{-1} (2S)^{-1/2} \hat{S}_{\mathbf{k}}^- |0\rangle = \hbar^{-1} (2SN)^{-1/2} \sum_i e^{i\mathbf{k}\cdot\mathbf{r}_i} \hat{S}_i^- |0\rangle, \quad (1.30)$$

where we divided $\hat{S}_{\mathbf{k}}^-$ by $\hbar\sqrt{2S}$ to obtain the normalized state $\hat{\Psi}_{\mathbf{k}}^\dagger|0\rangle$, i.e. $\langle 0|\hat{\Psi}_{\mathbf{k}}\hat{\Psi}_{\mathbf{k}}^\dagger|0\rangle = 1$. With this ansatz the commutator of $\hat{\Psi}_{\mathbf{k}}^\dagger$ with the Hamiltonian acting on the ground state becomes

$$\begin{aligned}
(\hat{\mathcal{H}} - \hbar\omega_0)\hat{\Psi}_{\mathbf{k}}^\dagger|0\rangle &\equiv [\hat{\mathcal{H}}, \hat{\Psi}_{\mathbf{k}}^\dagger]|0\rangle = \hbar^{-1}(2SN)^{-1/2} \sum_i e^{i\mathbf{k}\cdot\mathbf{r}_i} [\hat{\mathcal{H}}, \hat{S}_i^-]|0\rangle \\
&= 2J(2SN)^{-1/2} \sum_{\langle i,j \rangle} e^{i\mathbf{k}\cdot\mathbf{r}_i} (\hat{S}_j^z \hat{S}_i^- - \hat{S}_j^- \hat{S}_i^z)|0\rangle \\
&\quad + \gamma\mu_0 H(2SN)^{-1/2} \sum_i e^{i\mathbf{k}\cdot\mathbf{r}_i} \hat{S}_i^-|0\rangle \\
&= 2J\hbar S(2SN)^{-1/2} \sum_{\langle i,j \rangle} e^{i\mathbf{k}\cdot\mathbf{r}_i} (\hat{S}_i^- - \hat{S}_j^-)|0\rangle + \hbar\gamma\mu_0 H\hat{\Psi}_{\mathbf{k}}^\dagger|0\rangle \\
&= \hbar \left[2\hbar S \sum_{\mathbf{a}} J \sin^2(\mathbf{k} \cdot \mathbf{a}/2) + \gamma\mu_0 H \right] \hat{\Psi}_{\mathbf{k}}^\dagger|0\rangle \\
&= \hbar\omega(\mathbf{k})\hat{\Psi}_{\mathbf{k}}^\dagger|0\rangle. \tag{1.31}
\end{aligned}$$

Hence, $\hat{\Psi}_{\mathbf{k}}^\dagger|0\rangle$ is an eigenstate of the Heisenberg Hamiltonian with excitation energy $\hbar\omega(\mathbf{k})$ and a spin of \hbar . In the above we defined $\mathbf{a} = \mathbf{r}_i - \mathbf{r}_j$ as the spatial difference between nearest neighbours and we furthermore used $\hat{S}^z|0\rangle = \hbar S$. We thus find the exact dispersion relation for magnons to be $\omega(\mathbf{k}) = 2\hbar S \sum_{\mathbf{a}} J \sin^2(\mathbf{k} \cdot \mathbf{a}/2) + \gamma\mu_0 H$. In the long wavelength limit $ka \ll 1$ — where a is the lattice spacing — this magnon dispersion relation in a simple cubic lattice becomes

$$\omega(\mathbf{k}) \simeq \hbar S a^2 J \mathbf{k}^2 + \gamma\mu_0 H. \tag{1.32}$$

Comparing this long wavelength dispersion with the phenomenologically obtained spin wave dispersion in Eq. (1.11) we find $\bar{A}(T \rightarrow 0) = a^{2+d} J/2\gamma^2$, with d the number of spatial dimensions of the magnet.

For temperatures that are low compared to the atomic total spin — $k_B T \ll \hbar^2 S J$ — only relatively few magnons are excited and the total spin projection should still be close to $\hbar S N$. In this case magnons are approximately bosons, since the commutation relation of the magnon creation and annihilation

operators — which are the spin raising and lowering operators over $\hbar\sqrt{2S}$ — is approximately

$$\left[\hat{\Psi}_k, \hat{\Psi}_{k'}^\dagger \right] \simeq \delta_{k,k'}, \quad (1.33)$$

which is a bosonic commutation relation and this equality does not hold at high temperatures when a lot of magnon states are occupied. Note that the temperature range of validity becomes larger as the spin per unit cell increases. Thus in large-spin ferromagnets, magnons are bosons for most purposes. Hence, at low temperatures the amount of magnons should be given by the Bose distribution

$$n_B(\mathbf{k}) = 1/(e^{\beta\hbar\omega(\mathbf{k})} - 1), \quad (1.34)$$

with $\beta = 1/k_B T$. By noticing that the dispersion of occupied magnons is approximately quadratic at low temperatures and by ignoring the external magnetic field, we find the total decrease in magnetization in a three dimensional ferromagnet, due to occupation of magnons, to be proportional to $n_{\text{magnons}} = \int \frac{d\mathbf{k}}{(2\pi)^3} n_B(\mathbf{k}) = 4\pi \int \frac{dk}{(2\pi)^3} k^2 n_B(k) = T^{3/2} \times 4\pi \int \frac{dq}{(2\pi)^3} q^2 n_B(T^{1/2}q)$. Thus in the low temperature limit the magnetization decreases as

$$M(T) = M(0) \left(1 - \text{constant} \times T^{3/2} \right), \quad (1.35)$$

which is known as Bloch's law [56].

To conclude this section, we have derived the low energy magnetic excitations for the ferromagnetic Heisenberg model. We have found that the elementary excitations of the ferromagnetic Heisenberg model — called magnons — have a quadratic in k dispersion and have a spin of \hbar . And we found that these magnons behave like bosons at sufficiently low temperatures compared to the spin of the atoms. In Section 1.5.6, we will use an alternative method called the Holstein-Primakoff approximation to approximate the Heisenberg Hamiltonian and hence the magnon dispersion. In this formalism the connection between the bosonic nature of magnons and the magnitude of the atomic spin is more apparent. But before we end there, we first discuss different methods to inject angular momentum into magnetic materials.

1.4 SPIN INJECTION

Throughout this Thesis we propose applications to inject and amplify spin waves — or magnons — using the existence of negative magnetic energy excitations. Before we can exploit such excitations, we first need to know how one can create such excitations in a way that they are long lived. Usually, negative energy excitations signal an instability if the system is allowed to dissipate or redistribute its energy. As a result, such systems will reach a new ground state after some time and the concept of negative energy excitations is only relevant on timescales much smaller than the timescale in which the system reaches a new ground state. Things change drastically however, if we consider non-equilibrium magnetization dynamics. The inclusion of angular momentum injection into the magnetic may namely reverse the sign of the magnetic damping, making magnetic energetically unstable excitations dynamically stable. Hence, one can engineer a ground state in which long-lived dynamically stable negative energy excitations exist, and as a consequence, the magnetic system is dynamically not allowed to reach its energetic ground state. We will treat these cases in more detail in Section 1.5, but let us first focus on the two methods to inject angular momentum into magnetic systems that will be employed in this Thesis.

1.4.1 *Spin transfer torques in a magnetic continuum*

Spin transfer torques are torques on the magnetization that occur in metallic ferromagnets if an electric current is applied. This current has the property that it is spin-polarized in metallic ferromagnets which leads to torques on the magnetic texture by conservation of angular momentum. The polarization of the current stems from the microscopic details by which the magnetization is formed in metallic ferromagnets. In short, the exchange interaction that leads to the spontaneous ferromagnetic state creates a spin-splitting of the electron conduction bands. As a result, the spin-up and spin-down electron bands are shifted and typically have a different density of states at the Fermi-energy.

This leads to uneven charge transport of the spin-up and spin-down states and hence a spin polarized current.

Let us consider the case in which we have a spin-polarized current \mathbf{j}_α where α denotes the direction of the spin polarization. A common assumption is that the quantization axis of the spin polarized current follows that of the magnetization profile in the ferromagnet, i.e. the spin-polarized current in units of angular momentum per surface area per second is expressed as

$$\mathbf{j}_\alpha = \frac{g\mu_B P}{2eM_s} \mathbf{j} M_\alpha, \quad (1.36)$$

with μ_B the Bohr magneton, g the g-factor of the electron, e the electron charge, $P = (\sigma_\uparrow - \sigma_\downarrow)/(\sigma_\uparrow + \sigma_\downarrow)$ the spin polarization with $\sigma_{\uparrow,\downarrow}$ the conductivity of the respective spin along the $-\mathbf{M}$ direction and $M_s = |\mathbf{M}|$ the saturation magnetization. In the presence of a slowly varying magnetic profile — compared to the electron mean free path — the electron spin changes quantization axis and hence by conservation of angular momentum should exert a torque on the magnetization given by [57–59]

$$\partial_t M_\alpha|_{\text{STT adiabatic}} = -\nabla \cdot \mathbf{j}_\alpha = -\mathbf{v}_s \cdot \nabla M_\alpha, \quad (1.37)$$

with $\mathbf{v}_s = -g\mu_B P \mathbf{j}/2|e|M_s$ the spin-drift velocity. The above formula can be interpreted as follows. Consider a unit cell of volume a^3 with a total magnetization M_s . The change in the direction magnetic moment of the electrons per unit cell is $a^3 \nabla \cdot \mathbf{j}_\alpha$, hence it exerts a torque on the magnetization of the opposite sign $-a^3 \nabla \cdot \mathbf{j}_\alpha$. The phenomenologically derived torque in Eq. (1.37) is called the adiabatic spin-transfer torque (STT).

In the derivation of the adiabatic STT we neglected all processes that relax spin, and a gradient expansion shows that STTs may also induce the dissipative torque

$$\partial_t M_\alpha|_{\text{STT non-adiabatic}} = (\beta/M_s) \mathbf{M} \times (\mathbf{v}_s \cdot \nabla) \mathbf{M}, \quad (1.38)$$

with β the dimensionless constant characterizing this dissipative torque on the magnetization. In the literature this torque is called the non-adiabatic STT. Furthermore, microscopic calculations show the order of magnitude of

the dimensionless parameter β to be comparable to that of Gilbert damping $\beta \sim \alpha \sim 10^{-2}$ [58], where we used that $\alpha \sim 10^{-2}$ for typical metallic ferromagnets. In Chapter 2 we show that there exist regimes in which the non-adiabatic STT can stabilize negative energy excitations induced by the adiabatic STT. It does so by effectively reversing the sign of the damping.

1.4.2 *Spin orbit torques*

Another way of injecting angular momentum into the magnetic sample is by using spin-orbit torques (SOTs). SOTs can be used to inject angular momentum into the magnetic layer of magnetic heterostructures by using a charge current parallel to the interface between the layers. These heterostructures typically consist of a non-magnetic conducting layer with strong spin-orbit coupling and a magnetic — in our case ferromagnetic — layer on top. These setups are more versatile compared to the STT, since the magnetic layer is allowed to be insulating. This allows one to use low magnetic damping materials like the magnetic insulator yttrium-iron-garnet (YIG).

The generation of a torque in the magnetic layer is realized as follows. If we apply an electric field over the metallic layer it generates an electric current. This current gets partially converted into a spin current perpendicular to the direction of the electric current via the spin-Hall effect (SHE). The generation of the spin current in the SHE is due to an asymmetrical deflection of spin induced by spin-orbit coupling¹— which couples the electron spin to its orbital degree of freedom. This would describe the spin current if no boundaries are present. In heterostructures the spin current is flowing towards the interface of the conductor with the magnet. Not all the spin current is able to pass the interface and part of the spin accumulates, which is called the spin accumulation. The part of the spin current that can pass through

¹ Most models that consider the SHE restrict to the geometry of a two-dimensional electron gas (2DEG), in which the electrons are for instance only able to move in the let's say (x, y) plane. Typically, the spin polarized current generated by SHE in such a geometry is characterised by $\mathbf{j}_\alpha \propto (\hat{\zeta} \times \mathbf{j})\zeta_\alpha$, where \mathbf{j} is current density and $\hat{\zeta} = (\hat{z} \times \mathbf{j}/|\mathbf{j}|)$ the spin-polarization axis.

the interface into the magnet depends on the configuration of the magnet and on the spin accumulation. A long story short, the effective spin current through the interface is proportional to the torque on the magnetization, and is given by [60, 61]

$$\partial_t M_\alpha|_{\text{SH dampinglike}} = \hat{z} \cdot \mathbf{j}_\alpha = \frac{g\mu_B\eta\theta_{\text{SH}}}{2eM_s d} \mathbf{M} \times [\mathbf{M} \times (\hat{z} \times \mathbf{j})]_\alpha, \quad (1.39)$$

where μ_B is the Bohr magneton, g the g-factor of the electron, η gives the efficiency of the interface, d the thickness of the magnetic layer and $\theta_{\text{SH}} = \sigma_{\text{SH}}/\sigma$ the dimensionless spin-Hall angle, with σ_{SH} the spin-Hall conductivity and σ the conductivity of the conducting layer. Thus Eq. (1.39) gives a dissipative torque on the magnetization due to injection of angular momentum into the magnetic layer, and is referred to in literature as the damping-like torque.

For completeness, we discuss another torque on the magnetization that is induced by an electric current in such heterostructures. Namely the field like torque

$$\partial_t \mathbf{M}|_{\text{SH fieldlike}} \propto \mathbf{M} \times (\hat{z} \times \mathbf{j}). \quad (1.40)$$

This torque is due to interaction of the magnetization with spin density created by the SHE at the interface of the layers. This torque describes a shift in the effective magnetic field and for that reason is called the field-like torque. Since the field-like torque is often rather small compared to the effective magnetic field we neglect it in the remainder of this Thesis. The damping-like torque on the other hand competes with the dissipation of magnetic energy which is approximately related to the effective field via the Gilbert damping constant α which is a much smaller quantity to compete with. For sufficiently strong charge currents, SOTs may be used to effectively reverse the sign of the damping — which only the damping-like torque is capable of.

In the next sections we discuss how one can create long lived negative energy excitations with the use of SOTs. Furthermore, we discuss how these excitations are fundamentally different from positive energy excitations and cover some of the formalism necessary to treat them.

1.5 LOW ENERGY EXCITATIONS ON MAGNETICALLY STABLE AND MAGNETICALLY UNSTABLE GROUND STATES

In the sections below, we formally introduce magnons as excitations on energetically stable ground states and introduce the concept of antimagnons — which are excitations that occur in magnetically unstable ground states. While some of this discussion is well-known in the field of analogue gravity [27–29], it may not be familiar to researchers working in other fields of research. Because of this, we try to be detailed and complete in what follows. Moreover, while touching on treatments that have been presented in the field of analogue gravity, the discussion that follows adds the specific details for magnetic systems, such as the various magnetic interactions, damping, and spin currents. We also note that while in the first instance this discussion is fully based on the Landau-Lifshitz-Gilbert (LLG) equation, it also sets the stage for quantum effects that are beyond the LLG equation. For readers who wish to skip these details, we give here a brief summary: We discuss how the LLG equation yields an eigenvalue problem that is well-known in the Bogoliubov theory of excitations in superfluids, and which leads to the introduction of a specific conserved norm. This eigenvalue problem yields pairs of eigenfrequencies of which the eigenmodes have opposite norm and which physically correspond to the same excitation. Because of this doubling, it is sufficient to consider only positive or negative frequencies.

For linearization around the true magnetic ground state — referred to as the energetically-stable situation — the positive-norm modes have positive frequencies, while the negative-norm modes have negative frequencies. Upon quantization, we are left with excitations that correspond to magnons, either with positive norm and positive frequency or with negative norm and negative frequency. Typically, one restricts oneself to positive frequencies and therefore one does not need to introduce the negative-norm states.

The situation changes if one considers excitations on top of a state that is not the magnetic ground state, which we refer to as the energetically unstable situation. In this case, there may be positive-norm states with negative frequency, and negative-norm states with positive frequency. Re-

restricting oneself again to positive frequencies, one now has to consider the negative-norm states with positive frequencies. We define these excitations to be antimagnons, as they carry opposite spin to magnons and physically correspond to negative-energy excitations. This is because the system is now linearized around an energetically-unstable state, and the excitation lowers the total energy.

Adding any amount of dissipation would normally make the energetically-unstable situation dynamically unstable as well: because the environment is able to dissipate energy, the system dynamically evolves to its true ground state. The energetically-unstable situation may be made dynamically stable by external pumping that effectively reverses the sign of the damping. Below we discuss in detail the example of how this may be achieved by spin-orbit torque. Once the energetically-unstable state is dynamically stabilized it yields stable antimagnon excitations that may be coupled to magnons. Examples of the physics that results from this coupling are discussed in Part ii.

1.5.1 Preliminaries

We consider an insulating ferromagnetic (FM) thin film with hard-axis anisotropy in the y -direction adjacent to a heavy-metal layer (HM), as shown in Fig. 1.3. Furthermore, we consider an external magnetic field in the z -direction. The discussion below may be easily generalized to other examples of magnetic anisotropies and fields. Far below the Curie temperature, the dynamics is well described by the LLG equation for the direction $\mathbf{n} = \mathbf{M}/|\mathbf{M}|$ of the magnetization with spin-orbit torques (SOT),

$$\frac{\partial \mathbf{n}}{\partial t} = -\gamma \mathbf{n} \times \mathbf{h}_{\text{eff}} + \alpha \mathbf{n} \times \frac{\partial \mathbf{n}}{\partial t} + J_s \mathbf{n} \times \hat{z} \times \mathbf{n}, \quad (1.41)$$

with γ the gyromagnetic ratio, α the Gilbert damping and J_s the strength of SOTs generated by the spin current which depends on the current flowing in the HM layer, the spin Hall angle of the HM and the properties of the interface.

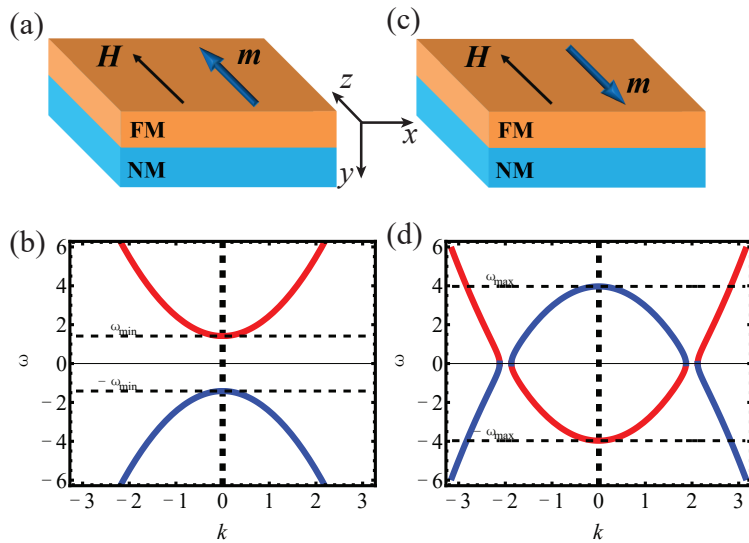


Figure 1.3: Scheme of a magnetic thin film adjacent to a heavy metal layer with magnetization parallel (a) and antiparallel (b) to the external field. The bottom panel shows the corresponding dispersion relations of magnetic excitations. The configuration in (a) corresponds to the energetically stable ground state and hence the dispersion in (b) is the usual spin wave dispersion. On the other hand, configuration (c) gives an energetically unstable situation, which is stabilized by SOT. As a result, the spin-wave dispersion in (d) has negative energy excitations.

The above equation describes damped precession around the effective magnetic field $\mathbf{h}_{\text{eff}} = -\delta E/(M_s \delta \mathbf{n})$, with M_s the saturation magnetization and

$$E = \int dV \left\{ A(\nabla_i \mathbf{n})^2 - \mu_0 H_e M_s n_z + \frac{1}{2} K n_y^2 \right\} \quad (1.42)$$

the magnetic energy functional of this set-up. In the above A is the exchange stiffness, H_e is the external magnetic field strength, μ_0 is the vacuum permeability with K the anisotropy, which may be caused by magnetocrystalline anisotropy or dipolar interactions.

We introduce spin waves as linearized dynamical fluctuations on top of the static magnetization. As discussed, we consider the static magnetization to be either in the direction of the external magnetic field or opposite to it, i.e. $\mathbf{n}_0 = \pm \hat{z}$. The former ($\mathbf{n}_0 = \hat{z}$) corresponds to the energetically stable configuration whereas the latter ($\mathbf{n}_0 = -\hat{z}$) corresponds to the energetically unstable configuration. We proceed by introducing the complex field $\Psi = (1/\sqrt{2})(\hat{e}_1 + i\hat{e}_2) \cdot \mathbf{n}$, with $\hat{e}_1 \times \hat{e}_2 = \mathbf{n}_0$. For convenience we consider $\hat{e}_1 = \hat{x}$, which automatically gives $\hat{e}_2 = \mp \hat{y}$. When linearizing the LLG equation (5.2) in $\delta n_1, \delta n_2$, according to $\mathbf{n} = \mathbf{n}_0 + (\delta n_1, \delta n_2, 0)^T$, it is recast as a Bogoliubov-DeGennes like equation

$$\frac{i(\mathbb{1} + i\alpha\sigma_z)\partial_t}{\gamma\mu_0 M_s} \begin{pmatrix} \Psi \\ \Psi^* \end{pmatrix} = (\mathcal{L}_\pm + iI_s\mathbb{1}) \begin{pmatrix} \Psi \\ \Psi^* \end{pmatrix}, \quad (1.43)$$

with

$$\mathcal{L}_\pm = (\Delta \pm h - \Lambda^2 \nabla^2) \sigma_z + i\Delta \sigma_y. \quad (1.44)$$

In the above, $\sigma_{y,z}$ are the Pauli matrices and $\mathbb{1}$ is the 2×2 identity matrix, $\Lambda = \sqrt{2A/\mu_0 M_s^2}$ the exchange length, $h = H_e/M_s$ the dimensionless external magnetic field, $\Delta = K/2\mu_0 M_s^2 = 1/2$ the dimensionless anisotropy constant and $I_s = J_s/\gamma\mu_0 M_s$ the dimensionless SOT.

1.5.2 Symmetries and the conserved norm of the equation of motion

We write the complex wavefunction Ψ in terms of Bogoliubov modes

$$\Psi(\mathbf{x}, t) = u(\mathbf{x})e^{-i\lambda t} + v^*(\mathbf{x})e^{i\lambda^* t} \quad (1.45)$$

and, for later convenience, we define the dimensionless frequency $\omega = \lambda/\gamma\mu_0 M_s$. At this point we make several observations. First of all, the dissipationless limit of Eq. (1.43) ($\alpha = I_s = 0$) is pseudo-Hermitian, in other words

$$\sigma_z \mathcal{L}_\pm^\dagger \sigma_z = \mathcal{L}_\pm. \quad (1.46)$$

A consequence of this statement is that the inner product $\langle \Psi, \Psi' \rangle \equiv \langle \Psi | \sigma_z | \Psi' \rangle = \int dV [u^*(\mathbf{x})u'(\mathbf{x}) - v^*(\mathbf{x})v'(\mathbf{x})]$ and hence the non-positive definite magnon norm

$$\|\Psi\| = \langle \Psi | \sigma_z | \Psi \rangle = \int dV (|u|^2 - |v|^2), \quad (1.47)$$

is conserved in the dissipationless limit. Secondly, Eq. (1.43) has the additional symmetry

$$\sigma_x (\mathcal{L}_\pm + i\alpha\omega^* \sigma_z + iI_\mu \mathbb{1}) \sigma_x = -(\mathcal{L}_\pm - i\alpha\omega \sigma_z + iI_\mu \mathbb{1})^*. \quad (1.48)$$

This implies that if ω is an eigenfrequency of Eq. (1.43) with eigenmode $(u \ v)^\top$, then $-\omega^*$ is an eigenfrequency with eigenmode $(v^* \ u^*)^\top$. These two modes have opposite norm by construction. Hence, the two branches of Eq. (1.43) are related to each other via particle-hole symmetry. In our magnetic system, this doubling is not physical, but merely a result of our choice to describe spin waves using complex scalar fields. Hence, in order to determine the full dynamics of the system it is sufficient to consider $\omega > 0$ and take into account the norm of different modes. As we see later, the sign of the norm in Eq. (1.47) describes whether we work with magnon or antimagnon commutation relations.

1.5.3 Spin waves, again

The ground state corresponds to $\mathbf{n}_0 = \hat{z}$. Because of translation invariance, we introduce spin-wave modes as the Fourier modes of $u(\mathbf{x})$ and $v(\mathbf{x})$ in the linearized LLG equation (5.2)–around the $+\hat{z}$ direction. Up to first order in dissipative terms α and I_s , these spin wave solutions have the following dispersion relation

$$\omega_{\mathbf{k}} \simeq \omega_{\mathbf{k}}^0 - i (\alpha [\Delta + h + \Lambda^2 k^2] - I_s), \quad (1.49)$$

with $\omega = \lambda/\gamma\mu_0 M_s$ the dimensionless frequency and

$$\omega_{\mathbf{k}}^0 = \|\Psi_k\| \sqrt{(\Delta + h + \Lambda^2 k^2)^2 - \Delta^2}, \quad (1.50)$$

the real part of the dispersion relation in which $\|\Psi_k\| = \pm 1$ is the norm of the modes. In Fig. 1.3(b) we show the real part of the dispersion relation, where the red curve corresponds to the positive norm mode and the blue curve corresponds to the negative norm mode. From the stability requirement we discussed in this section we find that the ground state is stable if $I_s/\alpha < [\Delta+h]$. Hence, the ground state becomes unstable if it is driven sufficiently strong such that the SOT overcompensates the damping. This is well known to happen in spin-torque-oscillators.

The energy functional (1.42) for spin-wave excitations per definition gives us

$$E \equiv \frac{1}{2} \langle \Psi | \sigma_z \mathcal{L}_+ | \Psi \rangle. \quad (1.51)$$

By expanding $|\Psi\rangle = \sum_k a_k |\Psi_k\rangle$ in spin-wave eigenmodes, we find

$$\begin{aligned} E &= \frac{1}{2} \sum_{l,k} a_l^* a_k \langle \Psi_l | \sigma_z \mathcal{L}_+ | \Psi_k \rangle \\ &= \frac{1}{2} \sum_{l,k} a_l^* a_k \langle \Psi_l | \sigma_z | \Psi_k \rangle \omega_k^0 \\ &= \frac{1}{2} \sum_k |a_k|^2 \|\Psi_k\| \omega_k^0, \end{aligned} \quad (1.52)$$

Thus, the contribution of the spin-wave modes to the energy is given by $\|\Psi_k\|\omega_k^0$. Hence, one may choose to work with the positive-norm modes which have positive frequency and the excitation of which leads to an increase of energy. Alternatively, one may work with negative-energy modes with negative frequency, the excitation of which also lead to an increase in energy. The former choice is the conventional one and, upon quantization, leads to conventional magnons. Choosing to restrict oneself to negative frequency would lead to the same magnonic excitations after a particle-hole transformation, but is an unnecessary complication. This, however, changes when one considers spin-wave excitations on top of an energetically-unstable state.

1.5.4 *Spin-wave excitations around an inverted ground state*

Now, we consider spin waves on top of the energetically-unstable configuration in which the static magnetization is pointing opposite to the external magnetic field, i.e. $\mathbf{n}_0 = -\hat{z}$. Due to this different quantization axis we find that the complex field becomes $\Psi = (1/\sqrt{2})(\hat{x} + i\hat{y}) \cdot \mathbf{n}$ instead of $\Psi = (1/\sqrt{2})(\hat{x} - i\hat{y}) \cdot \mathbf{n}$ which we used in the previous section. This, as we will see in Section 1.5.5, precisely corresponds to the choice of a different-norm branch and thus commutation relation for the excitations after quantization. As before, spin waves are introduced as the Fourier modes of $u(\mathbf{x})$ and $v(\mathbf{x})$ in the linearized LLG equation (5.2). We find that the dispersion relation, up to first order in dissipative constants α and I_s is given by

$$\omega_{\mathbf{k}} \simeq \omega_{\mathbf{k}}^0 - i(\alpha [\Delta - h + \Lambda^2 k^2] - I_s), \quad (1.53)$$

with

$$\text{Re}(\omega_{\mathbf{k}}^0) = \|\Psi_k\| \text{sgn}(\Lambda^2 k^2 - h) \sqrt{(\Delta - h + \Lambda^2 k^2)^2 - \Delta^2} \quad (1.54)$$

the real part of the dispersion relation in which

$$\|\Psi_k\| = \begin{cases} \pm 1, & |\Delta - h + \Lambda^2 k^2| > \Delta, \\ 0, & |\Delta - h + \Lambda^2 k^2| < \Delta, \end{cases}$$

is the norm of the modes. The real part of the dispersion relation in Eq. (1.54) is shown in Fig. 1.3(d), in which the red curve corresponds to the positive norm mode and the blue curve to the negative norm mode. Note that the above defined norm vanishes precisely in the interval for which the dispersion relation has a so called exceptional line [62]. In this interval the ground state becomes unstable towards excitations of specific wavelengths. This instability also has to overcome by the SOT for our theory to remain valid. Similar to the previous subsection, the classical stability follows from the sign of the imaginary part of the spin wave dispersion relation. Here, we see that this configuration is stable once

$$-I_s/\alpha \gtrsim \max(h - \Delta, \Delta/\alpha). \quad (1.55)$$

Thus the magnetization can in principle be held pointing opposite to the external field if the angular momentum injected by the SOT is sufficiently large. To determine this stability condition we furthermore used

$$\text{Im}(\omega_{\mathbf{k}}^0) = (1 - \|\Psi_{\mathbf{k}}\|^2) \sqrt{(\Delta - h + \Lambda^2 k^2)^2 - \Delta^2}.$$

We thus see that reducing the anisotropy Δ , which yields elliptical magnetization precession, will greatly reduce the critical current needed to keep the energetically-unstable state dynamically stable.

To continue, the energy functional for the excitations is given by

$$E \equiv \frac{1}{2} \langle \Psi | \sigma_z \mathcal{L}_- | \Psi \rangle. \quad (1.56)$$

By expanding in eigenmodes $|\Psi\rangle = \sum_k a_k |\Psi_k\rangle$ we find

$$\begin{aligned} E &= \frac{1}{2} \sum_{l,k} a_l^* a_k \langle \Psi_l | \sigma_z \mathcal{L}_- | \Psi_k \rangle \\ &= \frac{1}{2} \sum_k |a_k|^2 \|\Psi_k\| \omega_k^0. \end{aligned} \quad (1.57)$$

Once again we may chose to work with either positive or negative-norm excitations of which the excitation energy is given by $\|\Psi_k\| \omega_k^0$ which becomes negative in a specific region of phase space. What is, however, special in

this case is that at positive frequencies there now exist both positive-norm excitations and negative-norm excitations. Because they both have positive frequency, they may couple to each other and examples of this coupling are discussed in Part ii. Restricting oneself to positive frequencies, one now necessarily has to explicitly consider the negative-norm modes. Upon quantization, we define these latter modes to be antimagnons.

1.5.5 Canonical quantization

The formalism discussed in this section is restricted to the dissipationless limit, i.e. $\alpha \rightarrow 0$ and $I_s \rightarrow 0$, thereby assuming that the quantization procedure is still valid when turning on the small dissipation. We start out this section by canonically quantizing the complex scalar field in Eq. (1.43). In this case, canonical quantization should give us

$$[\Psi(\mathbf{x}, t), \Psi^\dagger(\mathbf{x}', t)] = \delta(\mathbf{x} - \mathbf{x}'), \quad (1.58)$$

since $i\Psi^\dagger$ is the canonical momentum associated with Ψ . For completeness, the canonical momentum of Ψ^\dagger is $-i\Psi$ making the above definition self consistent.

In Section 1.5.1 we have seen that the definition of Ψ depends on the choice of direction of the static magnetization \mathbf{n}_0 , where a sign change of \mathbf{n}_0 implies a complex conjugation of the complex scalar fields, i.e. $\mathbf{n}_0 = \hat{z} \rightarrow -\hat{z} \implies \Psi \rightarrow \Psi^*$. Hence, if the quantization axis describes the vacuum opposite to the fixed point direction used for linearization one obtains the anomalous commutation relations

$$[\Psi(\mathbf{x}, t), \Psi^\dagger(\mathbf{x}', t)] = -\delta(\mathbf{x} - \mathbf{x}'). \quad (1.59)$$

As we will see in the rest of this section, if we quantize our theory using the commutation relation in Eq. (1.58) for positive frequency excitations, the commutation relation for antimagnonic modes will satisfy anomalous commutations relations. And hence, intuitively, antimagnonic modes may also be seen as having an opposite quantization axis with respect to magnonic excitations.

1.5.6 Quantization from the microscopic Hamiltonian using the Holstein-Primakoff transformation

In this section we make the connection between the magnons in our canonically quantized theory and the magnons following from the Holstein-Primakoff transformation in a spin model [63]. We start from the spin Hamiltonian

$$\mathcal{H} = -J \sum_{\langle ij \rangle} \mathbf{S}_i \cdot \mathbf{S}_j - \gamma \mu_0 H \sum_i S_i^z + K_d \sum_i (S_i^y)^2 \quad (1.60)$$

where the first term is Heisenberg exchange interaction between neighbouring spins with J being exchange coefficient, which relates to the exchange coefficient in Eq. (1.42) via $A = Ja^{2+d}/2\gamma^2$, with d the number of spatial dimensions and a the lattice spacing. The second term is Zeeman energy of spins under an external field H with $H > 0$, which is related to H_e via $H_e = H$. In the above K_d is the shape anisotropy which is related to the anisotropy in Eq. (1.42) by $K = K_d a^d / \gamma^2$. The spin operator obeys the commutation relation $[S^i, S^j] = i\hbar \epsilon_{ijk} S^k$ with ϵ_{ijk} the Levi-Civita symbol. We consider the static state of the system around which we quantize to be $\mathbf{S} = \pm S e_z$. In the true ground state ($\mathbf{S} = +S e_z$) the decrease of S^z by \hbar corresponds to a magnon excitation. On the other hand, in the energetically unstable state ($\mathbf{S} = -S e_z$) an increase of \hbar gives rise to either a magnonic or an anti-magnonic excitation. The difference between the two is essentially their handedness and their energy. The antimagnonic excitations carry negative energy and have opposite handedness with respect to the magnonic ones. Formally, we introduce the (anti)magnonic excitations on top of the energetically (un-)stable ground state via the Holstein-Primakoff transformation

$$S_i^\pm = \hbar \sqrt{2S - \Psi_i^\dagger \Psi_i} \Psi_i, \quad (1.61a)$$

$$S_i^\mp = \Psi_i^\dagger \hbar \sqrt{2S - \Psi_i^\dagger \Psi_i}, \quad (1.61b)$$

$$S_{iz} = \pm \hbar (S - \Psi_i^\dagger \Psi_i), \quad (1.61c)$$

such that the commutation relations are given by

$$[\Psi_i, \Psi_j^\dagger] = \delta_{ij}, \quad [\Psi_i, \Psi_j] = 0. \quad (1.62)$$

We would like to stress here, that the definition of S^\pm is with respect to the quantization axis $\pm\hat{z}$. If $S \gg \langle \Psi_i^\dagger \Psi_i \rangle$ the spin Hamiltonian can be expanded up to second order in Ψ and Ψ^\dagger giving

$$\begin{aligned} \mathcal{H} = & \pm \gamma \hbar \mu_0 H \sum_i \Psi_i^\dagger \Psi_i - J \hbar S \sum_{\langle ij \rangle} \left[\Psi_i \Psi_j^\dagger + \Psi_i^\dagger \Psi_j - 2 \Psi_i^\dagger \Psi_i \right] \\ & - (K_d \hbar S / 2) \sum_i \left[\Psi_i^\dagger \Psi_i^\dagger + \Psi_i \Psi_i - 2 \Psi_i^\dagger \Psi_i \right]. \end{aligned} \quad (1.63)$$

When taking the continuum limit of the above we find

$$\mathcal{H} = \frac{1}{2} \int dV \begin{pmatrix} \Psi^\dagger & \Psi \end{pmatrix} (\sigma_z \mathcal{L}_\pm) \begin{pmatrix} \Psi \\ \Psi^\dagger \end{pmatrix}, \quad (1.64)$$

with \mathcal{L}_\pm defined in Eq. (1.44) and

$$[\Psi(x), \Psi^\dagger(x')] \rightarrow \delta(x - x'), \quad [\Psi(x), \Psi(x')] = 0. \quad (1.65)$$

We thus find that according to the Holstein-Primakoff transformation our canonically quantized fields Ψ and Ψ^\dagger correspond at quadratic order to the spin lowering and raising operators S^\pm and S^\mp . Hence, the anomalous operators b^\dagger and b describe a vacuum opposite of their quantization axis, up to second order in their fields.

1.5.7 Representations of magnons and antimagnons

Below we discuss two commonly used representations for magnons, namely the wavevector representation and the frequency representation. We put special emphasis on the case in which we linearize around the inverted ground state in which we need to consider both the magnonic and the antimagnonic excitations.

1.5.7.1 *Wavevector representation*

Let us in first instance restrict ourselves to the commutation relation in Eq. (1.58). In order to diagonalize the equation of motion (1.43) we take the following Bogoliubov ansatz

$$\Psi(\mathbf{x}, t) = \sum_k \left(u_k(x) a_k e^{-i\omega_k t} + v_k^*(x) a_k^\dagger e^{i\omega_k t} \right), \quad (1.66a)$$

$$\Psi^\dagger(\mathbf{x}, t) = \sum_k \left(v_k(x) a_k e^{-i\omega_k t} + u_k^*(x) a_k^\dagger e^{i\omega_k t} \right), \quad (1.66b)$$

where u_k and v_k are solutions of Eq. (1.43) and a^\dagger and a are the (anti)magnon creation and annihilation operators. We find that Eqs. (1.58) and (1.66) imply the commutation relations

$$\|\Psi_k\| \|\Psi_{k'}\| [a_k, a_{k'}^\dagger] = \langle \Psi_k, \Psi_{k'} \rangle = \|\Psi_k\| \delta_{k,k'}, \quad (1.67)$$

where the last equality in the above equation is only true if both states have the same norm and is otherwise zero. Thus, if we work with the positive-norm branch we use the commutation relations $[a_k, a_{k'}^\dagger] = \delta_{k,k'}$, while in the negative norm branch we have to use the anomalous commutations relations $[a_k, a_{k'}^\dagger] = -\delta_{k,k'}$. Furthermore, if two operators correspond to states with different norm we get the commutation relation

$$\|\Psi_k\| \|\Psi_{k'}\| [a_k, a_{k'}] = \|\Psi_{k'}\| \delta_{k,k'}, \quad (1.68a)$$

$$\|\Psi_k\| \|\Psi_{k'}\| [a_k^\dagger, a_{k'}^\dagger] = \|\Psi_k\| \delta_{k,k'}, \quad (1.68b)$$

and otherwise zero. The latter is a consequence of the particle-hole symmetry in the equations of motion Eq. (1.43) for the fields. From this point onward we relabel creation and annihilation operators of the negative norm branch as b_k^\dagger and b_k such that $[b_k, b_{k'}^\dagger] = -\delta_{k,k'}$ and the operators in the positive as a_k and a_k^\dagger with $[a_k, a_{k'}^\dagger] = \delta_{k,k'}$. Additionally we relabel solutions of the negative norm branch of Eq. (1.43) as $(\tilde{u} \ \tilde{v})^T$. From Eqs. (1.67) and (1.68) we unsurprisingly find that the operators in the different branches are related

by particle hole symmetry $b_k^\dagger = a_{-k}$ and $b_k = a_{-k}^\dagger$. We find that the field Ψ may now be written as

$$\begin{aligned} \begin{pmatrix} \Psi(\mathbf{x}, t) \\ \Psi^\dagger(\mathbf{x}, t) \end{pmatrix} &= \frac{1}{\sqrt{2}} \sum_{\|\Psi_k\|=1} \left[\begin{pmatrix} u_k \\ v_k \end{pmatrix} a_k e^{-i\omega_k t + ikx} + \begin{pmatrix} v_k^* \\ u_k^* \end{pmatrix} a_k^\dagger e^{i\omega_k t - ikx} \right] \\ &+ \frac{1}{\sqrt{2}} \sum_{\|\Psi_k\|=-1} \left[\begin{pmatrix} \tilde{u}_k \\ \tilde{v}_k \end{pmatrix} b_k e^{-i\omega_k t - ikx} + \begin{pmatrix} \tilde{v}_k^* \\ \tilde{u}_k^* \end{pmatrix} b_k^\dagger e^{i\omega_k t + ikx} \right] \end{aligned} \quad (1.69)$$

The fields $b^\dagger \equiv a$ and $b \equiv a^\dagger$ give a doubling of the modes, since the same information is essentially described by the fields a and a^\dagger of the positive norm branch. This can be made more intuitive when we remember that particle hole symmetry gives $(v^* \ u^*)^T$ as an eigenmode of Eq. (1.43) with frequency $-\omega^*$ if $(u \ v)^T$ is an eigenmode with frequency ω . Hence, we see that the negative norm sector can be mapped onto the positive norm sector via a particle-hole transformation. One may thus chose to work in whatever branch we find convenient. As argued previously, for excitations on top of a energetically-unstable state and after restricting oneself to positive frequency, one necessarily has to consider the negative-norm excitations. For the field in Eq. (1.69), this implies considering both the magnon operators a and a^\dagger and the antimagnon operators b and b^\dagger .

Let us consider the Hamiltonian for (anti)magnon excitations. Similar to the previous section this is given by

$$E \equiv \frac{1}{2} \int dV \begin{pmatrix} \Psi^\dagger & \Psi \end{pmatrix} (\sigma_z \mathcal{L}_\pm) \begin{pmatrix} \Psi \\ \Psi^\dagger \end{pmatrix}. \quad (1.70)$$

Using Eq. (1.69) we find that the Hamiltonian in second quantized form becomes

$$\begin{aligned} E &= \frac{1}{4} \sum_{\|\Psi_{k,l}\|=1} \left(a_l^\dagger a_k + a_k a_l^\dagger \right) \langle \Psi_l, \Psi_k \rangle \omega_k^0 \\ &+ \frac{1}{4} \sum_{\|\Psi_{k,l}\|=-1} \left(b_l b_k^\dagger + b_k^\dagger b_l \right) \langle \Psi_l, \Psi_k \rangle \omega_k^0. \end{aligned} \quad (1.71)$$

Thus we find

$$E = E_0 + \frac{1}{2} \sum_{\|\Psi_k\|=1} \|\Psi_k\| \omega_k^0 a_k^\dagger a_k + \frac{1}{2} \sum_{\|\Psi_k\|=-1} \|\Psi_k\| \omega_k^0 b_k b_k^\dagger. \quad (1.72)$$

In the above E_0 is the energy without excitations and b, b^\dagger and a, a^\dagger the (anti)magnon annihilation and creation operators. As in Section 1.5.4 we notice that on top of energetically-unstable states there exist negative energy modes of which, by definition, the product of norm and frequency is negative. This implies that these modes, which we call antimagnons, have opposite handedness with respect to their magnonic counterpart. More discussion on this can be found in Section 1.5.7.2.

1.5.7.2 Frequency representation

For processes in which the frequency ω is conserved but wavevector is no longer conserved, such as scattering, it is useful to change variables from $k \rightarrow \omega$. This representation is useful when coupling magnonic excitations to antimagnon excitations, of which examples are given in Chapters 2, 4 and 6. Furthermore, this representation makes the need to consider antimagnons on top of the energetically unstable state explicit. We proceed by expanding the Ψ and Ψ^\dagger in Section 1.5.7.1 in the frequency representation. Due to doubling of the modes we consider $\omega > 0$ throughout this section. Here, we consider k to be in the continuum. This implies $\sum_k \rightarrow \int d^d k$, furthermore we define $\|\Psi_k\|$ by $\langle \Psi_k | \sigma_z | \Psi_{k'} \rangle = \|\Psi_k\| \delta^d(k - k')$ and $\|\Psi_k\| \|\Psi_{k'}\| [a_k, a_{k'}^\dagger] = \langle \Psi_k, \Psi_{k'} \rangle \rightarrow \|\Psi_k\| \delta^d(k - k')$. We will see that a change in coordinates $k \rightarrow \omega$ proceeds very differently in the case where the static magnetization is pointing in the direction of the external magnetic field, i.e. $\mathbf{n}_0 = \hat{z}$, as compared to the case in which it points against the external magnetic field, i.e. $\mathbf{n}_0 = -\hat{z}$. Let us in first instance restrict ourselves to the case in which the magnetization is in the direction of the external magnetic field, i.e. $\mathbf{n}_0 = \hat{z}$, corresponding to true

equilibrium. From here we perform a coordinate transformation on Eq. (1.69) to frequency space giving us

$$\Psi(\mathbf{x}, t) = \int d\vec{\Omega} \int_{\omega_{\min}}^{\infty} d\omega \left[u_{\omega, \vec{\Omega}}(\mathbf{x}) a_{\omega, \vec{\Omega}} e^{-i\omega t} + v_{\omega, \vec{\Omega}}^*(\mathbf{x}) a_{\omega, \vec{\Omega}}^{\dagger} e^{i\omega t} \right], \quad (1.73a)$$

$$\Psi^{\dagger}(\mathbf{x}, t) = \int d\vec{\Omega} \int_{\omega_{\min}}^{\infty} d\omega \left[v_{\omega, \vec{\Omega}}(\mathbf{x}) a_{\omega, \vec{\Omega}} e^{-i\omega t} + u_{\omega, \vec{\Omega}}^*(\mathbf{x}) a_{\omega, \vec{\Omega}}^{\dagger} e^{i\omega t} \right]. \quad (1.73b)$$

Here, $\vec{\Omega}$ is a vector on the unit sphere of dimension $d - 1$, $(u_k \ v_k)^T$ is an eigenmode in the positive norm branch, $\omega_{\min} = \sqrt{(\Delta + h)^2 - \Delta^2}$ gives the ferromagnetic resonance and the rescaled fields and operators are given by

$$\begin{pmatrix} u_{\omega, \vec{\Omega}}(\mathbf{x}) \\ v_{\omega, \vec{\Omega}}(\mathbf{x}) \\ a_{\omega, \vec{\Omega}} \\ a_{\omega, \vec{\Omega}}^{\dagger} \end{pmatrix} = \sqrt{k^{d-1}} \sqrt{\frac{dk}{d\omega}} \begin{pmatrix} u_{\vec{k}}(\mathbf{x}) \\ v_{\vec{k}}(\mathbf{x}) \\ a_{\vec{k}} \\ a_{\vec{k}}^{\dagger} \end{pmatrix}. \quad (1.74)$$

Where these rescaled field and operators are chosen such that their commutation relations become

$$\left[a_{\omega, \vec{\Omega}}, a_{\omega', \vec{\Omega}'}^{\dagger} \right] = \delta(\omega - \omega') \delta^{d-1}(\vec{\Omega} - \vec{\Omega}'). \quad (1.75)$$

Due to the isotropic dispersion in Eqs. (1.50) and (1.54) the fields in Eq. (1.74) may be simplified further. Since the dispersion relation is independent of the direction of \vec{k} , the magnitude of k only depends on the magnitude of ω . We may thus express the fields as $(u_{\omega, \vec{\Omega}}(\mathbf{x}) \ v_{\omega, \vec{\Omega}}(\mathbf{x})) = (u_{\omega} \ v_{\omega}) \exp(ik(\omega)\vec{\Omega} \cdot \mathbf{x})$, with $(u_{\omega} \ v_{\omega}) = \sqrt{k^{d-1}} \sqrt{dk/d\omega} (u_k \ v_k)$ in which $(u_k \ v_k)$ is an eigenvector of Eq. (1.43) with $|u_k|^2 - |v_k|^2 = (2\pi)^{-d}$.

Next, we consider the case in which the equilibrium magnetization is pointing against the external magnetic field, hence $\mathbf{n}_0 = -\hat{z}$. In this instance the dispersion relation Eq. (1.54) becomes negative in the positive norm branch and positive for the negative norm branch. For frequencies below $\omega_{\max} = \sqrt{(\Delta - h)^2 - \Delta^2}$ we find an additional negative energy mode in every propagation direction. We stress that these modes carry negative energy since the product of their norm with their frequency is negative, and, following

our definition, we refer to these modes the antimagnons. For $\omega > \omega_{\max}$ on the other hand, these antimagnon modes do not exist. For excitations on top of the energetically unstable state the frequency representation of Eq. (1.69) becomes

$$\begin{aligned} \Psi(\mathbf{x}, t) = \int_{S^{d-1}} d\vec{\Omega} \int_0^{\omega_{\max}} d\omega & \left[u_{\omega, \vec{\Omega}}(\mathbf{x}) a_{\omega, \vec{\Omega}} e^{-i\omega t} + v_{\omega, \vec{\Omega}}^*(\mathbf{x}) a_{\omega, \vec{\Omega}}^\dagger e^{i\omega t} \right. \\ & \left. + \tilde{u}_{\omega, \vec{\Omega}}(\mathbf{x}) b_{\omega, \vec{\Omega}} e^{-i\omega t} + \tilde{v}_{\omega, \vec{\Omega}}^*(\mathbf{x}) b_{\omega, \vec{\Omega}}^\dagger e^{i\omega t} \right] \\ & + \int_{\omega_{\max}}^\infty d\omega \left[u_{\omega, \vec{\Omega}}(\mathbf{x}) a_{\omega, \vec{\Omega}} e^{-i\omega t} + v_{\omega, \vec{\Omega}}^*(\mathbf{x}) a_{\omega, \vec{\Omega}}^\dagger e^{i\omega t} \right], \end{aligned} \quad (1.76)$$

where the conjugated expression becomes

$$\begin{aligned} \Psi^\dagger(\mathbf{x}, t) = \int_{S^{d-1}} d\vec{\Omega} \int_0^{\omega_{\max}} d\omega & \left[v_{\omega, \vec{\Omega}}(\mathbf{x}) a_{\omega, \vec{\Omega}} e^{-i\omega t} + u_{\omega, \vec{\Omega}}^*(\mathbf{x}) a_{\omega, \vec{\Omega}}^\dagger e^{i\omega t} \right. \\ & \left. + \tilde{v}_{\omega, \vec{\Omega}}(\mathbf{x}) b_{\omega, \vec{\Omega}} e^{-i\omega t} + \tilde{u}_{\omega, \vec{\Omega}}^*(\mathbf{x}) b_{\omega, \vec{\Omega}}^\dagger e^{i\omega t} \right] \\ & + \int_{\omega_{\max}}^\infty d\omega \left[v_{\omega, \vec{\Omega}}(\mathbf{x}) a_{\omega, \vec{\Omega}} e^{-i\omega t} + u_{\omega, \vec{\Omega}}^*(\mathbf{x}) a_{\omega, \vec{\Omega}}^\dagger e^{i\omega t} \right]. \end{aligned} \quad (1.77)$$

In the above the modes $(\tilde{u} \tilde{v})$ have negative norm and positive frequency ω . Here, the rescaled fields and operator of the negative norm branch are defined by

$$\begin{pmatrix} \tilde{u}_{\omega, \vec{\Omega}}(\mathbf{x}) \\ \tilde{v}_{\omega, \vec{\Omega}}(\mathbf{x}) \\ b_{\omega, \vec{\Omega}}^\dagger \\ b_{\omega, \vec{\Omega}} \end{pmatrix} = \sqrt{k^{d-1}} \sqrt{\frac{dk}{d\omega}} \begin{pmatrix} \tilde{u}_{\vec{k}}(\mathbf{x}) \\ \tilde{v}_{\vec{k}}(\mathbf{x}) \\ b_{\vec{k}}^\dagger \\ b_{\vec{k}} \end{pmatrix}. \quad (1.78)$$

Via the particle-hole transformation $b_{\omega, \vec{\Omega}} \equiv a_{-\omega, -\vec{\Omega}}^\dagger$ and $b_{\omega, \vec{\Omega}}^\dagger \equiv a_{-\omega, -\vec{\Omega}}$ the same mode is described by positive norm and negative frequency $-\omega$.

In this representation the Hamiltonian becomes

$$\begin{aligned} \mathcal{H} = \int_{S^{d-1}} d\vec{\Omega} \int_0^{\omega_{\max}} d\omega \omega & \left[a_{\omega, \vec{\Omega}}^\dagger a_{\omega, \vec{\Omega}} - b_{\omega, \vec{\Omega}} b_{\omega, \vec{\Omega}}^\dagger \right] \\ & + \int_{S^{d-1}} d\vec{\Omega} \int_{\omega_{\max}}^\infty d\omega \omega \left[a_{\omega, \vec{\Omega}}^\dagger a_{\omega, \vec{\Omega}} \right]. \end{aligned} \quad (1.79)$$

Hence the antimagnons $b_{\omega, \vec{\Omega}}$, $b_{\omega, \vec{\Omega}}^\dagger$ or $a_{-\omega, \vec{\Omega}}^\dagger$, $a_{-\omega, \vec{\Omega}}$ after a particle-hole transformation, describe excitations with energy $-\omega$ and hence have opposite handedness as compared to the magnonic excitations. From the expression in Eqs. (1.76), (1.77) and (1.79) it is clear that for frequencies between 0 and ω_{\max} one has to consider both magnons and antimagnons, and, as a result, these excitations may couple.

1.6 THIS THESIS

This Thesis constitutes of two parts. In Part i we discuss dipole-exchange spin waves trying to make a close connection to experiments and include for magnetostatic — dipole-dipole — interactions, which is not the dominant energy scale, but nonetheless significant in the long wavelength physics of ferromagnets. In Chapter 2, we discuss the possibility for spin waves to carry negative magnetic energy driven by STT. To do so we include magnetostatic interactions, Dzyaloshinskii-Moriya interaction, crystalline anisotropies as well as surface anisotropies and the effect of STT, in a manner that should accurately model ferromagnetic conductors. We, most importantly, investigate the dynamical stability of these negative energy excitations. Since the spin waves also experience the non-adiabatic STT this could render these negative energy excitations dynamically stable. In Chapter 3 we present an analytic theory that accurately models the dipole-exchange spin wave dispersion for spin waves travelling perpendicular to an in-plane external magnetic field in a thin-film geometry. The currently widely used analytic approximation rests on a diagonal approximation that becomes inaccurate when the ferromagnetic film gets thick. We suggest a different method to analytically approximate the spin wave dispersion. This turns out to have an accurate analytic solution for both thin and thick ferromagnetic films.

The focus of Part ii is on applications of negative magnetic energy excitations and the discussion of non-linear magnetization dynamics due to the onset of dynamical instabilities. We start this part with Chapter 4, in which we discuss a method to amplify spin waves of an interface between a normal ferromagnet and ferromagnetic in which negative magnetic energy

spin waves exist. In this setup the spin quantization axis between the left magnet — containing only magnons — and the right region — containing also antimagnons — are opposite. This implies that magnons in the left magnet can only scatter to antimagnons in the right magnet since the handedness of the magnons and antimagnons are opposite. We find that the conservation of energy predicts a frequency range in which superradiant reflection $|R|^2 > 1$ of spin waves in the left magnet occurs. As we will show, this mechanism is rather similar to that of the bosonic Klein paradox — where the word paradox is actually not fitting anymore. In final two chapters, namely Chapters 5 and 6, we discuss non-linear dynamics in magnetic systems that develop a linear instability. Both chapters have in common that the onset of the instability is non-dissipative and stems from the coupling of positive magnetic energy to negative energy modes. In Chapter 5 we consider a spin-torque oscillator (STO), which consists of two macrospins. We describe the initial configuration before the onset of the instability as follows, the bottom macrospin is oriented against the external magnetic field may be driven by SOT to keep it stable while the magnetization of the top macrospin is aligned with the external magnetic field and is not driven. Both macrospins in principle experience dissipation in the form of Gilbert damping. At a special point in phase space, called the exceptional point (EP), this configuration becomes unstable due to coupling between positive energy excitations in the top macrospin and negative energy excitations in the bottom macrospin. Since the linear modes grow exponentially, a non-linear theory is quickly necessary. We thus develop an analytic theory that fully describes the non-linear limit cycles of the STO. We find that the dynamics of the STO becomes relatively simple near the EP and that this STO is extremely sensitive near the EP, for vanishing out of plane exchange couplings. For nonvanishing out of plane exchange couplings we find the point of extreme sensitivity to shift slightly away from the EP. Moreover, the predictions of this analytic theory agree with numerical spin simulations and give a complete understanding of the steady-state behaviour of the STO. In the final chapter, namely Chapter 6, we investigate the non-linear dynamics of a model in which the linear instability follows from the coupling of a continuum of spin wave excitations in the left magnet to

a discrete amount of negative energy spin waves in the right magnet. In the literature of analogue gravity, such a setup is described as a black-hole laser [41, 43]. Similar to the STO described in Chapter 5, we consider the right ferromagnet to be driven by SOT such that the magnetization is dynamically stabilized against the external magnetic field. The left ferromagnet on the other hand, is pointing in the direction of the external magnetic field and is not driven. Both magnets experience dissipation in the form of Gilbert damping. As the main result, we determine the possibility for this setup to form a one-mode laser and find the range in parameter space for which it should become a stable one-mode laser. This setup is quite different from the conventional lasing setup in which a specific mode(s) start lasing due to driving of the mode(s). Here, the onset of the lasing mode is due to the coupling between positive and negative energy excitations and this system is stabilized via the injection of SOT and non-linearities.

Part I

DIPOLE-EXCHANGE SPIN WAVES

“I bought a new notebook, and put at the front: "hoping for happy accidents". And that's basically what we were trying to do.”

—Thom Yorke.

2

DYNAMICALLY STABLE NEGATIVE-ENERGY STATES INDUCED BY SPIN-TRANSFER TORQUES

This Chapter is based on J. S. Harms, A. Rückriegel, and R. A. Duine, “Dynamically stable negative-energy states induced by spin-transfer torques,” *Physical Review B* **103**, 144408 (2021). R.A.D. conceived the project, J.S.H. performed the calculations and prepared the manuscript. All authors contributed to the manuscript.

In this Chapter, we investigate instabilities of the magnetic ground state in ferromagnetic metals that are induced by uniform electrical currents, and, in particular, go beyond previous analyses by including dipolar interactions. These instabilities arise from spin-transfer torques that lead to Doppler shifted spin waves. For sufficiently large electrical currents, spin-wave excitations have negative energy with respect to the uniform magnetic ground state, while remaining dynamically stable due to dissipative spin-transfer torques. Hence, the uniform magnetic ground state is energetically unstable, but is not able to dynamically reach the new ground state. We estimate this to happen for current densities $j \gtrsim (1 - D/D_c)10^{13}\text{A/m}^2$ in typical thin film experiments, with D the Dzyaloshinskii-Moriya interaction constant, and D_c the Dzyaloshinskii-Moriya interaction that is required for spontaneous formation of spirals or skyrmions. The critical current density can be made arbitrarily small for ultrathin film thicknesses at the order of nanometers, due to surface- and interlayer effects. From an analogue gravity perspective, the stable negative energy states are an essential ingredient to implement event horizons for magnons – the quanta of spin waves – giving rise to e.g. Hawking

radiation and can be used to amplify spin waves in a so-called black-hole laser.

2.1 INTRODUCTION

Unruh's 1981 paper "Experimental black hole evaporation" [26] proposed that following the argument for thermal black-hole radiation [39] a sonic analogue event horizon can be created by considering sound waves in a flowing medium. This sonic event horizon emits a thermal spectrum of sound waves and opens up possibilities for the experimental observation of Hawking radiation. The event horizon for sound waves is created by a transition from subsonic to supersonic background flow, such that sound waves incoming from the subsonic region cannot escape the supersonic region once they have passed the event horizon. Motivated by Unruh's work, theoretical proposals of analogue event horizons based on different systems were put forward [27–29]. These include phase oscillations in a Bose-Einstein condensate [33], slow light in dielectric media [34, 35], trapped ion rings [36, 37], Weyl semi-metals [38] and, as discussed in this Chapter, metallic magnets [31]. Although Unruh's original proposal considers waves in water which can not be pushed into the quantum regime, the existence of classically stimulated Hawking emission has been observed in Ref. [64]. Furthermore, thermal Hawking radiation in a Bose-Einstein condensate, a system which might be driven to the quantum regime, has been observed in Ref. [32].

Moreover, the combination of a black-hole and white-hole horizon – the time-reversed partner of a black-hole horizon – is proposed to lead to huge amplitude enhancements at specific resonant frequencies [41], thereby acting as a black-hole laser. The resonance frequencies occur due to constructive interference of particle-hole coupling at each horizon, which gives rise to Hawking radiation in the quantum regime. An implementation of the latter is the spin-wave laser proposed in Ref. [65], which provides a way of injecting spin angular momentum into a magnetic sample through amplification of spin waves, driven by current induced spin-transfer torques [57].

In the subsequent sections, we investigate energetic and dynamic instabilities of spin waves in metallic ferromagnetic thin films, induced by spin-transfer torques, i.e., torques arising from the interaction of the spin-polarized current and the magnetization dynamics [57, 66–70]. More specifically, spin waves are Doppler shifted in the presence of an electrical current [68, 71], with an effective spin-drift velocity proportional to the electrical current. This spin wave Doppler shift was experimentally observed by Vlaminck and Bailleul [72]. The spin-drift velocity, if large enough, can lead to instabilities in the ferromagnetic ground state [68, 70, 73]. For the existence of analogue horizons it is important to distinguish energetic and dynamic instabilities. Energetic instabilities are characterized by the existence of negative energy excitations, while dynamical instabilities lead to exponential growth of small amplitude excitations. Contrary to most physical systems, these instabilities do not necessarily coincide for spin waves in a ferromagnetic metal, due to dissipative spin-transfer torques [66]. We find that magnons – the quanta of spin waves – can be dynamically stable for a wide range of currents that make the ferromagnetic ground state energetically unstable.

In the context of analogue gravity, the magnonic event horizon is defined by the transition from a region of positive energy states to a region with dynamically stable negative energy states. For linearly dispersing sound waves, such as waves in water, the negative energy region corresponds to unidirectional movement of sound waves. In general, an event horizon is a region which couples positive energy states to negative energy states. For non-linearly dispersing sound waves one can still define the event horizon as the region that couples positive energy states and dynamically stable negative energy states. These generalized event horizons are referred to as dispersive horizons [74].

The ferromagnetic thin film set-up we consider in this Chapter is similar to Ref. [65], but treated more generally, including effects of surface- and volume anisotropies, Dzyaloshinskii-Moriya interaction, dipole-dipole interactions and finite thickness of the thin film. We find that the current density needed to create energetically unstable, but dynamically stable, states is of the order $j \gtrsim (1 - D/D_c)10^{13}\text{A/m}^2$ for typical thin film experiments, with D the

Dzyaloshinskii-Moriya constant, and D_c the Dzyaloshinskii-Moriya interaction that is required for spontaneous formation of spirals or skyrmions. The critical current density can be made arbitrarily small for thin film thicknesses at the order of a nanometer. This decrease is primarily due to the effects of surface anisotropy and interfacial Dzyaloshinskii-Moriya interaction.

The remainder of this Chapter is organized as follows. We put forward our model and discuss spin wave solutions in Section 2.2. Furthermore, the critical current needed for energetic instabilities to exist and the region of dynamical stability are derived in Section 2.3. Additionally, we derive the critical thickness at which the ferromagnetic ground state becomes unstable due to surface and interfacial effects in Section 2.A. A derivation of the lowest energy dipole-exchange spin wave mode is presented in Section 2.B. We conclude with a discussion and outlook.

2.2 METALLIC THIN FILM FERROMAGNET

2.2.1 *Model and set-up*

We consider a ferromagnetic metallic thin film of thickness L in the z direction with the surfaces corresponding to $z = \pm L/2$. We consider the set-up in Fig. 3.1 that involves a thin film subject to a static external field \mathbf{H}_e applied in the y direction and a uniform charge current \mathbf{j} pointing in the $-x$ direction. For temperatures far below the Curie temperature, amplitude fluctuations in the magnetization are negligible. In this case the dynamics of the magnetization direction $\mathbf{n} = \mathbf{M}/M_s$ is described by the Landau-Lifschitz-Gilbert (LLG) equation, with spin-transfer torques (STTs), and Maxwell's equations in the magnetostatic limit. The LLG equation with STTs is given by [66]

$$(\partial_t + \mathbf{v}_s \cdot \nabla) \mathbf{n} = -\gamma \mathbf{n} \times \mathbf{H}_{\text{eff}} + \alpha \mathbf{n} \times \left(\partial_t + \frac{\beta}{\alpha} \mathbf{v}_s \cdot \nabla \right) \mathbf{n}, \quad (2.1)$$

provided that spin-orbit coupling is not very strong so that spin-orbit torques are negligible. Inclusion of spin-orbit torques in our discussion is straightforward.

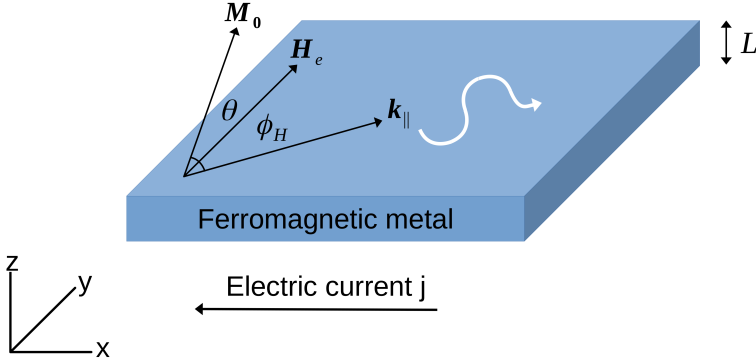


Figure 2.1: Sketch of the set-up. We consider a metallic ferromagnetic thin film of thickness L which is subjected to an external magnetic field \mathbf{H}_e pointing in the y direction and an electric current driven along the x direction. Furthermore, θ is the angle of the steady state magnetisation \mathbf{M}_0 with the plane and ϕ_H is the angle between the spin wave propagation direction and the y axis.

ward but omitted here to reduce the number of parameters. In the above equation, the adiabatic spin-transfer torque is parametrized by the velocity $\mathbf{v}_s = -gP\mu_B\mathbf{j}/2eM_s$ that is referred to as spin-drift velocity, which is proportional to the current density \mathbf{j} . Here g is the Landé factor, μ_B the Bohr magneton, e the elementary charge, P the spin polarization of the current and M_s the saturation magnetization. The LLG equation describes damped precession of the magnetization around the effective field $\mathbf{H}_{\text{eff}} = -\delta E/(M_s\delta\mathbf{n})$. Here, $E[\mathbf{n}]$ is the magnetic energy functional, which we consider to be of the general form

$$E = M_s \int dV \left\{ \frac{1}{2} J (\nabla_i \mathbf{n})^2 - \mu_0 \mathbf{H} \cdot \mathbf{n} - \frac{1}{2} K_v n_z^2 - \frac{1}{2} D [\hat{y} \cdot (\mathbf{n} \times \partial_x \mathbf{n}) - \hat{x} \cdot (\mathbf{n} \times \partial_y \mathbf{n})] \right\}. \quad (2.2)$$

In the above J is the spin stiffness, D the Dzyaloshinskii-Moriya interaction (DMI) constant that in this particular set-up may result from interfacing the magnet with a heavy metal, and K_v is the volume anisotropy constant – this type of anisotropy is e.g. typical in the Co layer spin wave spectroscopy

experiments in Ref. [75]. The dimensionless parameters α and β characterise the strength of the Gilbert damping parameter and the non-adiabatic spin-transfer torques, respectively. Usually these dissipative constants are comparable, $\alpha \sim \beta$, and of the order 10^{-2} [58]. For now, we neglect surface anisotropy in the energy functional, which we discuss in Section 2.B. Additionally, dipole-dipole interactions are taken into account by considering the magnetostatic Maxwell's equations [76]

$$\nabla \times \mathbf{H} = \mathbf{j}, \quad \nabla \cdot \mathbf{B} = 0. \quad (2.3)$$

Here \mathbf{H} is the magnetic field strength and $\mathbf{B} = \mu_0(\mathbf{H} + \mathbf{M})$ the total magnetic field. In the steady state, the internal magnetic field \mathbf{H}_0 and the magnetization \mathbf{M}_0 are parallel. For an external magnetic field pointing in the y direction with, $jL \ll 2H_e$, the internal magnetic field and magnetization are related to the external magnetic field by

$$\mu_0 j z \sin(\theta) \simeq (\mu_0 M_s - K_v) \sin(2\theta)/2 + \mu_0 H_e \sin(\theta), \quad (2.4)$$

with θ the angle between the magnetization direction and the $x - y$ plane. We find that the steady state magnetization points along the y axis if $K_v < \mu_0(H_e + M_s - jL/2)$. While the steady state magnetization deviates from the y axis if $K_v > \mu_0(H_e + M_s - jL/2)$, where it acquires a component in the z direction. From this point onward we assume $K_v < \mu_0(H_e + M_s - jL/2)$ such that the steady state magnetization is pointing in the y direction. Experimentally, this may be achieved by applying a sufficiently large external magnetic field.

2.2.2 Dipole-exchange spin wave modes

The dipole-exchange spin wave modes [75, 77–84] are generated by dynamical fluctuations of both the magnetization direction and the demagnetizing field, which are small compared to \mathbf{M}_0 and \mathbf{H}_0 ,

$$\mathbf{M} = \mathbf{M}_0 + \mathbf{m}(t), \quad \mathbf{H} = \mathbf{H}_0 + \mathbf{h}_D(t). \quad (2.5)$$

Notice that up to linear order in the dynamical fluctuations, \mathbf{m} is perpendicular to \mathbf{M}_0 , lying in the $x - z$ plane since we consider the magnitude of the magnetization to be constant $|\mathbf{M}| = M_s$. Both the static and dynamic part of the magnetization and magnetic field strength should satisfy the magnetostatic Maxwell equations (2.3). We accordingly require $\nabla \times \mathbf{h}_D = 0$, $\nabla \cdot \mathbf{b} = 0$, with $\mathbf{b} = \mu_0 (\mathbf{h}_D + \mathbf{m})$. The first Maxwell equation allows us to write the dynamic demagnetizing field in terms of a scalar potential $\mathbf{h}_D = \nabla \Phi_D$. The second Maxwell equation accordingly gives $\nabla^2 \Phi_D = -\nabla \cdot \mathbf{m}$, where the magnetization \mathbf{m} outside the film is zero. The Landau-Lifschitz-Gilbert- and magnetostatic Maxwell equations may be rewritten by means of $\mathbf{n} \simeq \hat{z} \sqrt{2} \text{Re}[\Psi] + \hat{x} \sqrt{2} \text{Im}[\Psi] + \hat{y} (1 - |\Psi|^2)$, with the complex field $\Psi = (1/\sqrt{2}) (\hat{z} + i\hat{x}) \cdot \mathbf{n}$. In these coordinates the linearised LLG and magnetostatic Maxwell equations become

$$\hat{\Omega} \Psi = - (\Omega_H - \Delta_v - \Lambda^2 \nabla^2) \Psi + \Delta_v \Psi^* + \frac{(\partial_z + i\partial_x) \Phi_D}{\sqrt{2} M_s}, \quad (2.6a)$$

$$\frac{\nabla^2 \Phi_D}{M_s^2} = - \frac{(\partial_z - i\partial_x) \Psi}{\sqrt{2} M_s} - \frac{(\partial_z + i\partial_x) \Psi^*}{\sqrt{2} M_s}. \quad (2.6b)$$

Additionally, the exchange boundary conditions for thin films [85] require

$$\pm \partial_z \Psi - (K_s/J) (\Psi + \Psi^*) \Big|_{z=\pm L/2} = 0, \quad (2.7)$$

with K_s the surface anisotropy constant. In the above, we defined the following dimensionless operators and variables ¹: dimensionless magnetic field $\Omega_H = \mu_0 H_e / \mu_0 M_s$, dimensionless volume anisotropy $\Delta_v = K_v / 2\mu_0 M_s$, exchange length $\Lambda = \sqrt{J/\mu_0 M_s}$ and the dimensionless frequency operator $\hat{\Omega} = i[(1 - i\alpha)\partial_t + (1 - i\beta)\mathbf{v}_s \cdot \nabla + \gamma D\partial_x]/(\gamma\mu_0 M_s)$.

Using the Bogoliubov ansatz, and taking \mathbf{v}_s in the x direction, we write $\Psi(\mathbf{x}, t) = u(\mathbf{x})e^{-i\omega t} + v^*(\mathbf{x})e^{i\omega^* t}$ and $\Phi_D(\mathbf{x}, t) = w(\mathbf{x})e^{-i\omega t} + w^*(\mathbf{x})e^{i\omega^* t}$, where $(u(\mathbf{x}), v(\mathbf{x}), w(\mathbf{x})) \propto e^{i\mathbf{k} \cdot \mathbf{r}_{\parallel}} (u(\mathbf{k}, z), v(\mathbf{k}, z), w(\mathbf{k}, z))$, with $\mathbf{k} = (k_x, k_y)$ and $\mathbf{r}_{\parallel} = (x, y)$. The above plane wave ansatz gives rise to a spectrum of spin wave solutions. The lowest energy dipole-exchange spin wave dispersion relation is obtained in Section 2.B for thin films with thicknesses comparable to the

¹ We neglected the contribution of the driving current \mathbf{j} to the magnetic field \mathbf{H} in Ω_H .

exchange length $L \sim \mathcal{O}(\Lambda)$. Up to linear order in α and β the lowest energy dipole-exchange spin wave dispersion relation is given by

$$(\omega_{\mathbf{k}} - v_s k_x) \simeq \omega_{\mathbf{k}}^0 - i\kappa\alpha\omega_{\mathbf{k}}^0 - i\kappa(\alpha - \beta)v_s k_x, \quad (2.8)$$

where

$$\begin{aligned} (\omega_{\mathbf{k}}^0 - \gamma D k_x) / (\gamma \mu_0 M_s) = & \quad (2.9) \\ \sqrt{[\Omega_H - \Delta + \Lambda^2 k^2 - 1/2 \cos^2(\phi_H) f(k)]^2 - [\Delta + 1/2 \{1 + \sin^2(\phi_H)\} f(k)]^2}, \end{aligned}$$

is the real part of the dispersion in the absence of an electrical current, which is plotted in Fig. 2.2. Here, $f(k) = 1 - (1 - e^{-kL})/kL$ is the form factor, ϕ_H the angle between the spin wave propagation direction and the y axis and $\Delta \equiv \Delta_v + \Delta_s - 1/2$, with $\Delta_s = (\Lambda/\mu_0 M_s L) K_s$ the dimensionless parameter corresponding to the sum of surface anisotropies [80, 85]. In the above, κ is an overall factor of the imaginary part of the dispersion relation, stemming from the fact that the isotropic Gilbert damping only enters in the diagonal part of Eq. (3.5a). This term is not of importance for the stability analyses, since it remains positive in the region of interest. The precise form of κ can be found in Section 2.B.

2.3 ENERGETIC AND DYNAMICAL SPIN WAVE INSTABILITIES

Motivated by theoretical predictions of magnonic black/white-hole horizons [31] and black-holes lasers [41, 65], we investigate energetic and dynamic instabilities in the spin wave spectrum, due to a spin-polarized electrical current [68], including effects of dipole-dipole interactions, volume- and surface anisotropies, and DMI. A negative real part of the spin wave dispersion relation, Eq. (2.8), indicates energetic instabilities, necessary for analogue black/white-hole setups [27–29]. Dynamical instabilities on the other hand are characterized by a positive imaginary part of the spin wave dispersion relation and classically lead to an exponential growth of unstable modes. In contrast to most physical systems, these two types of instabilities do not necessarily coincide for the magnetization dynamics in a metallic magnetic system, due

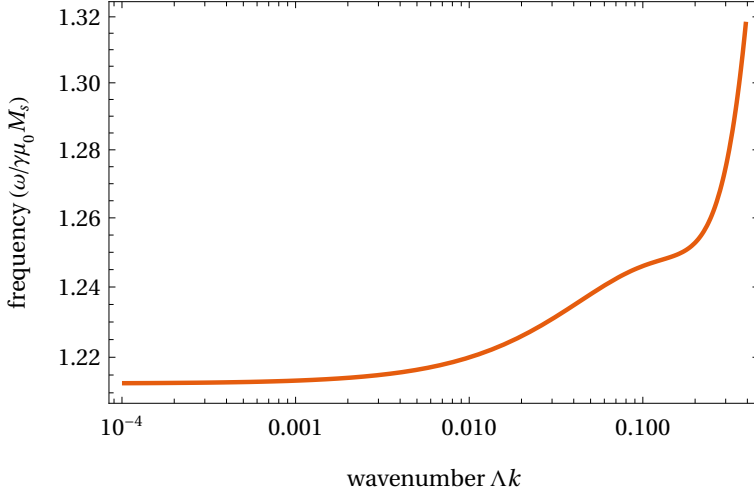


Figure 2.2: Dispersion relation (2.9) of the lowest energy spin wave mode including dipolar interactions and anisotropy. Here, we consider $\Omega_H = 1$, $D/\mu_0 M_s = 0$, $\Delta = -0.25$, $L \sim 40\text{nm}$ and $\phi_H = \pi/2$.

to the dissipative spin-transfer torques characterised by the parameter β . Accordingly, we investigate the regime in which the system is energetically unstable, but dynamically stable, see Fig. 2.3. From Eq. (2.8) we find that the system is dynamically stable if

$$|(\alpha - \beta)v_s k_x + \alpha \gamma D k_x| < \alpha(\gamma \mu_0 M_s) \Omega_{\mathbf{k}} \quad (2.10)$$

is satisfied for all \mathbf{k} , with $\gamma \mu_0 M_s \Omega_{\mathbf{k}} = \omega_{\mathbf{k}}^0 - \gamma D k_x$ the inversion symmetric part of the dispersion relation (2.9). Energetic instabilities on the other hand are present if $\text{Re} \omega_{\mathbf{k}} < 0$, for some \mathbf{k} . By considering minima of the dispersion relation we find the critical current above which energetic instabilities exist should satisfy $\partial_{k_c} \text{Re} \omega_{k_c}|_{v_s=v_c} = 0$ and $\text{Re} \omega_{k_c}|_{v_s=v_c} = 0$, for some k_c . Thus, energetic instabilities are present for currents $v_s > v_c$ and do not exist for $v_s < v_c$, which characterises the critical velocity v_c . The above constraints that determine the critical current are equivalent to

$$\partial_{k_c} \Omega_{k_c}^2 = 2\Omega_{k_c}^2/k_c, \quad (2.11a)$$

$$v_c/\gamma = [\mu_0 M_s / \sin(\phi_H)] \Omega_{k_c} / k_c - D. \quad (2.11b)$$

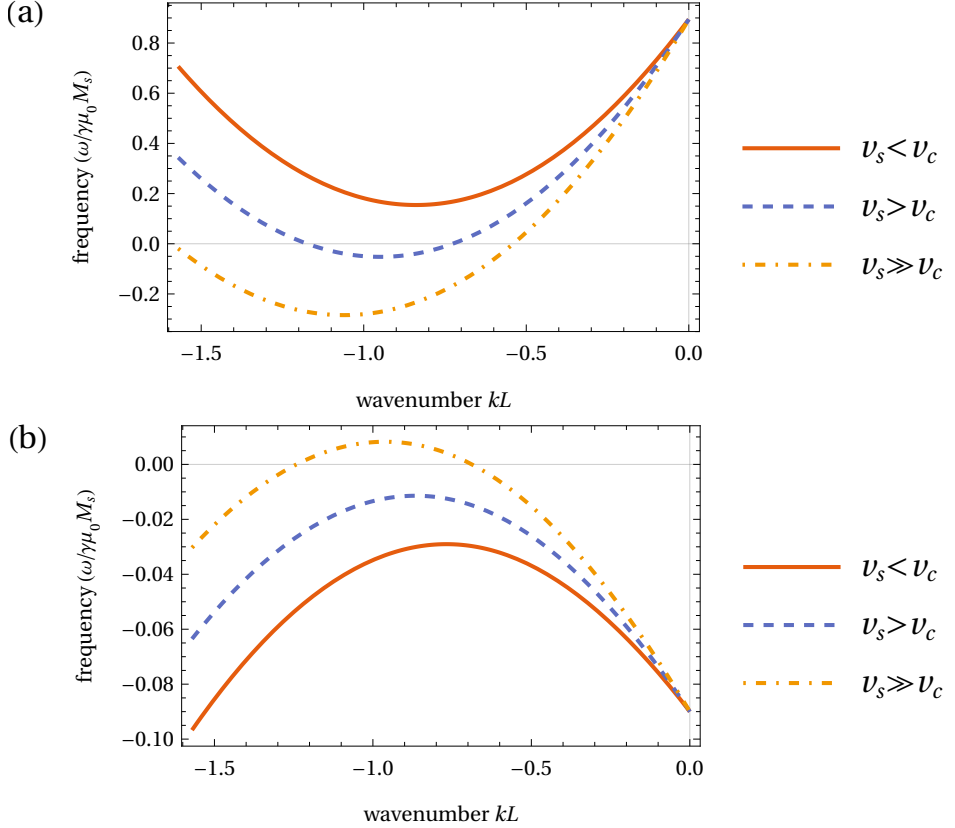


Figure 2.3: Dispersion relation (2.8) for different values of the spin drift-velocity v_s , with $\alpha = 0.1$ and $\beta = 0.01$. (a) Real part of the dispersion relation. (b) Imaginary part of the dispersion relation. For small $v_s < v_c$, spin waves are energetically and dynamically stable (red). For spin drift-velocities larger than the critical velocity, $v_s > v_c$, we obtain energetically unstable but dynamically stable spin waves (blue). For very large $v_s \gg v_c$ spin waves are both energetically and dynamically unstable (yellow).

For spin waves travelling perpendicular to the external magnetic field, $\phi_H = \pi/2$ in Eq. (2.9), the constraint in Eq. (2.11a) is explicitly written as

$$[\Omega_H - \Delta]^2 - \Lambda^4 k_c^4 \sim [\Delta + f(k_c)] [\Delta + f(k_c)^2], \quad (2.12)$$

where we used $f(k) - kf'(k) \sim f(k)^2$. We note that $f(k) \in [0, 1]$ and typically $\Delta = \Delta_v + \Delta_s - 1/2 \gtrsim -1/2$ with $\Omega_H \sim 1$. Accordingly, we assume $[\Delta + f(k_c)][\Delta + f(k_c)^2]/[\Omega_H - \Delta]^2$ to be small compared to unity around the critical wavelength k_c . Next, we expand $k_c^2 = \kappa_c^2 + \delta k_c^2$ around $\Lambda^2 \kappa_c^2 = \Omega_H - \Delta$, up to linear order in δk_c^2 and $[\Delta + f(k_c)][\Delta + f(k_c)^2]/[\Omega_H - \Delta]^2$ in Eq. (2.12). This gives

$$\Lambda^2 \delta k_c^2 \sim -\frac{1}{2} \frac{[\Delta + f(\kappa_c)] [\Delta + f(\kappa_c)^2]}{\Omega_H - \Delta}. \quad (2.13)$$

Similarly, we find that Ω_{k_c} , up to first order in δk_c^2 and $[\Delta + f(k_c)]^2/[\Omega_H - \Delta]^2$, is given by

$$\Omega_{k_c} \sim 2[\Omega_H - \Delta] + \Lambda^2 \delta k_c^2 - \frac{1}{4} \frac{[\Delta + f(\kappa_c)]^2}{\Omega_H - \Delta}. \quad (2.14)$$

Finally, using Eq. (2.11b) we find that the critical current that generates energetic instabilities is up to linear order in δk_c^2 and $[\Delta + f(k_c)]^2/[\Omega_H - \Delta]^2$ given by

$$v_c/\gamma\mu_0 M_s \simeq \left(\frac{\Omega_{k_c}}{\kappa_c} \right) \left(1 - \frac{1}{2} \frac{\delta k_c^2}{\kappa_c^2} \right) - D/\mu_0 M_s. \quad (2.15)$$

This can be rewritten as

$$v_c = \gamma(D_c - D), \quad (2.16)$$

where

$$D_c/2\mu_0 M_s \Lambda \simeq \sqrt[4]{[\Omega_H - \Delta]^2 - (1/2) [\Delta + f(\kappa_c)]^2} \quad (2.17)$$

is the critical DMI constant above which the ground state becomes both energetically and dynamically unstable. Once DMI reaches this value, the homogeneous ground state becomes unstable. This results in the spontaneous

formation of textures, typically spirals and skyrmions. Additionally, we note that the contribution of δk_c^2 drops out of the critical DMI, up to first order.

Finally, we find from Eq. (2.10) that the region in which electrical currents generate energetically unstable but dynamically stable spin waves is given by

$$\begin{cases} \gamma(D_c - D) < v_s < \gamma(D_c - D)|1 - \beta/\alpha|^{-1} & \beta < \alpha, \\ \gamma(D_c - D) < v_s < \gamma(D_c + D)|1 - \beta/\alpha|^{-1} & \beta > \alpha. \end{cases} \quad (2.18)$$

This provides a large window of stability, given that usually $\alpha \sim \beta$. We note that this region is determined by solely considering spin waves travelling along the x axis – perpendicular to the external magnetic field. This is a consequence of the fact that the critical current for energetic and dynamic instabilities increases as spin waves travel at increasing angles $|\phi_H - \pi/2|$ with respect to the x axis. In Fig. 2.4, we plotted the angular dependence of the critical current. Additionally, in the case where $\beta/\alpha > 2$ it is possible to have dynamically unstable but energetically stable states. This occurs when the right hand side of Eq. (2.18) becomes smaller than the left hand side. As a consequence, the DMI should be at least $D > D_c(1 - 2\alpha/\beta)$ for energetically unstable, but dynamically stable states to exist in the region where $\beta/\alpha > 2$. Therefore, dynamically stable negative energy states are difficult to create in materials when $\beta \gg \alpha$. For instance in Ref. [86] a value of $\beta \sim 5\alpha$ was found.

Taking typical values for the saturation magnetization $\mu_0 M_s \sim \mu_0 H_e \sim 1$ T, gyromagnetic ratio $\gamma/2\pi \sim 30\text{GHz T}^{-1}$ and exchange length $\Lambda = \sqrt{J/\mu_0 M_s} \sim 5$ nm, we find the typical order of magnitude of the critical current $j_c \sim M_s |e| v_c / \mu_b \sim 10^{13}$ A/m², where we took $g \sim P \sim 1$, $M_s/\mu_B \sim 10^2$ nm⁻³ and $v_c \sim \gamma \mu_0 M_s \Lambda \sim 10^3$ m/s. Furthermore, for typical values of DMI $DL/\mu_0 M_s \Lambda^2 \sim 0.1$ [75, 87, 88], anisotropies $\Delta_v = K_v/2\mu_0 M_s \sim 0.2$ and $\Delta_s L/\Lambda = K_s/\mu_0 M_s \Lambda \sim 0.4$ [75, 80], we find the critical current that is needed to create energetic instabilities, given in Eq. (2.16), is significantly reduced in thin films having thicknesses of a few nanometers, as is shown in Fig. 2.5. This reduction of the critical current is primarily due to the cumulative effect of DMI and surface anisotropies, which become prominent

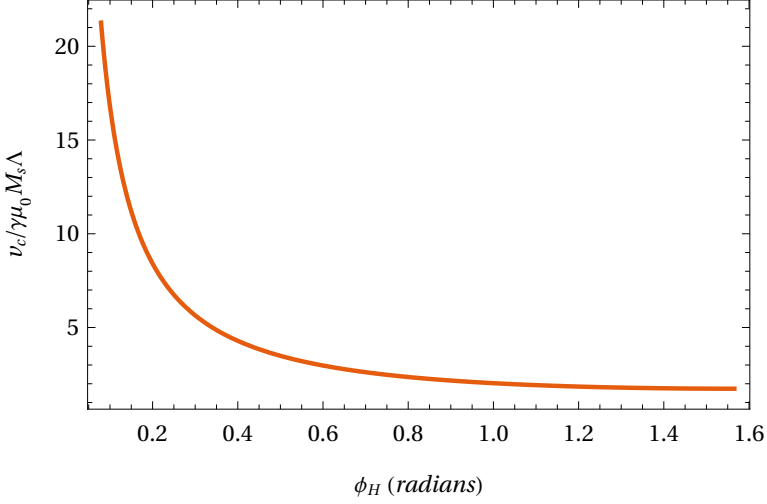


Figure 2.4: Numeric solution of the dimensionless critical velocity $v_c/\gamma\mu_0M_s\Lambda$ in Eq. (2.11) – for dispersion relation (2.9) – against the angle ϕ_H in radians. We took the typical values $\Omega_H \sim 1$, $DL/\mu_0M_s\Lambda \sim 0.1$, $\Delta_v = K_v/2\mu_0M_s \sim 0.2$, $\Delta_sL = K_s/\mu_0M_s\Lambda \sim 0.4$ and $L/\Lambda = 3$.

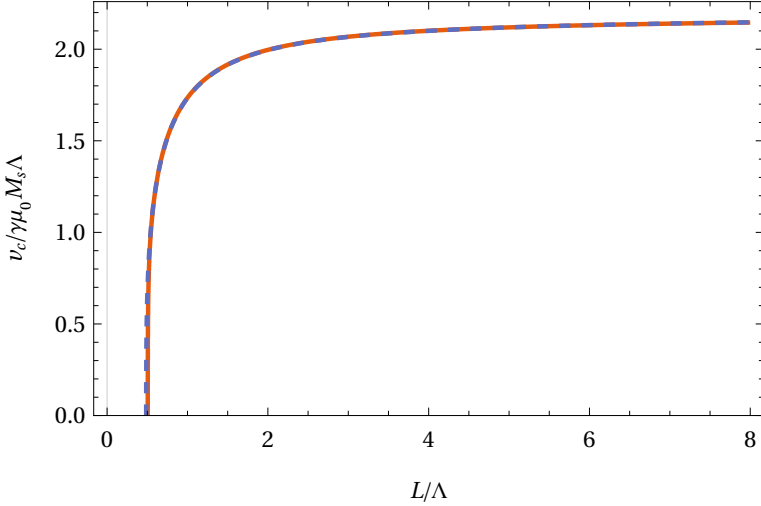


Figure 2.5: Dimensionless critical velocity $v_c/\gamma\mu_0M_s\Lambda$ against dimensionless thickness L/Λ , taking typical values $\Omega_H \sim 1$, $DL/\mu_0M_s\Lambda^2 \sim 0.1$, $\Delta_v = K_v/2\mu_0M_s \sim 0.2$, $\Delta_sL/\Lambda = K_s/\mu_0M_s\Lambda \sim 0.4$. The dashed line corresponds to the linear approximation in Eq. (2.16) and the solid line corresponds to the numerically obtained solution of Eq. (2.11) with dispersion relation (2.9).

in ultrathin films as a consequence of their inverse scaling with respect to the thickness of the thin film.

2.4 DISCUSSION AND OUTLOOK

We have investigated the occurrence of energetically unstable but dynamically stable spin wave excitations, due to spin-transfer torques, including effects of dipole-dipole interactions, anisotropies and DMI. We have shown that in typical thin film experiments [72, 75, 80], the critical current needed to create energetically unstable, but dynamically stable states is of the order $j \gtrsim (1 - D/D_c)10^{13} \text{ A/m}^2$. If one could experimentally enhance the DMI to be near the critical DMI, above which the homogeneous ground state becomes unstable towards the formation of textures, such as spirals and skyrmions, then a relatively small current should be sufficient to create the dynamically stable negative energy states. Additionally, we found that the critical current density becomes arbitrarily small for thin film thicknesses of the order of nanometers. This decrease is primarily due to the cumulative effect of DMI and surface anisotropies, which become dominant in ultrathin films.

Furthermore, the region in which dynamically stable negative energy spin wave excitations exist is found to be large, given that typically $\alpha \sim \beta$. In the case where $\beta \gg \alpha$ we note that energetically stable, dynamically unstable states could occur. Hence, dynamically stable negative energy states are difficult to create in materials when $\beta \gg \alpha$.

For the typical values considered in Section 2.3, we see a slight deviation of the first order critical velocity with respect to the numerical critical velocity at ultrathin film thicknesses, see Fig. 2.5. This is due to the surface anisotropy contribution becoming larger in the ultrathin film limit, where the increased inaccuracy stems from the fact that we determine the critical velocity in Eq. (2.16) up to first order assuming $[\Delta + f(k_c)][\Delta + f(k_c)^2]$ and $[\Delta + f(k_c)]^2/2$ to be small compared to $[\Omega_H - \Delta]^2$. This approximation is accurate when anisotropies are small compared to the external magnetic field, but describes the critical velocity less accurately when anisotropies become relatively large – especially volume anisotropy – approaching $2\Delta_v \lesssim \Omega_H + 1$.

Additionally, the critical momentum k_c becomes small for ultrathin film thicknesses – if surface anisotropies are dominating –, which makes the expansion of $1/k_c$ less accurate in this range. When dealing with relatively large anisotropies, it is more appropriate to expand the k_c^2 around $\kappa_c^2 = \sqrt{[\Omega_H - \Delta]^2 - [\Delta_v + \Delta_s]^2}$ in Eq. (2.12). In this case the critical DMI constant is given by $(D_c/\sqrt{2}\mu_0 M_s) \simeq \sqrt{(\Omega_H - \Delta + \kappa_c^2)^2 - \tilde{f}(\Delta_v + \Delta_s + \tilde{f})/\kappa_c^2}$, with $\tilde{f} = f(\kappa_c) - 1/2$.

Finally, energetically unstable, dynamically stable excitations are necessary to create analogue black/white-holes with spin waves [27–29, 31]. Furthermore, the combination of a black- and white-hole horizon is predicted to amplify spin waves of specific frequencies, giving rise to a spin-wave laser/amplifier [41, 65]. Future research could investigate energetic and dynamic instabilities in antiferromagnetic metals. Additionally, this model could be used to compute the resonance frequencies of the spin-wave laser in Ref. [65] more realistically. Moreover, one could investigate non-linear effects in such a setup, since non-linear effects quickly become important around the resonance frequencies. The non-linear regime could be investigated by means of the stochastic Landau-Lifschitz-Gilbert equation.

APPENDIX

2.A CRITICAL THICKNESS OF ENERGETIC INSTABILITIES AT ZERO CURRENT

In this Appendix, we determine the critical thickness at which spin wave excitations become energetically unstable at zero electrical current. These energetic instabilities are due the increase in magnitude of surface anisotropies and DMI in the ultra thin film limit and are dynamically unstable by Eq. (2.10). Additionally, the range of electrical currents that generate energetically unstable but dynamically stable spin wave excitations decreases when approaching the critical thickness. This is a direct consequence of decreasing the critical current, see Section 2.3. If surface anisotropies are dominant at small thick-

nesses, the critical thickness at which instabilities appear, at zero current and vanishing DMI, may be approximated at zero'th order by closing the spin-wave gap in Eq. (2.9), giving

$$\Omega_H - 2\Delta_0 \equiv \Omega_H + 1 - 2\Delta_v - 2\Delta_s^*/L_0 \sim 0, \quad (2.19)$$

with $k_c L \ll 1$ and $\Delta_s^* = \Delta_s L$ constant. For non-vanishing DMI, up to first order in $f(\kappa_c) \sim \kappa_c L/2 \ll 1$, we find that Eq. (2.11) is equivalent to

$$[\Omega_H - \Delta]^2 \sim [\Delta + f(k_c)] \Delta, \quad (2.20)$$

$$k_c [2(\Omega_H - \Delta) - (D^*/L)^2] \sim [\Delta + f(k_c)] f'(k_c), \quad (2.21)$$

where $D^* = (D/\mu_0 M_s \Lambda) L$ is constant. We expand the above equations around $\Delta = \Delta_0 + \delta\Delta$, with $\delta\Delta = -(\Delta_s^*/L_0^2)\delta L + \mathcal{O}(\delta L^2)$. Up to first order Eq. (2.20) gives

$$k_c L_0/2 \sim -4\delta\Delta. \quad (2.22)$$

We find that Eq. (2.21) in combination with the above equation leads to

$$\delta L \sim \frac{\Omega_H L_0^2}{32\Delta_s^*} \left/ \left\{ \Omega_H \left[\frac{1}{L_0^2} + \frac{1}{6} - \frac{L_0}{32\Delta_s^*} \right] - \frac{3}{16} - \left(\frac{D^*}{L_0^2} \right)^2 \right\} \right., \quad (2.23)$$

with $L_0 = 2\Delta_s^*/(2\Omega_H + 1 - 2\Delta_v)$ given by Eq. (2.19). We thus find that the critical thickness for spin wave instabilities is given by $L \sim L_0 + \delta L$, in the case that surface anisotropies dominate in the ultrathin film.

2.B APPROXIMATE DIPOLE-EXCHANGE MODE IN THIN FILMS

Here, we discuss an analytic approximation of the lowest energy spin wave dispersion relation for the setup discussed in Section 2.2, using the thin film magnetostatic Greens function [79, 80, 83, 84, 89]. We start by expressing the demagnetizing field \mathbf{h}_D in Eqs. (2.5), (3.5a) and (3.5b) in terms of the magnetization by using the magnetostatic Greens function. It is explicitly given by

$$\mathbf{h}_D(\mathbf{k}, z) = \int_{-L/2}^{L/2} dz' \mathbf{G}(\mathbf{k}; z - z') \mathbf{m}(\mathbf{k}; z'). \quad (2.24)$$

Where the magnetostatic Greens function [83, 89] satisfies the magnetostatic Maxwell equation Eq. (3.5b) along with the appropriate boundary conditions [49]. It is explicitly given by,

$$G_{\hat{\zeta}\hat{\eta}\hat{z}}(k; z, z') = \begin{pmatrix} -G_p & 0 & iG_q \\ 0 & 0 & 0 \\ iG_q & 0 & G_p - \delta(z - z') \end{pmatrix}, \quad (2.25)$$

with $\hat{\zeta} \propto \mathbf{k}$ the in-plane direction of spin wave propagation, $\hat{\eta}$ the orthogonal in-plane direction, \hat{z} the thickness direction, $G_p = \frac{|k|}{2} \exp(-|k||z - z'|)$ and $G_q = G_p \text{sign}(z - z')$. By substituting Eq. (2.24) into the linearised Landau-Lifschitz-Gilbert equation Eq. (3.5a) we obtain the effective linearised LLG equation

$$\hat{\Omega}\Psi = - [\Omega_H - \Delta_{v/s} - \Lambda^2 \nabla^2] \Psi + \Delta_{v/s} \Psi^* + \int_{-L/2}^{L/2} \frac{1}{2} [A_k \Psi_k + B_k \Psi_{-k}^*] dz', \quad (2.26)$$

where $A_k = \cos^2(\phi_H)G_p - \delta(z - z')$, $B_k = \{1 + \sin^2(\phi_H)\}G_p - 2 \sin(\phi_H)G_q - \delta(z - z')$ and ϕ_H the angle between wave vector \mathbf{k} and the y axis. Additionally we introduced the dimensionless anisotropy constant $\Delta_{v/s} = K_{v/s}/2\mu_0 M_s$, where we took $K_{v/s} = K_v + K_s^- \delta(z - L/2) + K_s^+ \delta(z + L/2)$. Here K_s correspond to the surface anisotropies of the thin film. Following Gladii *et al.* [80] we add the term $(K_s^\pm/2)\delta(z \pm L/2)n_z^2$ in the energy functional Eq. (4.2) to account for surface anisotropies. This differs from the approach used by Kalinikos and Slavin [84] where surface anisotropies determine the exchange boundary conditions of the thin film [85].

Using the Bogoliubov ansatz $\Psi(\mathbf{x}, t) = u(\mathbf{x})e^{-i\omega t} + v^*(\mathbf{x})e^{i\omega^* t}$, with $(u(\mathbf{x}), v(\mathbf{x})) = \int \frac{d^2\mathbf{k}}{2\pi} e^{i\mathbf{k}\cdot\mathbf{r}\parallel} (u(\mathbf{k}, z), v(\mathbf{k}, z))$, the linearised LLG equation becomes

$$\begin{pmatrix} \hat{F} + 1/2 & 1/2 - \Delta_{v/s} \\ \Delta_{v/s} - 1/2 & -\hat{F}^* - 1/2 \end{pmatrix} \begin{pmatrix} u(k, z) \\ v(k, z) \end{pmatrix} + \int_{-L/2}^{L/2} dz' \begin{pmatrix} -C(s) & D^+(s) \\ -D^-(s) & C(s) \end{pmatrix} \begin{pmatrix} u(k, z') \\ v(k, z') \end{pmatrix} = 0, \quad (2.27)$$

with $s = z - z'$, $\hat{F} = \Omega + (\Omega_H - \Delta_v + \Lambda^2 k^2 - \Lambda^2 \partial_z^2)$, $\hat{F}^* = -\Omega^* + (\Omega_H - \Delta_v + \Lambda^2 k^2 - \Lambda^2 \partial_z^2)$, $C(s) = (1/2) \cos^2(\phi_\zeta) G_p$ and $D^\pm(s) = -(1/2) \{1 + \sin^2(\phi_\zeta)\} G_p \pm |\sin(\phi_\zeta)| G_q$. Furthermore, $\gamma \mu_0 M_s \Omega = (1 + i\alpha)\omega + (1 + i\beta)v_s k_x + \gamma D k_x$ and $\gamma \mu_0 M_s \Omega^* = (1 - i\alpha)\omega + (1 - i\beta)v_s k_x + \gamma D k_x$.

The magnetization profile in the thickness direction may be expanded in eigenfunctions of the unpinned exchange boundary conditions, which form a complete basis [83]. We approximate the magnetization profile of the lowest mode by the lowest Fourier mode, for thicknesses of the order $L \sim \mathcal{O}(\Lambda)$,

$$\begin{pmatrix} u(k, z) \\ v(k, z) \end{pmatrix} \sim u^0(k) \sqrt{\frac{1}{L}} \begin{pmatrix} 1 \\ 0 \end{pmatrix} + v^0(k) \sqrt{\frac{1}{L}} \begin{pmatrix} 0 \\ 1 \end{pmatrix}, \quad (2.28)$$

which is the uniform mode approximation. Using the above ansatz the linearised LLG equation Eq. (2.27) becomes

$$\begin{pmatrix} \Omega + \Omega_d & -\Omega_i \\ \Omega_i & \Omega^* - \Omega_d \end{pmatrix} = 0, \quad (2.29)$$

where

$$\Omega_d = \Omega_H - \Delta + \Lambda^2 k^2 - 1/2 \cos^2(\phi_H) f(k), \quad (2.30a)$$

$$\Omega_i = \Delta + 1/2 \{1 + \sin^2(\phi_H)\} f(k). \quad (2.30b)$$

With $f(k) = 1 - (1 - e^{-kL})/kL$, $\Delta = \Delta_v + \Delta_s - 1/2$ and $\Delta_s = (\Lambda/2\mu_0 M_s L)(K_s^- + K_s^+)$. Hence, the lowest mode dispersion relation, up to first order in α and β , is given by

$$(\omega_{\mathbf{k}} - v_s k_x) \simeq \omega_{\mathbf{k}}^0 - i\kappa\alpha\omega_{\mathbf{k}}^0 - i\kappa(\alpha - \beta)v_s k_x, \quad (2.31)$$

with $(\omega_{\mathbf{k}}^0 - \gamma D k_x)^2 / (\gamma \mu_0 M_s)^2 = \Omega_{\mathbf{k}}^2$, $\kappa = (\Omega_d / \Omega_{\mathbf{k}})$ and

$$\begin{aligned} \Omega_{\mathbf{k}}^2 = & [\Omega_H - \Delta + \Lambda^2 k^2 - 1/2 \cos^2(\phi_H) f(k)]^2 \\ & - [\Delta + 1/2 \{1 + \sin^2(\phi_H)\} f(k)]^2. \end{aligned} \quad (2.32)$$

3

THEORY OF THE DIPOLE-EXCHANGE SPIN WAVE SPECTRUM IN FERROMAGNETIC FILMS WITH IN-PLANE MAGNETIZATION REVISITED

This Chapter is based on J. S. Harms and R. A. Duine, “Theory of the dipole-exchange spin wave spectrum in ferromagnetic films with in-plane magnetization revisited,” *Journal of Magnetism and Magnetic Materials* **557**, 169426 (2022). R.A.D. and J.S.H. conceived the project, J.S.H. performed the calculations and prepared the manuscript. All authors contributed to the manuscript.

We present a refinement of the widely accepted spin-wave spectrum that Kalinikos and Slavin [83, 84] computed for magnetic films with an in-plane magnetization. The spin wave spectrum that follows from the diagonal approximation in this theory becomes inaccurate for relatively thick films, as has already been noted by Kreisel *et al.* [77]. Rather than solving an integrodifferential equation which follows from the magnetostatic Green’s function, as done by Kalinikos and Slavin [83, 84], we impose the exchange and magnetostatic boundary conditions on bulk spin-wave solutions. This boundary problem has an accurate analytical solution which is quantitatively different from the commonly used diagonal theory [83, 84] for magnetic films.

3.1 INTRODUCTION

Dipole-exchange spin waves propagating in in-plane magnetized magnetic thin films have attracted a lot of attention in recent years, due to their potential

applications in magnonic devices [90]. Of special interest is the case in which spin waves travel perpendicular to the external magnetic field – in which case the spin wave velocity is the largest. As noted by Kreisel *et al.* [77] the spin wave spectrum that follows from the diagonal approximation in the commonly used theory [83, 84] is inaccurate in this case for relatively thick films. The inaccuracy stems from the diagonal approximation, and disappears when solving the system numerically with interband interactions. This approach on the other hand is not feasible for analytic approximations.

In this Chapter, we present an alternative analytic derivation of the dipole-exchange spin wave spectrum for this scenario. Rather than solving an integrodifferential equation following from the magnetostatic Green's functions as done by Kalinikos and Slavin [83, 84], we use an approach resembling that of Wolfram and DeWames [82] which previously had no analytical solution. A similar approach has been used by Sonin [91] to derive the spectrum of spin waves propagating parallel to an in-plane magnetic field for sufficiently large wave numbers. Moreover, Arias [92] used this approach to find the spin-wave dispersion numerically and presented a uniform mode solution in the ultrathin-film limit similar to the uniform mode solution in the diagonal approximation by Kalinikos and Slavin [83, 84]. Kalinikos and Slavin [83, 84] approximately solved the integrodifferential equations by assuming a superposition of magnetization profiles which satisfy the exchange boundary conditions but do not satisfy the bulk equations of motion. Here, however we impose both the exchange and magnetostatic boundary conditions on bulk spin wave solutions. This boundary problem turns out to have an accurate analytical solution – compared with the numerical spectrum – and is quantitatively different from the commonly used diagonal spin wave theory [83, 84] for relatively thick films.

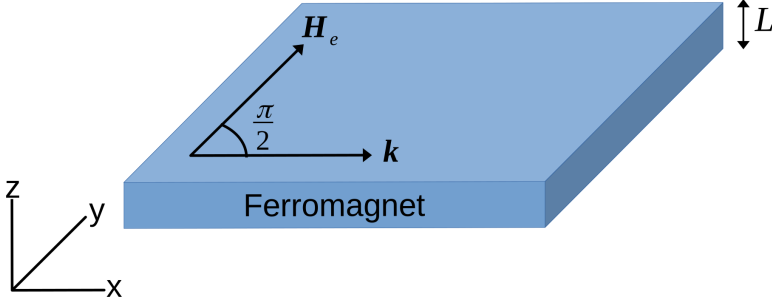


Figure 3.1: Sketch of the set-up. We consider a ferromagnetic thin film of thickness L with the equilibrium magnetization pointing in the y direction.

3.2 THIN-FILM FERROMAGNET

3.2.1 Model and set-up

We consider the set-up in Fig. 3.1 of a ferromagnetic thin film of thickness L subject to an in-plane external magnetic field \mathbf{H}_e . We chose the $x - y$ axes to correspond to the in-plane directions, with the external magnetic field $\mathbf{H}_e = H_e \hat{y}$ pointing in the y direction. Furthermore, the z axis corresponds to the out of plane direction where the surfaces of the thin film are located at $z = \pm L/2$. For temperatures below the Curie temperature, amplitude fluctuations in the magnetization are negligible. Hence, the dynamics of the magnetization direction $\mathbf{n} = \mathbf{M}/M_s$ is described by the Landau-Lifshitz equation (LL), and the Maxwell equations in the magnetostatic limit – accounting for dipole-dipole interactions. The LL equation is given by

$$\partial_t \mathbf{n} = -\gamma \mathbf{n} \times \mathbf{H}_{\text{eff}}, \quad (3.1)$$

which describes precession of the magnetization direction around the effective field $\mathbf{H}_{\text{eff}} = -\delta E / \delta(M_s \mathbf{n})$. Here, we consider the magnetic energy functional $E[\mathbf{n}]$ of the form

$$E[\mathbf{n}] = M_s \int dV \left[-\frac{1}{2} J \mathbf{n} \cdot \nabla^2 \mathbf{n} - \mu_0 \mathbf{H} \cdot \mathbf{n} \right]. \quad (3.2)$$

In the above J is the spin stiffness and $\mathbf{H} = \mathbf{H}_e + \mathbf{H}_D$ is the magnetic field strength, where \mathbf{H}_D is the demagnetization field originating from dipole-dipole interactions. Furthermore, the magnetostatic Maxwell equations [49] – accounting for dipole-dipole interactions – are given by

$$\nabla \times \mathbf{H} = 0, \nabla \cdot \mathbf{B} = 0, \quad (3.3)$$

with $\mathbf{B} = \mu_0(\mathbf{H} + \mathbf{M})$ the total magnetic field. The boundary conditions require the normal component of \mathbf{B} and the tangential components of \mathbf{H} to be continuous at the thin film surfaces.

In equilibrium the LL equation requires the equilibrium magnetization \mathbf{M}_{eq} and the effective magnetic field strength \mathbf{H}_{eff} to be parallel $\mathbf{M}_{\text{eq}} \parallel \mathbf{H}_{\text{eff}}$. In this case the internal magnetic field strength $\mathbf{H}_{\text{eq}} = \mathbf{H}_e + \mathbf{H}_D$ has a contribution from the external magnetic field \mathbf{H}_e and the demagnetization field $\mathbf{H}_D = -\hat{z}M_z$, originating from the magnetostatic boundary conditions. For an external magnetic field pointing in the y direction, as discussed in this Chapter, the uniform equilibrium magnetization \mathbf{M}_{eq} should also point in the y direction.

Dipole-exchange spin-wave modes are generated by dynamical fluctuations of the magnetization and the demagnetizing field around the magnetostatic equilibrium

$$\mathbf{M} = \mathbf{M}_{\text{eq}} + \mathbf{m}(t), \quad \mathbf{H} = \mathbf{H}_{\text{eq}} + \mathbf{h}_D(t), \quad (3.4)$$

where \mathbf{m} is perpendicular to \mathbf{M}_{eq} up to linear order in m_x and m_z , lying in the $x-z$ plane. The latter is a consequence of the magnitude of the magnetization being constant $|\mathbf{M}| = M_s$. Since the magnetostatic Maxwell equations (3.3) are linear we require $\nabla \times \mathbf{h}_D = 0$, $\nabla \cdot \mathbf{b} = 0$, with $\mathbf{b} = \mu_0(\mathbf{h}_D + \mathbf{m})$. Using that the dynamic demagnetizing field has vanishing curl, we express the dynamic demagnetization field in terms of a scalar potential $\mathbf{h}_D = \nabla\Phi_D$. Hence, the magnetostatic Maxwell equations become $\nabla^2\Phi_D = -\nabla \cdot \mathbf{m}$, where the magnetization outside the thin film vanishes.

The Landau-Lifschitz and magnetostatic Maxwell equations may be rewritten by means of $\mathbf{n} \simeq \hat{z}\sqrt{2}\text{Re}[\Psi] - \hat{x}\sqrt{2}\text{Im}[\Psi] + \hat{y}(1 - |\Psi|^2)$, with $\Psi =$

$(1/\sqrt{2})(\hat{z} - i\hat{x}) \cdot \mathbf{n}$. Consequently the linearised LL and magnetostatic Maxwell equations become

$$\hat{\Omega}\Psi = -(\Omega_H - \Lambda^2\nabla^2)\Psi + \frac{(\partial_z - i\partial_x)}{\sqrt{2}M_s}\Phi_D, \quad (3.5a)$$

$$\frac{\nabla^2\Phi_D}{M_s^2} = -\frac{(\partial_z + i\partial_x)}{\sqrt{2}M_s}\Psi - \frac{(\partial_z - i\partial_x)}{\sqrt{2}M_s}\Psi^*. \quad (3.5b)$$

Additionally, the exchange boundary conditions for thin films [85, 93] in the absence of surface anisotropy require

$$\pm\partial_z\Psi\Big|_{z=\pm L/2} = 0. \quad (3.6)$$

In the above, we defined the dimensionless magnetic field $\Omega_H = \mu_0 H_e / \mu_0 M_s$, exchange length $\Lambda = \sqrt{J/\mu_0 M_s}$ and the dimensionless frequency operator $\hat{\Omega} = i\partial_t / \gamma\mu_0 M_s$.

3.2.2 Bulk dipole-exchange spin-waves and it's boundary conditions

Using the Bogoliubov ansatz, we write $\Psi(\mathbf{x}, t) = u(\mathbf{x})e^{-i\omega t} + v^*(\mathbf{x})e^{i\omega t}$ and $\Phi_D(\mathbf{x}, t) = w(\mathbf{x})e^{-i\omega t} + w^*(\mathbf{x})e^{i\omega t}$, where $(u(\mathbf{x}), v(\mathbf{x}), w(\mathbf{x})) \propto e^{i\mathbf{k}\cdot\mathbf{r}\parallel}(u(\mathbf{k}, z), v(\mathbf{k}, z), w(\mathbf{k}, z))$, with $\mathbf{k} = (k_x \ k_y)$ and $\mathbf{x} = (x \ y \ z)$. In these coordinates the linearised LL and magnetostatic Maxwell equation Eq. (3.5) become

$$\mathcal{G} \cdot (u(\mathbf{k}, z) \ v(\mathbf{k}, z) \ w(\mathbf{k}, z)) = 0, \quad (3.7)$$

with

$$\mathcal{G} = \begin{pmatrix} -\sqrt{2}M_s F & 0 & (\partial_z + k_x) \\ 0 & -\sqrt{2}M_s F^* & (\partial_z - k_x) \\ \frac{M_s}{\sqrt{2}}(\partial_z - k_x) & \frac{M_s}{\sqrt{2}}(\partial_z + k_x) & (\partial_z^2 - k^2) \end{pmatrix}. \quad (3.8)$$

and $\hat{F} = \Omega + \Omega_h + \Lambda^2(k^2 - \partial_z^2)$, $\hat{F}^* = -\Omega + \Omega_h + \Lambda^2(k^2 - \partial_z^2)$ the dimensionless LL spin-wave operators and $\Omega = \omega / \gamma\mu_0 M_s$ the dimensionless frequency. Furthermore, $k^2 = k_x^2 + k_y^2$, which becomes $k^2 = k_x^2$ for spin waves travelling perpendicular to the external magnetic field. The above bulk equation of

motion gives rise to a sixth order homogeneous differential equation in position space, which is cubic with respect to ∂_z^2 . For spin waves travelling in the x direction, perpendicular to the external magnetic field, the general solution of Eq. (3.7) is given by the linear combination of plane waves

$$\begin{pmatrix} u(\mathbf{x}) \\ v(\mathbf{x}) \\ w(\mathbf{x}) \end{pmatrix} = \sum_{l=1}^6 C_{k_l} \begin{pmatrix} F_l^*(k_l + k_x)/\sqrt{2}M_s \\ F_l(k_l - k_x)/\sqrt{2}M_s \\ F_l^*F_l \end{pmatrix} e^{k_l z + i k_x x}, \quad (3.9)$$

where $F_l = \Omega + \Omega_h + \Lambda^2(k^2 - k_l^2)$ and $F_l^* = -\Omega + \Omega_h + \Lambda^2(k^2 - k_l^2)$. The wave numbers k_l satisfy the bulk equations of motion which follow from setting the determinant of Eq. (3.8) to zero

$$F_l^*F_l(k^2 - k_l^2) + (1/2)(F_l^* + F_l)(k_x^2 - k_l^2) = 0. \quad (3.10)$$

This is explicitly written as

$$(k^2 - k_l^2) \left\{ [\Omega_h + 1/2 + \Lambda^2(k^2 - k_l^2)]^2 - 1/4 - \Omega^2 \right\} = 0. \quad (3.11)$$

We find that the bulk equation of motion in Eq. (3.10) gives rise to one volume mode $k_l = \pm iq$ and two real surface modes $k_l = \pm k_{1,2}$, with $\{q, k_1, k_2\}$ real and positive. Furthermore, the bulk equation of motion Eq. (3.11) may be rewritten in the dispersive form

$$\Omega^2 = [\Omega_H + 1/2 + \Lambda^2 k^2 + \Lambda^2 q^2]^2 - 1/4, \quad (3.12)$$

where the precise form of the volume mode q follows from the boundary conditions on the system. From Eqs. (3.10) and (3.12) we find that the remaining two surface modes $k_{1,2}$ may be expressed as

$$k_1^2 = k_x^2, \quad (3.13a)$$

$$k_2^2 = k_x^2 + \Lambda^{-2} [2\Omega_H + 1 + \Lambda^2 k^2 + \Lambda^2 q^2]. \quad (3.13b)$$

The surface mode with wavelength k_1 is the Damon-Eshbach (DE) surface mode [76], which is confined to the surface with width $1/k_x$. The remaining surface mode $k_2 \gg k_1$ is a much more confined to the surface with a width of

$1/k_2$. We will find this mode to be evanescent due to the boundary conditions of the thin film.

The exchange boundary conditions in Eq. (3.6) evaluated for the spin-wave modes in Eq. (3.9) give

$$\sum_{l=1}^6 C_{k_l} k_l F_l^*(k_l + k_x) e^{\pm k_l L/2} \Big|_{z=\pm L/2} = 0, \quad (3.14a)$$

$$\sum_{l=1}^6 C_{k_l} k_l F_l(k_l - k_x) e^{\pm k_l L/2} \Big|_{z=\pm L/2} = 0, \quad (3.14b)$$

with $k_l \in \{\pm k_1, \pm k_2, \pm iq\}$ as defined in Eqs. (3.10) and (3.13). The magnetostatic boundary conditions on the other hand require a bit more work. We start by noting that the magnetization vanishes $\Psi = 0$ outside the magnetic thin film ($z < -L/2$ and $L/2 < z$). Hence, the magnetostatic Maxwell equations (3.3) outside the thin film give $\nabla^2 w(\mathbf{x}) = (-k^2 + \partial_z^2)w(\mathbf{k}, z)e^{i\mathbf{k}\cdot\mathbf{r}_{\parallel}} = 0$. The asymptotically bound solutions outside the magnet are thus given by

$$w(\mathbf{k}, z) \propto \begin{cases} e^{-kz}, & z > L/2, \\ e^{kz}, & z < -L/2. \end{cases} \quad (3.15)$$

Since the tangential components of \mathbf{h}_D are continuous across the thin film surfaces, the scalar field $w(\mathbf{k}, z)$ should also be continuous across the thin film surface. Furthermore, continuity of the normal component of \mathbf{b} in the Bogoliubov ansatz requires

$$\partial_z w(\mathbf{k}, z^{\pm}) = \partial_z w(\mathbf{k}, z^{\mp}) + \frac{M_s}{\sqrt{2}} [u(\mathbf{k}, z^{\mp}) + v(\mathbf{k}, z^{\mp})] \Big|_{z=\pm L/2}, \quad (3.16)$$

with $z^{\pm} = z \pm 0^+$. This boundary condition (3.16) in combination with Eq. (3.15) gives the effective magnetostatic boundary condition

$$(\pm k + \partial_z)w(\mathbf{k}, z) + \frac{M_s}{\sqrt{2}} [u(\mathbf{k}, z) + v(\mathbf{k}, z)] \Big|_{z=\pm L/2} = 0. \quad (3.17)$$

Evaluated for the spin-wave modes in Eq. (3.9) the above effective magneto-static boundary condition (3.17) gives

$$\sum_{\pm} C_{\pm k_1} [(2F_1^* F_1 + F_1^*) \delta_{\pm} - F_1 \delta_{\mp}] e^{\pm k_1 L/2} - \sum_l C_{k_l} F_l^* e^{k_l L/2} |_{z=L/2} = 0, \quad (3.18a)$$

$$\sum_{\pm} C_{\pm k_1} [(2F_1^* F_1 + F_1) \delta_{\mp} - F_1^* \delta_{\pm}] e^{\mp k_1 L/2} - \sum_l C_{k_l} F_l e^{-k_l L/2} |_{z=-L/2} = 0, \quad (3.18b)$$

with $\delta_{\pm} \equiv \delta_{1,\pm 1}$ the Kronecker delta and $k_l \in \{\pm k_2, \pm iq\}$ as defined in Eqs. (3.10) and (3.13). Note here that we used the bulk equation of motion in Eq. (3.10) to simplify the above boundary conditions.

3.3 DIPOLE-EXCHANGE DISPERSION RELATION

3.3.1 General derivation

For notational simplicity we introduce the dimensionless wavenumbers $\Lambda k \rightarrow k$, $\Lambda q \rightarrow q$ and the dimensionless thickness $L/\Lambda \rightarrow L$.

3.3.1.1 Effective boundary conditions for spin waves

We start this section by noting that Eq. (3.13) yields $k_2 \gg k \equiv k_x$, $e^{k_2 L/2} \gg e^{-k_2 L/2}$ and $|F_2^*| \gg |F_2|$. This allows us to approximate the exchange boundary conditions in Eq. (3.14) by

$$a_+ F_k^* k^2 e^{kL/2} + b_+ = c F_q^* (q^2 \cos[(q + \delta)L/2] + kq \sin[(q + \delta)L/2]), \quad (3.19a)$$

$$a_+ F_k^* k^2 e^{-kL/2} + b_- = c F_q^* (q^2 \cos[(q - \delta)L/2] - kq \sin[(q - \delta)L/2]), \quad (3.19b)$$

$$a_- F_k k^2 e^{-kL/2} = c F_q (q^2 \cos[(q + \delta)L/2] - kq \sin[(q + \delta)L/2]), \quad (3.19c)$$

$$a_- F_k k^2 e^{kL/2} = c F_q (q^2 \cos[(q - \delta)L/2] + kq \sin[(q - \delta)L/2]). \quad (3.19d)$$

where $a_{\pm} = C_{\pm k}$, $b_{\pm} \simeq C_{\pm k_2} F_2^* k_2^2 / 2 e^{k_2 L/2}$ and $e^{\pm i\delta L/2} c = C_{\pm q}$. Note that δ can in principle be a complex number. For future convenience we rewrite the above exchange boundary conditions to

$$\bar{b}_+ + a_- F_k k^2 e^{-kL/2} = 2c F_q q^2 \cos[(q + \delta)L/2], \quad (3.20a)$$

$$\bar{b}_+ - a_- F_k k^2 e^{-kL/2} = 2c F_q k q \sin[(q + \delta)L/2], \quad (3.20b)$$

$$\bar{b}_- + a_- F_k k^2 e^{kL/2} = 2c F_q q^2 \cos[(q - \delta)L/2], \quad (3.20c)$$

$$-\bar{b}_- + a_- F_k k^2 e^{kL/2} = 2c F_q k q \sin[(q - \delta)L/2]. \quad (3.20d)$$

where $\bar{b}_+ = (F_q/F_q^*)b_+ + a_+(F_q/F_q^*)F_k^* k^2 e^{kL/2}$ and $\bar{b}_- = (F_q/F_q^*)b_- + a_+(F_q/F_q^*)F_k^* k^2 e^{-kL/2}$ are free parameters since $k_2 \gg k$ implies that b_+ and b_- are – to good approximation – not restricted by the magnetostatic boundary conditions. From here we find that the contributions of q and δ can be separated by making use of the trigonometric identities

$$\begin{cases} \cos[(q \pm \delta)L/2] = \cos(qL/2) \cos(\delta L/2) \mp \sin(qL/2) \sin(\delta L/2), \\ \sin[(q \pm \delta)L/2] = \sin(qL/2) \cos(\delta L/2) \pm \cos(qL/2) \sin(\delta L/2). \end{cases}$$

The above trigonometric identities allow us to express \bar{b}_+ and \bar{b}_- in Eq. (3.20) in terms of the variables a_- , k and q , which gives

$$\bar{b}_+ = \frac{a_- F_k k^2}{k^2 + q^2} \left[(q^2 - k^2) e^{-kL/2} + 2kq \left(\csc(qL) e^{kL/2} - \cot(qL) e^{-kL/2} \right) \right], \quad (3.21a)$$

$$\bar{b}_- = \frac{a_- F_k k^2}{k^2 + q^2} \left[(q^2 - k^2) e^{kL/2} + 2kq \left(\cot(qL) e^{kL/2} - \csc(qL) e^{-kL/2} \right) \right], \quad (3.21b)$$

where $\csc(qL) \equiv 1/\sin(qL)$ and $\cot(qL) \equiv \cos(qL)/\sin(qL)$. Hence, Eqs. (3.20) and (3.21) allow us to express $2c F_q^* F_q q^2 \cos[(q \pm \delta)L/2]$ in terms of the variables a_- , k and q , which to leading order in exponential functions is given by

$$c F_q \cos[(q + \delta)L/2] = \frac{a_- F_k k^2 e^{kL/2}}{k^2 + q^2} \left(e^{-kL} + kL \csc(qL)/qL \right), \quad (3.22a)$$

$$c F_q^* \cos[(q - \delta)L/2] = \frac{a_- F_k k^2 e^{kL/2}}{k^2 + q^2} \frac{F_q^*}{F_q} (1 + kL \cot(qL)/qL). \quad (3.22b)$$

So far we have used the exchange boundary conditions Eq. (3.19) to express $2cF_q^*F_qq^2 \cos[(q \pm \delta)L/2]$ in terms of the variables a_- , k and q . From here, we impose the magnetostatic boundary conditions to find a closed expression for q satisfying all boundary conditions.

The remaining magnetostatic boundary conditions (3.18), for $k_2 \gg k_x$, $e^{k_2L/2} \gg e^{-k_2L/2}$ and $|F_2^*| \gg |F_2|$, are well approximated by

$$a_+(2F_kF_k^* + F_k^*)e^{kL/2} - a_-F_ke^{-kL/2} = 2cF_q \cos[(q + \delta)L/2], \quad (3.23a)$$

$$a_-(2F_kF_k^* + F_k^*)e^{kL/2} - a_+F_k^*e^{-kL/2} = 2cF_q^* \cos[(q - \delta)L/2]. \quad (3.23b)$$

3.3.1.2 Dipole-exchange spin-wave modes

The above magnetostatic boundary conditions together with the effective exchange boundary conditions in Eq. (3.22) give two linear homogeneous equations in a_+ and a_- . Hence, we have spin-wave solutions when the determinant of this square matrix vanishes. At leading order in exponential functions of the trigonometric contribution we find this to be the case when

$$\det \begin{bmatrix} (2F_k + 1) & (3k^2 + q^2)e^{-kL} \\ e^{-kL} & D(k, q) \end{bmatrix} = 0, \quad (3.24)$$

with

$$D(k, q) = (2F_k^* + 1) [(3k^2 + q^2) + 2k^3L \cot(qL)/qL] \\ + 4k^2(k^2 + q^2)(1 + kL \cot(qL)/qL).$$

In the above we used the bulk equation of motion $2F_qF_q^* + F_q + F_q^* = 0$ to obtain $F_q^*/F_q = -(2F_q^* + 1)$. Note that we neglected $2k^3L \csc(qL)/qL$ in Eqs. (3.22a) and (3.24) since it is exponentially suppressed in the equation of motion and thus not of importance for the dispersion relation. The spin-wave modes hence satisfy

$$\begin{aligned} & [(F_k + 1/2)(F_k^* + 1/2) - e^{-2kL}/4](3k^2 + q^2) \\ & + (F_k + 1/2)2k^2(k^2 + q^2) \\ & + (F_k + 1/2)(F_k^* + 1/2 + k^2 + q^2)2k^3L \cot(qL)/qL \\ & = 0. \end{aligned} \quad (3.25)$$

When interested in the n -th spin-wave mode the above equation is well approximated by

$$\begin{aligned}
& [(F_{k,n} + 1/2)(F_k^* + 1/2) - e^{-2kL}/4](3k^2 + n^2\pi^2/L^2 + \delta_n\pi^2/4L^2) \\
& + (F_{k,n} + 1/2)2k^2(k^2 + n^2\pi^2/L^2) \\
& + (F_{k,n} + 1/2)(F_{k,n}^* + 1/2 + k^2 + n^2\pi^2/L^2)2k^3L \cot(qL)/qL \\
& = 0,
\end{aligned} \tag{3.26}$$

with $\delta_n \equiv \delta_{n,0}$ the Kronecker delta, $F_{k,n} \equiv F_k|_{q \rightarrow n\pi/L}$ and $F_{k,n}^* \equiv F_k^*|_{q \rightarrow n\pi/L}$. In order to proceed we use the identity

$$\pi \cot(\pi x) = \frac{1}{x} + 2x \sum_{n=1}^{\infty} \frac{1}{x^2 - n^2}. \tag{3.27}$$

To make use of the above identity we consider $\pi x = qL$. Furthermore, we note that q for n -th spin-wave is in the interval $n\pi/L < q < (n+1)\pi/L$. For the n -th spin wave mode we obtain

$$\frac{\cot(qL)}{qL} \simeq \frac{2 - \delta_n}{q^2L^2 - n^2\pi^2} + \frac{2}{q^2L^2 - (n+1)^2\pi^2} - \alpha_n, \tag{3.28}$$

with $\delta_n \equiv \delta_{n,0}$ the Kronecker delta and

$$\alpha_n = \frac{4}{3\pi^2} \frac{1}{(1+n)^2}. \tag{3.29}$$

We expand q^2L^2 around $n^2\pi^2$ for the n -th spin-wave mode. From here it follows that Eq. (3.26) can be written explicitly as

$$a_{n,k}z^3 + b_{n,k}z^2 + c_{n,k}z + d_{n,k} = 0, \tag{3.30}$$

with $z = q^2L^2 - n^2\pi^2$. Furthermore,

$$a_{n,k} \approx -1, \tag{3.31a}$$

$$b_{n,k} = B_{n,k} - \alpha_n C_{n,k} - a_{n,k} (2n+1)\pi^2, \tag{3.31b}$$

$$c_{n,k} = (4 - \delta_n)C_{n,k} - (B_{n,k} - \alpha_n C_{n,k})(2n+1)\pi^2, \tag{3.31c}$$

$$d_{n,k} = -C_{n,k}(2 - \delta_n)(2n+1)\pi^2, \tag{3.31d}$$

and

$$B_{n,k} \simeq \frac{1 - e^{-2kL}}{4\gamma_{n,k}/L^2} - (k^2L^2 + n^2\pi^2) \frac{k^2L^2 + n^2\pi^2 + \delta_n\pi^2/4}{3k^2L^2 + n^2\pi^2 + \delta_n\pi^2/4}, \quad (3.32a)$$

$$2C_{n,k} \simeq \frac{k^3L^5 \times \gamma_{n,k}^{-1}}{3k^2L^2 + n^2\pi^2 + \delta_n\pi^2/4}, \quad (3.32b)$$

where $\gamma_{n,k} = 2(\Omega_H + 1/2 + k^2 + n^2\pi^2/L^2)$. For the n -th spin-wave mode Eq. (3.30) gives the formal solution

$$z_{n,k} = -\frac{1}{3} \frac{b_{n,k}}{a_{n,k}} + \sqrt{\frac{-4P_{n,k}}{3}} \cos \left[\frac{1}{3} \arccos \left(\frac{3Q_{n,k}}{2P_{n,k}} \sqrt{\frac{-3}{P_{n,k}}} \right) - \frac{2\pi}{3} \right], \quad (3.33)$$

with

$$Q_{n,k} = \frac{d_{n,k}}{a_{n,k}} - \frac{1}{3} \frac{b_{n,k}}{a_{n,k}} \frac{c_{n,k}}{a_{n,k}} + \frac{2}{27} \left(\frac{b_{n,k}}{a_{n,k}} \right)^3, \quad (3.34a)$$

$$P_{n,k} = \frac{c_{n,k}}{a_{n,k}} - \frac{1}{3} \left(\frac{b_{n,k}}{a_{n,k}} \right)^2. \quad (3.34b)$$

The dispersion relation of the n -th spin-wave mode is accordingly given by Eq. (3.12)

$$\Omega_n^2 = \left[\Omega_H + \frac{1}{2} + k^2 + \frac{n^2\pi^2}{L^2} + \frac{z_n}{L^2} \right]^2 - \frac{1}{4}. \quad (3.35)$$

Note that Eqs. (3.33) and (3.35) are expressed in terms of the dimensionless wavenumber $\Lambda k \rightarrow k$ and the dimensionless thickness $L/\Lambda \rightarrow L$. Furthermore, Eq. (3.35) gives the dispersion relation for the dimensionless frequency $\Omega = \omega/\gamma\mu_0 M_s$. This is the main result of this paper. In Fig. 3.2 we compare the analytic dipole-exchange mode in Eq. (3.35) with the full numeric solution. We see that the analytic dispersion derived above is in good agreement with the full numeric solution of Eqs. (3.14) and (3.18). We like to stress that the analytic spin wave modes given in Eq. (3.35) do not experience level crossing. Hence, the n -th mode does not cross the $(n-1)$ and $(n+1)$ -th energy modes. In the remaining Subsections 3.3.2 and 3.3.3 we will simplify Eq. (3.35) for relative thin and thick films respectively.

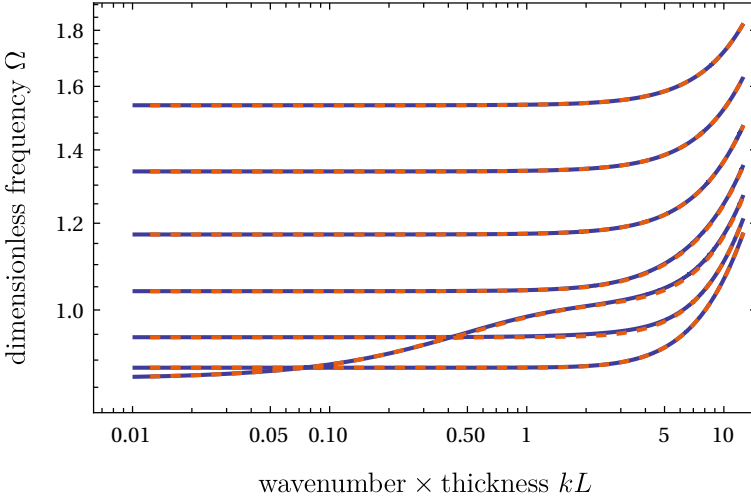


Figure 3.2: The first seven modes of the dipole-exchange spin-wave dispersion relation for $\Omega_H = 1/2$ and $L = 24$ are shown. The dashed lines correspond to the analytic dispersion in Eq. (3.35), while the solid lines correspond to the full numeric solution of Eqs. (3.14) and (3.18).

3.3.2 Thick thin-film approximation for the lowest exchange mode

In relatively thick films, $L > \mathcal{O}(10\sqrt{J/\mu_0 M_s})$, for sufficiently long wavelengths, the lowest energetic mode will be dominated by the first exchange mode. Away from the DE mode, we may approximate exchange mode solutions of Eq. (3.24) by $D(k, q) = 0$ with $F_k^* \rightarrow F_{k,n}^*$. This is equivalent to $a_{n,k} \rightarrow 0$ in Eq. (3.30) and $e^{-2kL} \rightarrow 0$ and $\delta_n \pi^2/4/L^4 \rightarrow 0$ in Eq. (3.32). The above results in a second order equation in z when the exchange mode has a small avoided crossing with the DE mode. For the lowest exchange mode $n \rightarrow 0$ this becomes

$$2kL \cot(qL)/qL = 4k^2 \gamma_k - 3. \quad (3.36)$$

Hence, we obtain a quadratic equation in z

$$b_k z^2 + c_k z + d_k = 0, \quad (3.37)$$

where

$$b_k = B_k - \frac{4C_k}{3\pi^2}, \quad (3.38a)$$

$$c_k = \frac{13}{3}C_k - \pi^2 B_k, \quad (3.38b)$$

$$d_k = -\pi^2 C_k, \quad (3.38c)$$

and

$$B_k \simeq 3 - 8(\Omega_H + 1/2 + k^2)k^2, \quad (3.39a)$$

$$C_k \simeq 2kL. \quad (3.39b)$$

We thus find

$$z = -\frac{c_k}{2b_k} + \text{sgn}(b_k) \sqrt{\left(\frac{c_k}{2b_k}\right)^2 - \frac{d_k}{b_k}}. \quad (3.40)$$

The lowest exchange mode dispersion is thus

$$\Omega^2 = [\Omega_H + 1/2 + k^2 + z/L^2]^2 - 1/4. \quad (3.41)$$

In Fig. 3.3 we compare the above dispersion relation with the numeric solution of the lowest energy mode. We find good agreement between the approximated dispersion relation in Eq. (3.41) and the numerical lowest energy mode for wavelengths k larger than the level crossing point with the DE mode. Note that the above simplification is not restricted to the lowest energy exchange mode, but can be applied to the higher exchange modes as long as there is no large avoided crossing with the DE mode.

3.3.3 Thin film approximation for the lowest energy mode

For very thin films, $L \sim \mathcal{O}(\sqrt{J/\mu_0 M_s})$, only the DE wave is of importance for the lowest energy mode. For very thin films it is reasonable to assume $q^2 L^2 < (3/4)^2 \pi^2$, we may thus approximate

$$\frac{\cot(qL)}{qL} \simeq \frac{1}{(qL)^2} - \frac{1}{3}. \quad (3.42)$$

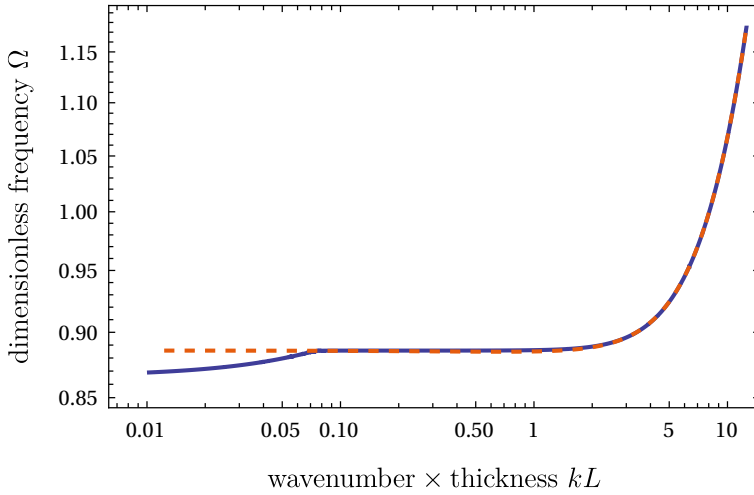


Figure 3.3: Dipole-exchange dispersion relation of the lowest energy mode for $\Omega_H = 1/2$ and $L = 24$. The dashed line correspond to the analytically derived dispersion in Eq. (3.41), while the solid line gives the numeric solution to Eqs. (3.14) and (3.18) for the lowest energy mode.

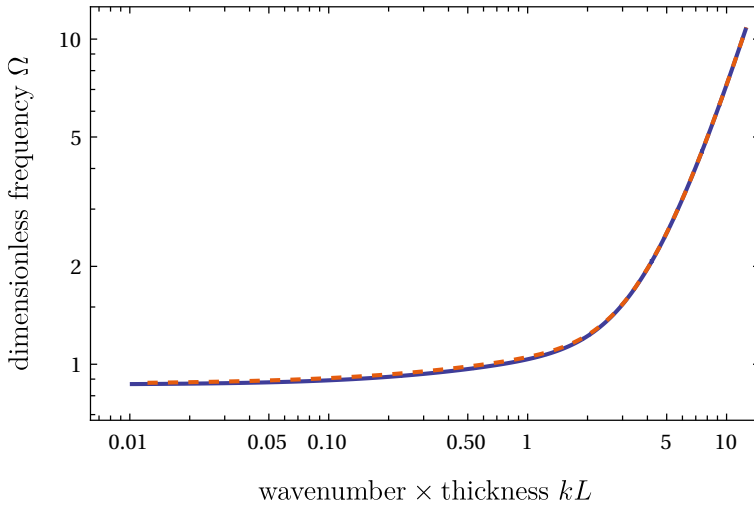


Figure 3.4: Dipole-exchange dispersion of the lowest energy mode for $\Omega_H = 1/2$ and $L = 4$. The dashed line corresponds to the approximate dispersion relation in Eq. (3.47). The solid line corresponds to the numeric solution of Eqs. (3.14) and (3.18).

Thus the lowest energy mode in very thin films is described by a quadratic equation in z

$$a_k z^2 + b_k z + c_k = 0. \quad (3.43)$$

Where

$$a_k \approx -2(\Omega_H + 1/2 + k^2)/L^2, \quad (3.44a)$$

$$b_k \simeq B_k - c_k/3, \quad (3.44b)$$

$$c_k \simeq kL/6, \quad (3.44c)$$

and

$$B_k \simeq \frac{1 - e^{-2kL}}{4} - \frac{2}{3}(\Omega_H + 1/2 + k^2)k^2. \quad (3.45a)$$

The lowest energy mode in very thin films is thus given by

$$z = -\frac{b_k}{2a_k} + \sqrt{\left(\frac{b_k}{2a_k}\right)^2 - \frac{c_k}{a_k}}, \quad (3.46)$$

where the lowest energy dispersion relation is given by

$$\Omega^2 = [\Omega_H + 1/2 + k^2 + z/L^2]^2 - 1/4. \quad (3.47)$$

This is plotted in Fig. 3.4. We again find good agreement between the analytic result in Eq. (3.47) and the numerical solution of the full boundary conditions in Eqs. (3.14) and (3.18). Note that we took $\delta_n \pi^2 / 4L^2 \rightarrow 0$ of Eq. (3.32) in the very thin-film limit, since it simplifies the expressions for B_k and c_k and does not have a big impact on the dispersion relation for very thin-films.

3.3.4 Comparison with Kalinikos and Slavin [83, 84]

In the paper by Kalinikos and Slavin [83, 84] the dipole-exchange spin-wave spectrum that follows from the diagonal approximation for spin waves propagating perpendicular to a tangentially magnetized thin-film was given by

$$\Omega_n^2 = [\Omega_H + 1/2 + k^2 + n^2 \pi^2 / L^2]^2 - [P_n - 1/2]^2, \quad (3.48)$$

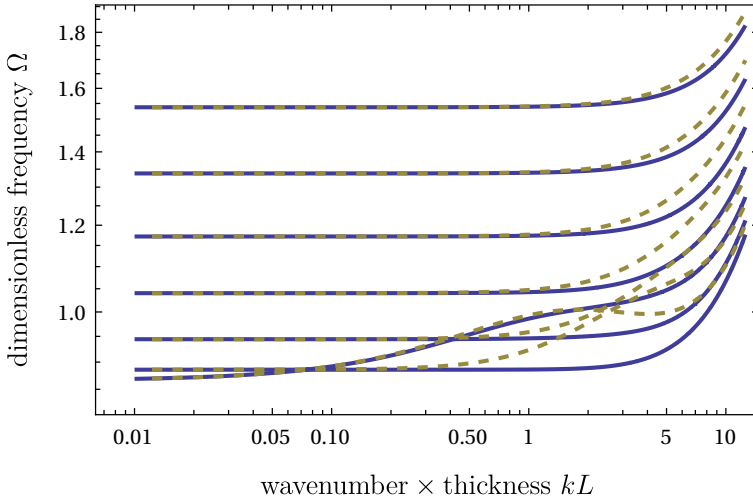


Figure 3.5: The first seven modes of the dipole-exchange spin-wave dispersion relation for $\Omega_H = 1/2$ and $L = 24$ are shown. The dashed lines correspond to the analytic dispersion derived by Kalinikos and Slavin [83, 84] in Eq. (3.48). The solid lines correspond to the full numerical solution of Eqs. (3.14) and (3.18). We did not plot the analytic results in Eq. (3.35) and Fig. 3.2, since it agrees very well with the numerical solution.

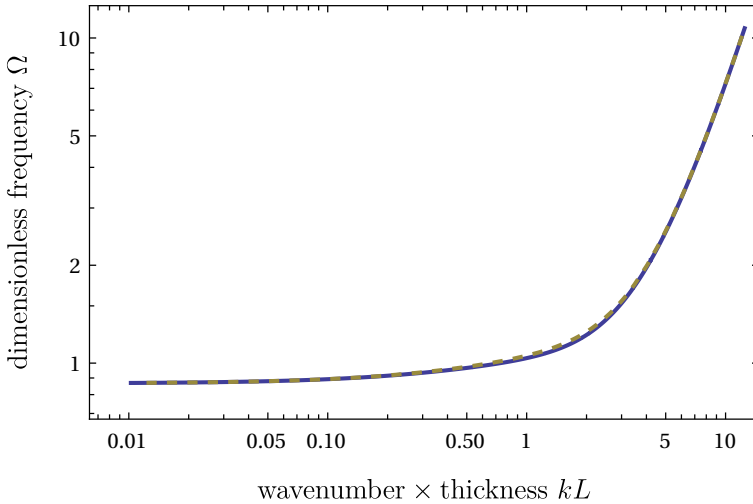


Figure 3.6: Dipole-exchange dispersion of the lowest energy mode for $\Omega_H = 1/2$ and $L = 4$. The dashed line corresponds to the dispersion relation by Kalinikos and Slavin [83, 84] in Eq. (3.48). The solid line on the other hand corresponds to the numeric solution of Eqs. (3.14) and (3.18). We did not plot the analytic results in Eq. (3.35) and Fig. 3.4, since it agrees very well with the numerical solution.

with

$$P_n = \frac{k^2 L^2}{k^2 L^2 + n^2 \pi^2} \left[1 - \frac{k^2 L^2}{k^2 L^2 + n^2 \pi^2} \frac{2}{1 + \delta_n} \left(\frac{1 - (-1)^n e^{-kL}}{kL} \right) \right]. \quad (3.49)$$

In Fig. 3.5 we plotted the spin-wave dispersion by Kalinikos and Slavin [83, 84] in Eq. (3.48) for relatively thick films. We see that the analytic spin-wave dispersion by Kalinikos and Slavin [83, 84] shows quantitative differences with the analytic spin-wave dispersion derived in this Chapter Eqs. (3.35) and (3.41) and the numerical solution of the full problem. For very thin films on the other hand, we find good agreement between the theory of Kalinikos and Slavin [83, 84], the analytic results derived in this Chapter Eqs. (3.35) and (3.47) and the numeric solution of the full boundary conditions, see Fig. 3.6.

3.4 DISCUSSION AND CONCLUSIONS

We considered the theory of spin waves in ferromagnetic films. More specifically, the theory of spin waves propagating perpendicular to an in-plane magnetic field. This case is of special interest since it is the most typical configuration used in spin wave experiments. The main result of this Chapter is the spin wave spectrum in Eq. (3.35) which we derived by imposing the exchange and magnetostatic boundary conditions on bulk spin wave solutions. This derivation differs significantly from the derivation of Kalinikos and Slavin [83, 84] where the magnetostatic Green's function was used to construct the spin wave spectrum. The boundary problem we obtained has an accurate analytical solution which agrees well with the numerical solution and shows quantitative differences with the commonly used theory in Refs. [83, 84] in relative thick films. This inaccuracy of the spin wave spectrum that follows from the diagonal approximation in the theory by Kalinikos and Slavin [83, 84] has already been observed by Kreisel *et al.* [77]. Furthermore, our results could be verified experimentally, for example using Brillouin light scattering and spin-wave spectroscopy [94].

Future research could generalize the method presented here to describe spin waves propagating in an arbitrary direction with respect to a generally

oriented external magnetic field. This is relatively straightforward for in-plane magnetizations. Another way to generalize this model is to include the effects of both surface and boundary anisotropies. Lastly, the magnetization profile of spin wave modes could relatively straightforwardly be determined from the spin wave spectrum in Eqs. (3.35), (3.41) and (3.47).

ACKNOWLEDGMENTS

J.S.H. would like thank A. Rückriegel for helpful discussions and D. A. Bozhko for useful comments on the preprint.

Part II

APPLICATIONS OF NEGATIVE ENERGY MODES AND NON-LINEAR DYNAMICS

“If you think you’re boring your audience, go slower not faster.”

—Credited to Gustav Mahler.

“How wonderful that we have met with a paradox. Now we have some hope of making progress.”

—Niels Bohr.

4

ENHANCED MAGNON SPIN CURRENT USING THE BOSONIC KLEIN PARADOX

This Chapter is based on J. S. Harms, H. Y. Yuan, and R. A. Duine, “Enhanced magnon spin current using the bosonic Klein paradox,” *Physical Review Applied* **18**, 064026 (2022). R.A.D. conceived the project, J.S.H. did the analytic calculations and H.Y.Y performed the numerical simulations. H.Y.Y and J.S.H. prepared the manuscript. All authors contributed to the manuscript.

We propose to amplify magnon currents based on the realization of the bosonic Klein paradox in magnetic nanostructures. This paradox involves the antimagnon, carrying opposite spin and energy, whose existence is usually precluded by ferromagnetic instabilities as it is an excitation at negative energy. We show that, by appropriately tuning the effective dissipation through spin-orbit torques, both magnons and antimagnons are dynamically stabilized. As a result, we find that the reflection coefficient of incident magnons at an interface between two coupled magnets can become larger than one, thereby amplifying the reflected magnon current. Our findings can lead to magnon amplifier devices for spintronic applications. Furthermore, our findings yield a solid-state platform to study the field theoretical behavior of bosonic particles, which is an outstanding challenge with fundamental particles.

4.1 INTRODUCTION

We show that the magnon spin current can be significantly amplified at an interface between a magnet that is not driven externally and a magnet into which angular momentum is injected using spin-orbit torque (SOT) [60, 95–98]. By designing the balance of this external driving with intrinsic dissipation, both magnons (positive-energy excitations) and antimagnons (negative-energy excitations) are dynamically stabilized. This results in enhanced reflection of magnons from the interface with the driven-dissipative magnet. The enhanced reflection is accompanied by a transmitted antimagnon current. This suggests a method to amplify magnon spin currents that is relatively straightforward to implement, which may be generalized to both ferromagnetic and antiferromagnetic materials, different types of driving, and to both metals and insulators. Below, we explicitly illustrate the basic physics for a magnetic heterostructure involving yttrium-iron-garnet (YIG) and platinum.

Our result can be interpreted as a realization of the bosonic Klein paradox, which refers to the counterintuitive reflection or transmission of relativistic particles from a potential barrier [99–104], and is a natural consequence of quantum field theories. The experimental test of this paradox using fundamental particles is nearly impossible because of the extremely high energy barrier that needs to be overcome [105]. While its solid-state realization for fermionic particles in 2D materials with gapless excitations was recently reported [106–108], the study of the Klein paradox for bosonic quasiparticles remains an outstanding challenge because the presence of bosonic antiparticles in a solid-state system usually signals instabilities. In our implementation, these instabilities are prevented by the external driving via SOT. Hence, in addition to the application-motivated magnon amplification that is discussed above, our results launch driven magnetic systems as a suitable solid-state platform to experimentally study field theoretical of bosonic particles.

4.2 PHYSICAL MODEL

4.2.1 Set-up and magnonic and antimagnonic excitations

We consider two exchange coupled ferromagnetic (FM) insulating thin films adjacent to a heavy-metal layer (HM) subject to an in-plane external magnetic field in the z direction, as shown in Fig. 4.1(a). The magnetization of the right FM aligns antiparallel to the external field. This situation is energetically unstable but dynamically stable due to the presence of an electrical current in the HM layer which exerts a SOT on the magnetization dynamics. This can be understood as follows: the spin current produced by the electric current through the spin Hall effect in the HM will keep injecting angular momentum to the FM layer to counteract the damping of magnetization and to prevent the magnetization to align with the external field, thereby yielding a region with dynamically stable antimagnons. In general, the dynamics of the magnetization $\mathbf{n}_\nu = \mathbf{M}_\nu/M_s$ is well described by the Landau-Lifschitz-Gilbert (LLG) equation with SOT [60], i.e.,

$$\frac{\partial \mathbf{n}_\nu}{\partial t} = -\gamma \mathbf{n}_\nu \times \mathbf{h}_{\text{eff},\nu} + \alpha \mathbf{n}_\nu \times \frac{\partial \mathbf{n}_\nu}{\partial t} + J_\nu \mathbf{n}_\nu \times \hat{z} \times \mathbf{n}_\nu, \quad (4.1)$$

where $\nu = L, R$ labels the (L)eft and (R)ight magnet, and, γ is the gyromagnetic ratio, α is the Gilbert damping and J_ν characterizes the strength of SOTs generated by the spin current which depends on the current flowing in the HM layer, the spin Hall angle of the HM and the properties of the interface. The LLG equation describes damped precession around the effective magnetic field $\mathbf{h}_{\text{eff},\nu} = -\delta E_\nu/(M_s \delta \mathbf{n}_\nu)$, with M_s being saturation magnetization. Here, we consider the magnetic energy functional $E_\nu[\mathbf{n}_\nu]$ in the left and right magnet to be of the form

$$E_\nu = \int dV \left\{ A(\nabla_i \mathbf{n}_\nu)^2 - \mu_0 H_{e,\nu} M_s n_{z,\nu} + \frac{1}{2} K n_{y,\nu}^2 \right\}, \quad (4.2)$$

with A the exchange stiffness, $H_{e,\nu}$ is the external magnetic field strength, μ_0 is the vacuum permeability and $K = \mu_0 M_s^2$ the effective shape anisotropy caused by the dipolar interaction.

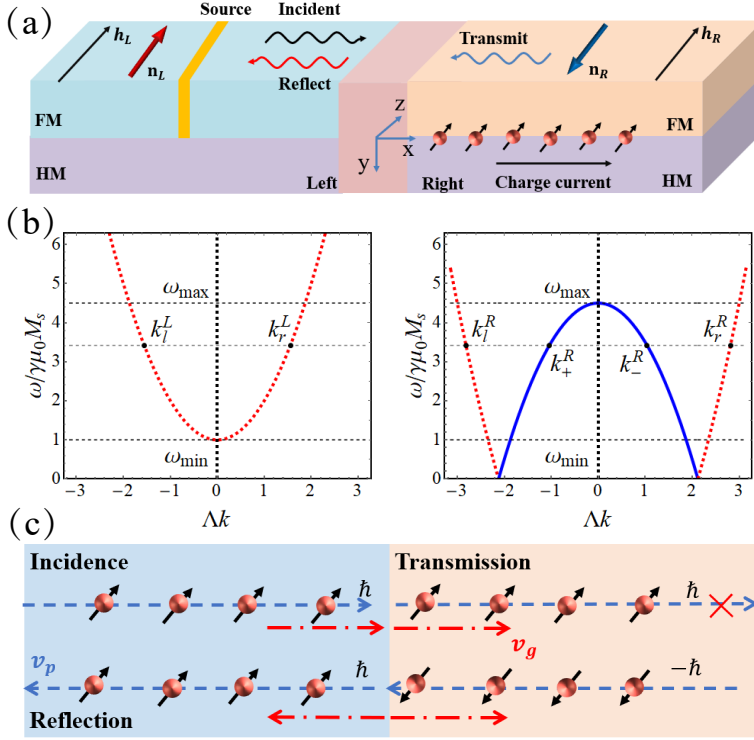


Figure 4.1: (a) Schematic of the driven-dissipative magnetic system containing two exchange-coupled magnetic films. (b) Magnon dispersion for the left and right ferromagnets respectively. The red dotted curves give the positive energy excitations while the blue curve corresponds to the negative energy excitations. In other words, negative energy excitations exist for the wavenumbers $-2.1 \lesssim \Delta k \lesssim 2.1$ between the zeros of the dispersion in the right magnet. (c) Physical picture of the anomalous magnon reflection. Blue and red arrows represent the directions of phase and group velocity, respectively.

Spin waves or magnons are introduced as linear dynamical fluctuations on top of the equilibrium magnetization $\mathbf{n}_{0,\nu}$ with $\mathbf{n}_{0,L} = e_z$ and $\mathbf{n}_{0,R} = -e_z$. By introducing the complex field $\Psi_\nu = (1/\sqrt{2})(\hat{x} \mp i\hat{y}) \cdot \mathbf{n}_\nu$, the linearized LLG equation [109–111] accordingly becomes

$$\frac{i(\mathbb{1} + i\alpha\sigma_z)\partial_t}{\gamma\mu_0M_s} \begin{pmatrix} \Psi_\nu \\ \Psi_\nu^* \end{pmatrix} = (\mathcal{L}_\pm + iI_\nu\mathbb{1}) \begin{pmatrix} \Psi_\nu \\ \Psi_\nu^* \end{pmatrix}, \quad (4.3)$$

with

$$\mathcal{L}_\pm = (\Delta \pm h_\nu - \Lambda^2\nabla^2) \sigma_z + i\Delta\sigma_y. \quad (4.4)$$

In the above, $\sigma_{y,z}$ are the Pauli matrices, $\Lambda = \sqrt{2A/\mu_0M_s^2}$ the exchange length, $h_\nu = H_{e,\nu}/M_s$ the dimensionless external magnetic field, $\Delta = K/2\mu_0M_s^2 = 1/2$ the dimensionless anisotropy constant and $I_\nu = J_\nu/\gamma\mu_0M_s$ the dimensionless SOT. The \pm sign in the definition of Ψ_ν and Eqs. (4.3) and (4.4) comes from the linearization around the $\pm e_z$ direction in the left and right ferromagnets respectively. We introduce spin wave solutions of the linearized LLG equation (4.3) in the form of Bogoliubov modes

$$\Psi_\nu(\mathbf{x}, t) = u_\nu(\mathbf{x})e^{-i\lambda t} - v_\nu^*(\mathbf{x})e^{i\lambda^* t}. \quad (4.5)$$

Here, the Fourier transform of $u_\nu(\mathbf{x})$ and $v_\nu(\mathbf{x})$ satisfy, up to first order in α and I_ν , the following dispersion relation

$$\omega_{\mathbf{k},\nu} \simeq \omega_{\mathbf{k},\nu}^0 - i(\alpha[\Delta \pm h_\nu + \Lambda^2k^2] - I_\nu), \quad (4.6)$$

with $\omega = \lambda/\gamma\mu_0M_s$ the dimensionless frequency,

$$(\omega_{\mathbf{k},\nu}^0)^2 = (\Delta \pm h_\nu - \Lambda^2k^2)^2 - \Delta^2, \quad (4.7)$$

the dissipationless dispersion relation and

$$\|\Psi_{\mathbf{k},\nu}\| = |u_{\mathbf{k},\nu}|^2 - |v_{\mathbf{k},\nu}|^2, \quad (4.8)$$

the norm of the two different branches of Eq. (4.3) [112]. In Fig. 4.1(b) we plot an example of the real part of the dispersion relation for both the left and right ferromagnets, with $h_L = 0.5$ and $h_R = 4.5$ and $\omega > 0$.

At this point it is good to take a step back to stress a couple of things. First of all, the dissipationless limit of Eq. (4.3) is pseudo-Hermitian, in other words

$$\sigma_z \mathcal{L}_\pm^\dagger \sigma_z = \mathcal{L}_\pm. \quad (4.9)$$

A consequence of this statement is that the magnon norm $\|\Psi_{\mathbf{k},\nu}\|$ in Eq. (4.8) is conserved in the dissipationless limit. Secondly, Eq. (4.3) has the additional symmetry

$$\sigma_x (\mathcal{L}_\pm + i\alpha\omega^* \sigma_z + iI_\mu \mathbb{1}) \sigma_x = -(\mathcal{L}_\pm - i\alpha\omega \sigma_z + iI_\mu \mathbb{1})^*. \quad (4.10)$$

This implies that if ω is an eigenfrequency of Eq. (4.3) with eigenmode $(u_\nu \ v_\nu)^\top$, then $-\omega^*$ is also an eigenfrequency with eigenmode $(v_\nu^* \ u_\nu^*)^\top$. These two modes have opposite norm by construction. Hence, the two branches of Eq. (4.3) are related to each other via particle hole symmetry. In our magnetic system, this doubling is not physical, but merely a result of our choice to describe spin waves using complex scalar fields. Hence, in order to describe the full dynamics of the system it is sufficient to consider $\omega > 0$ and take into account the norm of different modes.

From this point onwards we refer to the positive norm excitations as magnons, and the excitations carrying negative norm as antimagnons. This distinction between magnons and antimagnons is only allowed if one would solely consider excitation with positive sign of ω , i.e. $\omega > 0$. Note that it is sufficient to consider $\omega > 0$, due to the particle doubling. We can make two important observations. One, anti-magnons only exist in the right magnet. And second, antimagnons carry negative energy and most importantly they have opposite handedness w.r.t. the magnonic excitations.

The antimagnons in this setup can be stabilized, since in driven magnetic systems, energetic and dynamical stability do not necessarily coincide. For the system to be dynamically stable we need

$$\text{Im}(\omega_{\mathbf{k},\nu}) \simeq \text{Im}(\omega_{\mathbf{k},\nu}^0) - \alpha [\Delta \pm h_\nu + \Lambda^2 k^2] + I_\nu < 0, \quad (4.11)$$

for all wavenumbers \mathbf{k} , because then small-amplitude fluctuations die out. This identity imposes that the magnons on the right side are dynamically

stable if $-I_R \gtrsim \max[\alpha(h_R - \Delta), \Delta]$. Whereas, energetic instabilities exist if the (anti)magnon excitation energy is negative, i.e. $\|\Psi_{\mathbf{k},\nu}\| \omega_{\mathbf{k},\nu}^0 < 0$. We thus note that the magnons on the right FM are energetically unstable for a range of wavenumbers but may be stabilized by injecting angular momentum via SOT, see Fig. 4.1. Physically, this means that the internal energy of the right ferromagnet can be lowered by small spin fluctuations (antimagnons), but injection of angular momentum prohibits the system to reach a new ground state.

4.2.2 Exchange coupling at the interface

Additionally, the left and right thin films are exchange coupled ¹, which results in effective boundary conditions for the magnetization. In terms of the Bogoliubov ansatz (4.5), the four boundary conditions follow from varying the energy functional in Eq. (4.2) after including the boundary term $E_{bn} = -J_c \mathbf{n}_L(0) \cdot \mathbf{n}_R(0)$ at the interface ($x = 0$). This gives

$$\Lambda \partial_x \varphi_L - \Lambda_c (\varphi_R + \varphi_L) = 0, \quad (4.12a)$$

$$\Lambda \partial_x \varphi_R + \Lambda_c (\varphi_L + \varphi_R) = 0, \quad (4.12b)$$

with $\varphi = u, v$ and $\Lambda_c = J_c / \Lambda \gamma \mu_0 M_s$. To analytically solve the scattering problem, we shall first focus on the isotropic case ($\Delta = 0$) and further show the essential physics still holds for elliptical magnons ($\Delta \neq 0$).

¹ Here the interface of left and right domains may be a normal-metal layer that generates the interlayer exchange interaction between left and right domain, an irradiated region where magnetic parameters can be effectively designed or other regions that could induce an effective exchange coupling between left and right domains.

4.3 SCATTERING OFF THE INTERFACE

Due to doubling of the modes we consider $\omega > 0$ without loss of generality. Solutions of Eq. (4.3) without dissipative terms have the form

$$\begin{pmatrix} u(x) \\ v(x) \end{pmatrix} = \begin{pmatrix} u_k \\ v_k \end{pmatrix} e^{ikx}. \quad (4.13)$$

At a given $\omega > \omega_{\min} \equiv h_L$, we find four different wavenumbers k . In the left region with only positive energy excitations, we find two real k_r^L, k_l^L and two complex k_+^L, k_-^L wavenumbers. These wavenumbers are, according to Eq. (4.6), given by

$$\Lambda k_{r/l}^L = \pm \sqrt{\omega - h_L}, \quad \Lambda k_{\pm}^L = \pm i \sqrt{\omega + h_L}. \quad (4.14)$$

The complex modes are either blowing up or are damped, where only the damped mode is physically allowed [113]. However, in the right magnet – magnetized against the external magnetic field – there are four real wavenumbers if $\omega < \omega_{\max} \equiv h_R$, which are explicitly given by

$$\Lambda k_{r/l}^R = \pm \sqrt{\omega + h_R}, \quad \Lambda k_{\pm}^R = \pm \text{sgn}(\omega - h_R) \sqrt{h_R - \omega}. \quad (4.15)$$

The k_r and k_l modes correspond to positive energy modes (magnons) with positive and negative group velocity respectively. Furthermore, k_+ and k_- correspond respectively to additional right- and left moving modes carrying negative energy (antimagnons). We included $\text{sgn}(\omega - h_R)$ in the expression of k_{\pm} here, such that k_+ corresponds both to the right moving negative energy mode and the exponentially damped mode when $\omega > \omega_{\max} \equiv h_R$.

We now construct the scattering solutions satisfying the boundary conditions in Eq. (4.12). The general solution for bulk modes at frequency ω are given by

$$u_{\nu}(x) = A_r^{\nu} u_{k_r, \nu} e^{ik_r x} + A_l^{\nu} u_{k_l, \nu} e^{ik_l x} + A_+^{\nu} u_{k_+, \nu} e^{ik_+ x} + A_-^{\nu} u_{k_-, \nu} e^{ik_- x}, \quad (4.16a)$$

$$v_{\nu}(x) = A_r^{\nu} v_{k_r, \nu} e^{ik_r x} + A_l^{\nu} v_{k_l, \nu} e^{ik_l x} + A_+^{\nu} v_{k_+, \nu} e^{ik_+ x} + A_-^{\nu} v_{k_-, \nu} e^{ik_- x}, \quad (4.16b)$$

with A_j^{ν} are amplitudes of the scattering modes in Eqs. (4.14) and (4.15) and $(u_{k,\nu}, v_{k,\nu})$ solutions to Eq. (4.3) with ansatz (4.13) and normalization condition $||u_{\nu,k}|^2 - |v_{\nu,k}|^2| = 1$. By disregarding spatially growing modes, the boundary conditions in Eq. (4.12) for incident magnons from the left imply

$$\mathbf{M} \begin{pmatrix} 1 \\ A_l^L \\ 0 \\ A_-^L \end{pmatrix} = \begin{pmatrix} A_v^R \\ 0 \\ A_+^R \\ 0 \end{pmatrix}. \quad (4.17)$$

Here, the matrix \mathbf{M} is defined by the boundary conditions given in Eq. (4.12) and is given by

$$\begin{aligned} \mathbf{M} = & \frac{1}{\lambda_{u,l}^R - \lambda_{u,r}^R} \begin{pmatrix} 0 & 1 \\ 0 & 0 \end{pmatrix} \otimes \begin{pmatrix} \lambda_{u,l}^R \lambda_{v,+}^L - 1 & \lambda_{u,l}^R \lambda_{v,-}^L - 1 \\ 1 - \lambda_{u,r}^R \lambda_{v,+}^L & 1 - \lambda_{u,r}^R \lambda_{v,-}^L \end{pmatrix} \\ & + \frac{1}{\lambda_{v,-}^R - \lambda_{v,+}^R} \begin{pmatrix} 0 & 0 \\ 1 & 0 \end{pmatrix} \otimes \begin{pmatrix} \lambda_{v,-}^R \lambda_{u,r}^L - 1 & \lambda_{v,-}^R \lambda_{u,l}^L - 1 \\ 1 - \lambda_{v,+}^R \lambda_{u,r}^L & 1 - \lambda_{v,+}^R \lambda_{u,l}^L \end{pmatrix}, \end{aligned} \quad (4.18)$$

with

$$\lambda_{\varphi,j}^L = +i\Lambda_c^{-1}\Lambda k_j - 1 \text{ and } \lambda_{\varphi,j}^R = -i\Lambda_c^{-1}\Lambda k_j - 1. \quad (4.19)$$

By solving (4.17), we derive the reflection amplitudes as,

$$A_l^L = -\frac{1 - \lambda_{v,+}^R \lambda_{u,r}^L}{1 - \lambda_{v,+}^R \lambda_{u,l}^L}, \quad A_-^L = 0. \quad (4.20)$$

We want to find the ratio between the incoming and reflected magnon spin current. Here, we define the spin current as the spatial current following from the conservation of the norm – without dissipative terms – $\|\Psi\| = |u|^2 - |v|^2$, i.e., $-i\partial_t \|\Psi\| \mp \Lambda i \partial_x J_s = 0$. Using the equations of motion (4.3), we find that the spin current is given by $iJ_s \Lambda = u \partial_x u^* - u^* \partial_x u + v \partial_x v^* - v^* \partial_x v$. Far from the interface, the Fourier transform of the spin current is dominated – for wave packets – by

$$J_s / \Lambda = \sum_{k_j} |A_j|^2 k_j (|u_{k_j}|^2 + |v_{k_j}|^2). \quad (4.21)$$

Finally, we derive the reflection coefficient as the ratio of reflected and incident spin currents, by combining Eqs. (4.14), (4.20) and (4.21),

$$R^2 \equiv -J_s^R/J_s^I = |A_l^I|^2. \quad (4.22)$$

We now distinguish between the cases $\omega > h_R$ and $h_L < \omega < h_R$. (i) If $\omega > h_R$ then $|A_l^I|^2 = 1$, hence we have perfect reflection in this instance. (ii) If $h_L < \omega < h_R$, then the reflection coefficient

$$R^2 = \frac{h_R - h_L + \Lambda_c^{-2}(\omega - h_L)(h_R - \omega) + 2\sqrt{\omega - h_L}\sqrt{h_R - \omega}}{h_R - h_L + \Lambda_c^{-2}(\omega - h_L)(h_R - \omega) - 2\sqrt{\omega - h_L}\sqrt{h_R - \omega}}. \quad (4.23)$$

For $\Lambda_c > \sqrt{h_R - h_L}/2$, the above expression is maximal at $\omega = (h_L + h_R)/2$ with the maximal reflection

$$R_{\max}^2 = 1 + 8\Lambda_c^2/(h_R - h_L). \quad (4.24)$$

On the other hand, if $\Lambda_c < \sqrt{h_R - h_L}/2$, the expression (4.23) is maximal for $\omega = (h_R + h_L)/2 \pm \sqrt{(h_R + h_L)(h_R + h_L - 4\Lambda_c^2)}/4$ with the maximal reflection

$$R_{\max}^2 = \frac{\sqrt{h_R - h_L} + |\Lambda_c|}{\sqrt{h_R - h_L} - |\Lambda_c|}. \quad (4.25)$$

For both cases, we find the maximum reflection $R_{\max} > 1$, which gives rise to spin wave amplification and is the magnonic analogue of the Klein paradox.

The physical picture of this anomalous reflection is illustrated in Fig. 4.1(c). Magnons with angular momentum (AM) \hbar are excited in the left domain and incident at the interface. The overlap of the magnon band in the left magnet with the antimagnon band in the right magnet, produced by the unequal external fields, guarantees that the magnons can propagate into the right film. According to AM conservation, a magnon current with AM \hbar propagating forward is expected to be produced in the right domain. However, magnons with AM \hbar are forbidden due to the antiparallel orientation of magnetization with respect to external field. To conserve AM, antimagnon currents with AM $-\hbar$ propagating backward are generated and thus enlarge the reflected current. Throughout the scattering process, the group velocity of transmitted

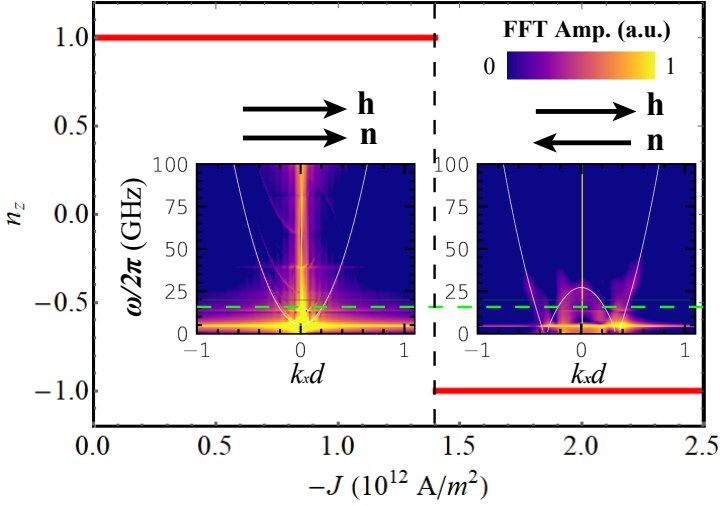


Figure 4.2: Steady state n_z of the right magnet as a function of current density (J) obtained by simulations. The insets show the simulated magnon spectrum for $J = 0$ and $-1.5 \times 10^{-12} \text{ A/m}^2$, respectively. The white lines are the analytical dispersions. The horizontal dashed line is the driving frequency of the microwave ($\omega_0/2\pi = 20$ GHz) to initiate magnon scattering.

antimagnons (v_g) is always positive to guarantee the forward flow of energy. As a comparison, in the original Klein paradox, an electrostatic potential lifts the positron band in the right region and makes it overlap with the electron band in the incident region, while in the present case an inhomogeneous field lifts the antimagnon band and makes it overlap with the magnon band (see Appendix A).

4.4 NUMERICAL VERIFICATION

To verify the analytical predictions and to account for effects of dissipation and non-linearities, we perform micromagnetic simulations on two exchange-coupled ferromagnetic thin films as shown in Fig. 4.1(a) (see Appendix B for simulation details). Here the inter-domain coupling A_i is a tunable coefficient

and is related to J_c in the theory as $J_c = -2A_i/d$. By applying a global driving microwave $\mathbf{h}(t) = h_0 \text{sinc}(\omega_c t) \hat{x}$ with $\omega_c/2\pi = 100$ GHz and $h_0 = 50$ mT, we first quantify the response of the magnetic system and identify two regimes as shown in Fig. 4.2. (i) When the current density $J > -1.4 \times 10^{12}$ A/m², the antiparallel state of the right domain ($\mathbf{n}_R \parallel -\mathbf{h}_R$) is dynamically unstable and the magnetization switches to the parallel state spontaneously ($\mathbf{n}_R \parallel \mathbf{h}_R$). The magnon spectrum of the right magnet for the steady parallel state is a normal parabola (left inset of Fig. 4.2)². (ii) When $J < -1.4 \times 10^{12}$ A/m², the antiparallel state becomes dynamically stable and the antimagnon states in the negative energy branch are excited, and a sombrero-like spectrum is identified (right inset of Fig. 4.2), consistent with the theory.

To study the magnon scattering off the interface between left and right magnets, a microwave source $\mathbf{h}(t) = h_0 \sin(\omega_0 t) \hat{x}$ is applied at the left domain at $x = -d_{si}$, with $d_{si} = 800$ nm. The excited magnons propagate in the $+\hat{x}$ direction and scatter at the interface ($x = 0$). By making a Fourier transform of $n_x(x, y, t)$ in the propagating direction (\hat{x})³, we derive the response of the system in momentum space as shown in Fig. 4.3(a). An antimagnon state with $k_x < 0$ is clearly identified in the right domain while the reflection coefficient is larger than one. This demonstrates the enhancement of magnon spin current via an analogue of the Klein paradox. In the absence of injection, the antimagnon current is barely excited. A detailed analysis of the evolution of incident, transmitted and reflected magnon current further verifies their correlation (see Appendix C).

Figure 4.3(b) shows that the reflected coefficient, defined as the peak-height ratio of the reflection magnons and incident magnons, increases with inter-

2 Here the lineshape of dispersion is consistent with the theoretical predictions (white lines), while we also notice a series of standing wave modes in the transverse direction ($k_y w = n\pi$, $n = 0, 1, 2, \dots$). For a real magnetic film with a sufficiently larger width, the lower modes of the standing waves will merge together. This will not have a significant influence on our results.

3 Here to eliminate the influence of magnons on the regions $x < -d_i$, which have the same wavevector and propagating direction as the reflecting magnons, the FFT is only performed at the region between the microwave source and the interface while same sized region is taken in the right domain.

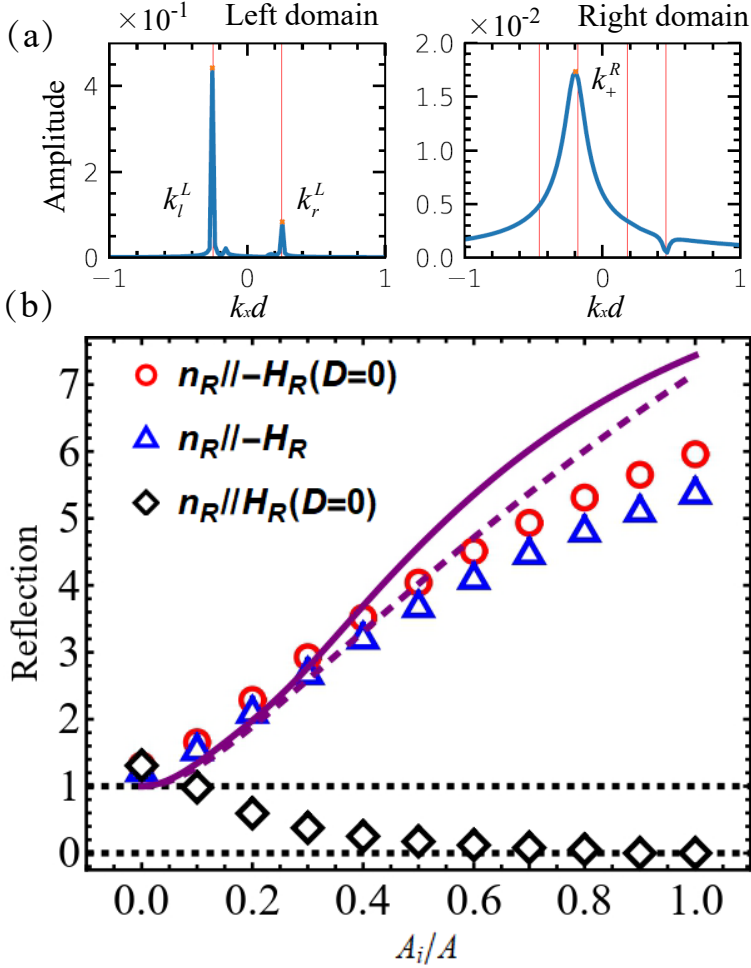


Figure 4.3: (a) Scattering of magnons at the interface of left and right domains. $h_0 = 10$ mT, $A_i/A = 1$. The red vertical lines represent the theoretical predictions of magnon wavevectors. (b) Reflection of magnons as a function of inter-domain exchange couplings. The DMI strength is $D = 0$ (red circles) and $D = 0.1$ mJ/m² [114] (blue triangles). The purple dashed line is prediction by Eq. (4.23), and the solid line is the prediction with shape anisotropy.

domain exchange coupling. For comparison, we also simulate the magnon scattering in the parallel configuration ($\mathbf{n}_R \parallel \mathbf{h}_R$) and find that the reflection keeps decreasing to zero with increasing the coupling between the magnetic films (black diamonds). As expected, no antimagnon state is excited in this case. We find a good agreement between the analytical prediction in Eq. (4.23) and the micromagnetic simulations for small couplings. For large exchange couplings, however, we see quantitative differences, which are not explained by including dipolar anisotropy – see purple solid line in Fig. 4.3(b). We expect the quantitative difference at large couplings to stem from non-linear effects, which are not treated in the analytical formalism. The reflection amplitudes become increasingly large at increasing couplings, thereby making non-linear effects important.

4.5 DISCUSSIONS AND CONCLUSIONS

In conclusion, we have analytically shown and numerically confirmed that the magnon spin current can be amplified through the realization of the bosonic Klein paradox in a driven-dissipative magnetic system. The Dzyaloshinskii-Moriya interaction (DMI) caused by the interfacial symmetry breaking in the hybrid system does not change the results significantly, as shown in Fig. 4.3(b). In our proposal, we dynamically stabilize the antimagnons by the SOT. The essential physics is applicable to a wide class of materials and driving knobs which are able to maintain the magnetization against the external field. For example, electric currents through spin-transfer torque [115], optical waves through magneto-optical interaction [116] and other effective techniques capable of producing a positive damping of the magnons. Our proposal therefore can be realized in ferromagnetic insulators as well as metals. Experimentally, the magnons may be detected by optical, inductive and even electric techniques [117–119].

4.A DETAILED COMPARISON BETWEEN THE ORIGINAL AND THE MAGNON KLEIN PARADOX

In this section, we address the analogue between the original Klein paradox and the magnon Klein paradox presented in the main text. In the original Klein paradox, Klein studied scattering of an electron off a potential barrier [99], as shown in the top panel of Fig. 4.4(a). The electrostatic potential in the right domain will lift the negative energy band of positrons [blue line in Fig. 4.4(a)] and makes it overlap with the positive energy band of electrons on the left (red line). Then, the incident electrons from the left domain can excite positron current moving to the right in the right domain. This corresponds to left-moving electron current and thus could enhance the reflection of electrons at the interface. A detailed treatment of this scattering process can be found in the literature [104]. In the magnon Klein paradox, an inhomogeneous external field, for example, can induce the band overlap of the magnons band in the left domain with the antimagnon band in the right domain, as shown in Fig. 4.4(b). Again, the antimagnon current generated at the interface enhances the strength of the reflected magnon current. The underlying physics of the original and magnon Klein paradox is therefore the same. This is so despite that the magnon bands on the left and right domains also overlap, but their coupling is very weak in our setup, and thus does not change the essential physics.

4.B PARAMETER SPECIFICATION IN NUMERICAL SIMULATIONS

The magnetization dynamics of the two exchange-coupled magnetic films are simulated by numerically solving Eq. (5.2). Note that the dissipation of magnon spin current caused by its interaction with the environment is phenomenologically covered by the Gilbert damping, while identifying its microscopic mechanism including spin-orbit interaction, spin pumping and two-magnon scattering [25] is not the focus of our current work.

The dimensions of the nanostrip on each domain are length $l = 2048$ nm, width $w = 64$ nm and thickness $d = 2$ nm. The SOT strength $J_L = 0$, and

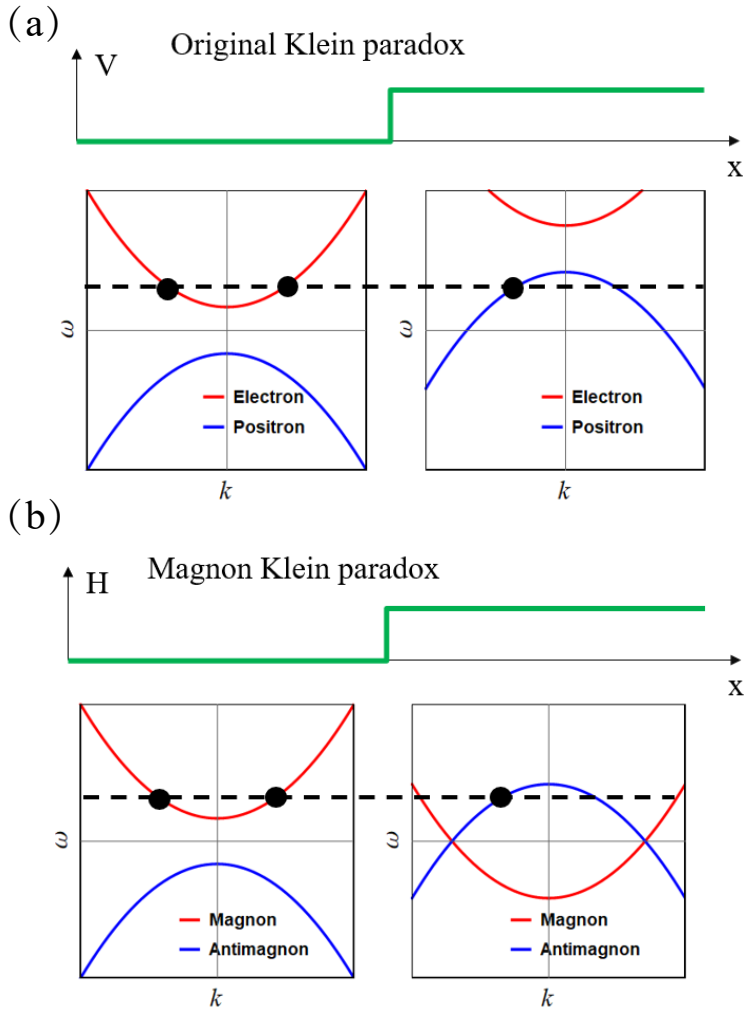


Figure 4.4: Comparison between the original and magnon Klein paradox. The top panel (green line) sketches the “potential” distribution while the bottom panel sketches the dispersion relation of particles (red lines) and antiparticles (blue lines).

$J_R = J\hbar\theta_{SH}/(2M_s|e|d)$, where J is current density, θ_{SH} is the spin-Hall angle of the heavy-metal layer, and e is electron charge. Here we use the magnetic parameters of YIG/Pt, i.e., exchange coefficient $A = 3.1 \times 10^{-12}$ J/m, saturation magnetization $M_s = 1.92 \times 10^5$ A/m, spin-Hall angle $\theta_{SH} = 0.1$ [120], Gilbert damping $\alpha = 10^{-2}$. The inter-domain coupling A_i is assumed to be a tunable coefficient and it is related to the coupling coefficient J_c in the theory as $J_c = -2A_i/d$. The mesh size is $2 \times 2 \times 2$ nm³. Absorptive boundary conditions are taken on the left domain to eliminate the influence of boundary reflection of magnons. The *Mumax*³ [121] package is employed to numerically solve the LLG equation (5.2).

4.C CORRELATIONS OF INCIDENT, REFLECTED, AND TRANSMITTED MAGNON SPIN CURRENT

In the main text, we consider a classical model in which the antimagnons in the right domain can only be excited by an incoming magnon current from the left domain dynamically stabilized by SOTs. Without an incoming spin current from the left magnet, the right domain stays in the dynamically stabilized state, where the magnetization is pointing against the external field. Continuous emission of antimagnons would be present in a quantum mechanical treatment of the problem since there is no true ground state of the system. This can be interpreted as an analogue of Hawking radiation. Since we are considering a classical theory in this Letter, spontaneous emission of antimagnons is not captured by our classical model.

To verify the temporal correlation of antimagnon excitation and injected magnons, we plot the evolution of incident, reflected and transmitted magnon spin current in Fig. 4.5. Right after the microwave source located in the left domain is turned on, the excitations of both magnons and antimagnons are nearly zero [Fig. 4.5(a)], where the tiny excitations are mainly resulting from the fluctuation of spins in the ground state. Around 0.5 ns, the magnons on the left domain are significantly injected and propagate toward the interface [Fig. 4.5(b)]. Around 0.7 ns, the magnons reach the interface of left and right domains and inject the antimagnon current in the right domain [Fig. 4.5(c)].

Meanwhile, the reflected spin current appears and is amplified. As more antimagnons are excited, the reflection also becomes stronger [Fig. 4.5(d)]. This indeed verifies the temporal correlation between incident, reflected and transmitted magnon spin current.

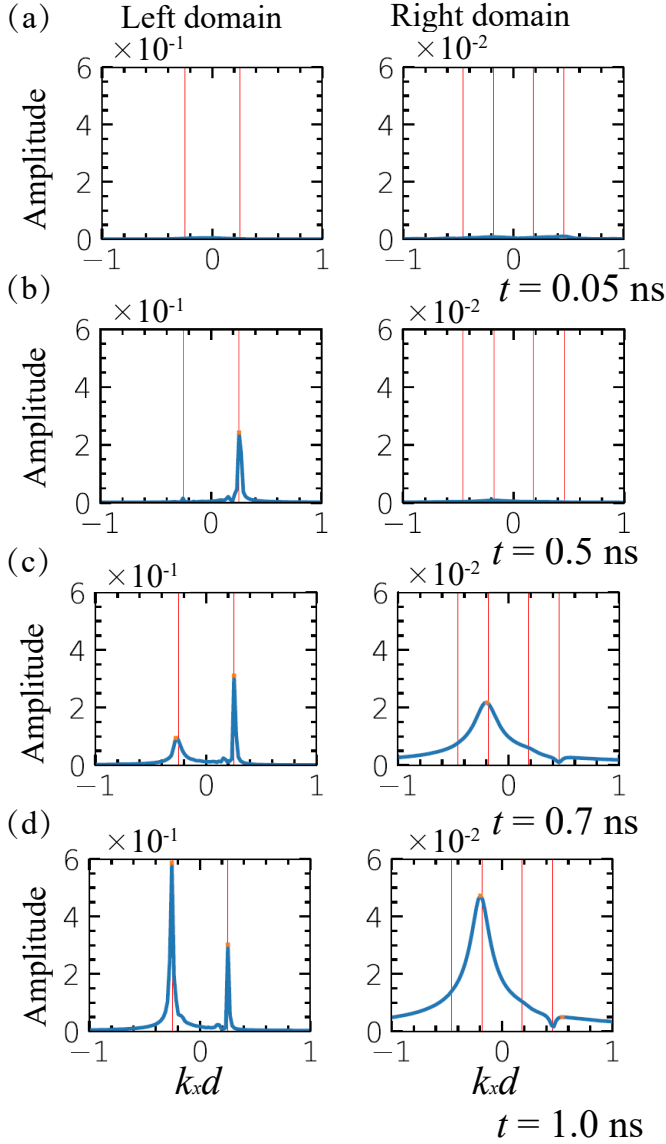


Figure 4.5: Evolution of incident, reflected and transmitted magnons at $t = 0.05$ ns (a), 0.5 ns (b), 0.7 ns (c) and 1.0 ns (d), respectively. The microwave source located on the left domain is turned on at $t = 0$ ns to excite magnons and then the magnons propagate toward the interface 800 nm away from the microwave source. All the other parameters are the same as Fig. 3(a) of the main text.

5

NON-LINEAR DYNAMICS NEAR EXCEPTIONAL POINTS OF SYNTHETIC ANTIFERROMAGNETIC SPIN-TORQUE OSCILLATORS

This Chapter is based on R. A. Duine, V. Errani, and J. S. Harms, “Nonlinear dynamics near exceptional points of synthetic antiferromagnetic spin-torque oscillators,” *Phys. Rev. B* **108**, 054428 (2023). R.A.D. conceived the project, J.S.H. did the analytic calculations and V.E performed the numerical simulations. V.E. and J.S.H. prepared the manuscript. All authors contributed to the manuscript.

In this chapter, we consider a synthetic antiferromagnetic spin-torque oscillator with anisotropic interlayer exchange coupling. This system exhibits exceptional points in its linearized dynamics. We find the non-linear dynamics and the dynamical phase diagram of the system both analytically and numerically. Moreover, we show that, near one of the exceptional points, the power of the oscillator depends extremely sensitively on the injected spin current. Our findings may be useful for designing sensitive magnetometers and for other applications of spin-torque oscillators.

5.1 INTRODUCTION

For the design of many applications, such as magnetometers, converters and amplifiers, a strong response to perturbations is preferred. One way to achieve this strong response, is to make use of the existence of exceptional points (EPs) [122–124]. EPs are characterized by a square-root dependence of the

imaginary part of the eigenfrequencies on some system parameters, which enables a large dynamic response as a result of a small change in a parameter. Mathematically, EPs correspond to the coalescence of different eigenvalues and eigenvectors in parameter space [62, 125]. EPs are studied intensely since they might lead to better sensors [122–124], and yield a variety of interesting phenomena such as lasing [126], spontaneous emission [127], and give rise to geometric phases when encircling them [128]. Examples of physical systems that exhibit EPs are optical microcavities [129] and other photonic systems [124, 130], optical lattices with engineered defects [131], electromechanical systems [132], superconducting resonators [133], nodal superconductors [129], semimetals [134–136] and magnetic systems [137–143]. While EPs have been studied intensely in the linear regime, the non-linear regime remains relatively unexplored.

In this Chapter, we consider a synthetic antiferromagnetic (SAF) spin-torque oscillator (STO), i.e., a spin-torque oscillator that consists of two magnetic layers that are coupled by the Ruderman–Kittel–Kasuya–Yosida (RKKY) interactions. We consider the situation that one of the two magnetic layers is driven by means of the injection of spin current. This could be achieved by spin-orbit torque or by spin-transfer torque [144]. Generically, an STO is a magnetic system in which the damping is compensated by the injection of spin angular momentum from a spin current to yield precessional magnetic dynamics [143, 145–147]. These oscillators have potential for a wide range of applications, such as detectors, microwave signal sources [148, 149], microwave-assisted magnetic recording and neuromorphic computation [150, 151].

The SAF STO that we consider has anisotropic RKKY coupling and exhibits EPs in its linearized dynamics. We consider the full non-linear dynamics analytically and find the limit cycles of the magnetization dynamics. Moreover, we show that the dynamics becomes relatively simple close to the EPs because the power and precessing frequency depend linearly on the injected spin current. These analytical results agree with numerical computations and lead to a complete understanding of the steady-state behaviour of the system. Furthermore, we find from our analysis that the

magnetization dynamics is extremely sensitive to small changes in parameters in the sense that the slope of the steady-state power with respect to injected spin current diverges close to one of the EPs. This result cannot be obtained from a linear analysis and the non-linear description is therefore needed. A complementary work to ours is that of Deng *et al.* [152] who numerically consider the non-linear dynamics of an STO near a different type of EP. Another recent closely-related complementary work is that of Ref. [153].

The remainder of this Chapter is organized as follows. In the next section, we present the model and determine the eigenfrequencies and stability conditions from a linear analysis. In the second section, we consider the non-linear dynamics close to the EPs and find the limit circles of the magnetic dynamics. In the third section, we consider the magnetization dynamics numerically and find the dynamical phase diagram. We end with a brief conclusion and outlook.

5.2 LINEAR ANALYSIS

We consider a spin-torque oscillator composed of two RKKY coupled nanomagnets subject to the same external magnetic field and uniaxial anisotropy, see Fig. 5.1. For simplicity, we take both magnetic layers to be identical. Furthermore, spin angular momentum is injected into the bottom magnetic layer. The magnetic energy is given by

$$E = -B(m_{U,z} + m_{L,z}) - K(m_{U,z}^2 + m_{L,z}^2)/2 \quad (5.1)$$

$$- J_{\perp}(m_{U,x}m_{L,x} + m_{U,y}m_{L,y}) - J_z m_{U,z}m_{L,z} ,$$

where U denotes the upper- and L the lower macrospin, and $m_{L/U,i}$ the i -th Cartesian component of the macrospin. Furthermore, K is the uniaxial anisotropy constant, $B > 0$ the external magnetic field directed along the z axis, J_{\perp} the in-plane RKKY interaction, and J_z its out-of-plane component. We take the RKKY interaction to be anisotropic because, first of all, it will typically be anisotropic, and second, the anisotropic coupling enriches the phase diagram.

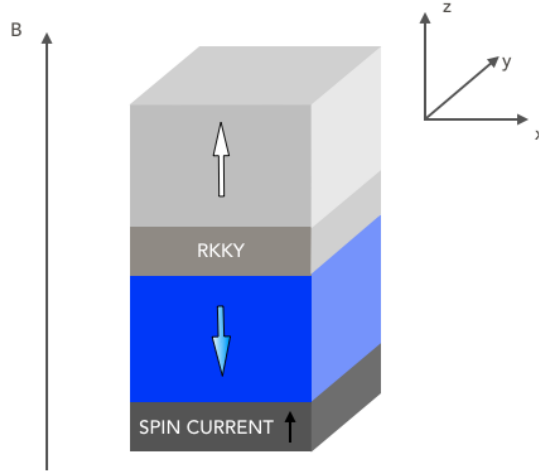


Figure 5.1: A synthetic antiferromagnetic spin torque oscillator in an external magnetic field $B\hat{z}$. Spin angular momentum is injected into the bottom magnetic layer.

For temperatures below the Curie temperature the magnetization dynamics is well described by the Landau-Lifschitz-Gilbert (LLG) equation with the inclusion of the injected spin current

$$\frac{\partial \mathbf{m}_\nu}{\partial t} = -\mathbf{m}_\nu \times \mathbf{h}_{\text{eff},\nu} + \alpha \mathbf{m}_\nu \times \frac{\partial \mathbf{m}_\nu}{\partial t} + I_{s,\nu} \mathbf{m}_\nu \times (\mathbf{m}_\nu \times \hat{z}), \quad (5.2)$$

with the effective field $\mathbf{h}_{\text{eff},\nu} = -\gamma \delta E / \delta \mathbf{m}_\nu$. Here, ν denotes either the lower (L) or the upper (U) macrospin, α the dimensionless Gilbert damping and $I_{s,U} = 0$, $I_{s,L} = I_s > 0$ the spin current. The sign of the spin current is such that it tends to align the bottom magnetic layer against the external field. Since the Gilbert damping is typically small, $\alpha \ll 1$, we work in most of what follows to lowest order in α and discard terms of the order αI_s as well. Furthermore, we set $\gamma = 1$ so that B, K, J_\perp and J_z have units of frequency.

For the case that $K > 0$, the magnetic energy (5.1) yields four configurations where the torques on the magnetization direction in both layers vanish simultaneously: these are both layers pointing up, both pointing down, and

the two anti-parallel configurations. Depending on the parameters, these configurations are energy extrema that are stable, or unstable. For large fields, the configuration with both spins pointing up is stable. For large spin currents, the bottom layer is forced to point downward, while, depending on the strength and sign of the RKKY coupling, the top layer may point down or up.

The most interesting configuration for our purposes is the antiparallel configuration. As we shall see below, the linearized dynamics around this configuration yields an EP. This may be anticipated because, in the absence of dissipation, i.e., when $\alpha = 0$ and $I_s = 0$, the antiparallel configuration in an external field is reminiscent of a system of two coupled harmonic oscillators with one of the oscillators having a potential energy that is inverted. This latter system is known to yield an EP [154]. Because $I_s > 0$ we consider the situation where the bottom magnetic layer is pointing against the field.

We investigate the stability of a given magnetic state by linearizing the LLG equations for small deviations around that state. For the reasons mentioned above, we focus on the antiparallel configuration with the magnetization of the bottom layer pointing against the external field, which yields the eigenfrequencies

$$\begin{aligned}
 (\alpha^2 + 1)\omega_{\pm} &= B - i\alpha(K - J_z) - (i - \alpha)I_s/2 \\
 &\pm \sqrt{[K - J_z - i\alpha B + (i - \alpha)I_s/2]^2 - (\alpha^2 + 1)J_{\perp}^2}.
 \end{aligned}
 \tag{5.3}$$

From this expression, we find that the parameters for which the system exhibits an EP by setting the expression under the square root equal to zero. To lowest order in α and I_s this yields $J_{\perp}^2 = (K - J_z)^2$ and $I_s = 2\alpha B$. Close to this EP and, in particular, when the expression underneath the square-root is negative, the imaginary part of the eigenvalues depends strongly on small changes in parameters. Physically, this implies that a small change in parameters may yield a strong dynamic response, because a positive imaginary part of the eigenfrequency corresponds to exponential growth of small-amplitude fluctuations. By determining when the imaginary part of the

above eigenfrequency changes sign, we find that the antiparallel configuration is stable when

$$\frac{I_s}{2\alpha} > \frac{-K - J_z + |K - J_z|B/\sqrt{(K - J_z)^2 - J_\perp^2}}{1 + |K - J_z|/\sqrt{(K - J_z)^2 - J_\perp^2}}, \quad (5.4a)$$

$$\frac{I_s}{2\alpha} < \frac{-K - J_z - |K - J_z|B/\sqrt{(K - J_z)^2 - J_\perp^2}}{1 - |K - J_z|/\sqrt{(K - J_z)^2 - J_\perp^2}}. \quad (5.4b)$$

In the next section we focus on the non-linear dynamics outside this range of dynamical stability. As we shall see, the power of the STO is extremely sensitive to small changes in the current around this EP for $K > 0$, but not when $K < 0$.

5.3 NON-LINEAR DYNAMICS

In this section we discuss the non-linear dynamics of the system described in Section 5.2 and in specifically focus on the limit cycles of the model.

The reactive dynamics is formulated by means of the Poisson bracket $\{m_\alpha, m_\beta\} = \epsilon_{\alpha\beta\gamma}m_\gamma$. From here we define the canonical coordinates $p_{U/L} = m_{U/L,z}$ and $\theta_{U/L} = \arctan(m_{U/L,y}/m_{U/L,x})$, that correspond to the total power and angle of the oscillator and which have non-zero Poisson brackets $\{p_{U/L}, \theta_{U/L}\} = 1$. We continue performing yet another coordinate transformation that makes use of the rotational symmetry around the z -axis:

$$\begin{aligned} \mu &= (p_U + p_L)/2, & \eta &= (p_U - p_L)/2, \\ \theta &= \theta_U + \theta_L, & \phi &= \theta_U - \theta_L, \end{aligned} \quad (5.5)$$

where $\mu \in [-1, 1]$ and $\eta \in [-1 + \mu, 1 - \mu]$. The above coordinates have $\{\mu, \theta\} = 1$ and $\{\eta, \phi\} = 1$ as non-vanishing Poisson brackets. In these coordinates the Hamiltonian (internal energy) in Eq. (5.1) becomes

$$\begin{aligned} h \equiv E &= -2B\mu - K(\mu^2 + \eta^2) - J_z(\mu^2 - \eta^2) \\ &\quad - J_\perp \sqrt{[1 - (\mu + \eta)^2][1 - (\mu - \eta)^2]} \cos(\phi), \end{aligned} \quad (5.6)$$

where the rotation symmetry around the z -axis ensures that the right-hand side of the above does not depend on θ . The Hamilton equations of motion are accordingly given by

$$\dot{\mu} = \{\mu, E\} = \{\mu, \theta\} \partial_\theta E = 0, \quad (5.7a)$$

$$\dot{\theta} = 2B + 2(K + J_z)\mu - \frac{2J_\perp \mu (1 + \eta^2 - \mu^2) \cos(\phi)}{\sqrt{[1 - (\mu + \eta)^2][1 - (\mu - \eta)^2]}}, \quad (5.7b)$$

$$\dot{\phi} = 2(K - J_z)\eta - \frac{2J_\perp \eta (1 + \mu^2 - \eta^2) \cos(\phi)}{\sqrt{[1 - (\mu + \eta)^2][1 - (\mu - \eta)^2]}}, \quad (5.7c)$$

$$\dot{\eta} = 2J_\perp \sqrt{[1 - (\mu + \eta)^2][1 - (\mu - \eta)^2]} \sin(\phi), \quad (5.7d)$$

where the rotation symmetry guarantees that the total power is conserved. For the limit cycles we expect $\dot{\phi} = \dot{\eta} = 0$, since both spins experience the same magnetic field strength and are thus expected to have equal angular velocity. Using this ansatz, we find two possible expressions for the difference in power η in terms of the total power μ for $J_\perp^2 < K^2$, which are given by

$$\eta = 0, \quad \eta^2 = 1 + \mu^2 - \frac{2|K - J_z||\mu|}{\sqrt{(K - J_z)^2 - J_\perp^2}}. \quad (5.8)$$

In case $J_\perp^2 > (K - J_z)^2$ we are only left with $\eta = 0$ as a solution, since we require η to be real.

The model under consideration furthermore has dissipative contributions in the form of Gilbert damping and the injection of spin angular momentum. Up to first order in the Gilbert damping constant α the dynamics of total power μ and the relative power η due to Gilbert damping is given by

$$\begin{aligned} \dot{\mu}/\alpha &= [B + (K + J_z)\mu] (1 - \mu^2 - \eta^2) - 2(K - J_z)\eta^2\mu \\ &\quad - J_\perp \sqrt{[1 - (\mu + \eta)^2][1 - (\mu - \eta)^2]} \cos(\phi)\mu \end{aligned} \quad (5.9a)$$

$$\begin{aligned} &= B(1 + \mu^2 - \eta^2) + [h + J_z + K(1 - 2\eta^2)]\mu. \\ \dot{\eta}/\alpha &= [-2B\mu + K(1 - 3\mu^2 - \eta^2) - J_z(1 + \mu^2 - \eta^2) \\ &\quad - J_\perp \sqrt{[1 - (\mu + \eta)^2][1 - (\mu - \eta)^2]} \cos(\phi)]\eta. \end{aligned} \quad (5.9b)$$

$$= [h + K(1 - 2\mu^2) - J_z]\eta.$$

The influence of SOT, up to first order in I_s , on the dissipative dynamics is, on the other hand, given by

$$\dot{\mu}/I_s = [(\mu - \eta)^2 - 1]/2, \quad (5.10a)$$

$$\dot{\eta}/I_s = [1 - (\mu - \eta)^2]/2. \quad (5.10b)$$

With this set up we are in the position to discuss the limit cycles of the model and their stability. Again for all values of J_\perp , $\eta = 0$ will be a solution of $\dot{\phi} = \dot{\eta} = 0$. Furthermore, for $J_\perp^2 < K^2$ we additionally have $\eta^2 = 1 + \mu^2 - 2|K||\mu|/\sqrt{K^2 - J_\perp^2}$ as a solution. Below we address limit cycles and stability in for the solution $\eta = 0$, which covers, as we shall see, the behaviour near the EP. For completeness, we address the other type of limit cycles and their stability in Sections 5.A to 5.D.

When $\eta = 0$ the equation for the total power μ becomes

$$\dot{\mu}/\alpha = [B - I_s/2\alpha + (K + J_z - |J_\perp|)\mu](1 - \mu^2). \quad (5.11)$$

This has two steady state solutions

$$\mu = \pm 1, \quad \mu = \frac{B - I_s/2\alpha}{|J_\perp| - J_z - K}, \quad (5.12)$$

with $\mu = m_{U,z} = m_{L,z}$. The first solution describes both macrospins aligning in the $\pm \hat{z}$ direction. The second solution on the other hand describes the limit cycle towards which the system converges for sufficiently large times. Furthermore, this limit cycle has a precessional frequency of

$$\dot{\theta} = I_s/\alpha. \quad (5.13)$$

From the fixed point analyses presented in Section 5.B these fixed points are stable if $\partial_\mu \dot{\mu} < 0$ and $|J_\perp|(1 + \mu^2) > (K - J_z)(1 - \mu^2)$. Alternatively, these limit cycles are unstable if one of the above constraints is not satisfied. The limit cycle solution $\mu = (B - I_s/2\alpha)/(|J_\perp| - J_z - K)$ is thus stable if $\max[K + J_z, (K - J_z)(1 - \mu^2)/(1 + \mu^2)] < |J_\perp|$. While the static solution with $\mu = \pm 1$ on the other hand is stable if $\mp(B - I_s/2\alpha) < K + J_z - |J_\perp|$.

In conclusion, we find that the power of the SAF is quite sensitive to small perturbations around the point $|J_\perp| \gtrsim K + J_z$, where the slope of the total

power $\mu = m_{U,z} = m_{L,z}$ with respect to $I_s/2\alpha$ is given by $(|J_\perp| - J_z - K)^{-1}$ in Eq. (5.12). The total power of the oscillator therefore depends sensitively on injected spin current around this point. Hence, we find an enhanced sensitivity if $K + J_z > 0$ for $J_\perp > K + J_z$.

5.4 NUMERICAL RESULTS

In this section we determine all the dynamical phases of the synthetic anti-ferromagnetic oscillator using numerical solutions. For concreteness, we focus on the case that $J_z = 0$. We solve the LLG equation (5.2) numerically for different values of the coupling J_\perp and current I_s starting from the antiparallel configuration with a small initial perturbation. In Fig. 5.2 we present the long-time behaviour in each region of the dynamical phase diagram, with the blue spin denoting the magnetic layer that is driven by spin current. We note that a change in the external magnetic field B results in a rigid upward- or downward shift of the phase diagram. The black lines in Fig. 5.2 are the analytically predicted phase boundaries from Eqs. (5.4) and (5.12). We find a very good agreement between the analytic predictions and the results from numerical solutions.

There are three regions where the spin configuration is static (I, II, and III), and one region, IV, where the magnetization is oscillating. The region in Fig. 5.2 with $J_\perp < K$ may be interpreted in the following way. If we start from zero coupling and increase the current we observe that the configuration is initially parallel with both macrospin aligned upward (region I). This is what we expect since for small values of the current the spin current is not large enough to compensate the Gilbert damping and the two macro-spins both align with the external magnetic field. Increasing the current further, the system is able to keep the initial configuration (region II), since now the current is enough to compensate for the damping (light-blue macro-spin pointing downwards), but the coupling is too small to make the white macrospin, i.e., the magnetic layer into which no spin current is injected, flip. Indeed for increasing values of the coupling and sufficiently high current both macro-spins are aligned against the external field (region III).

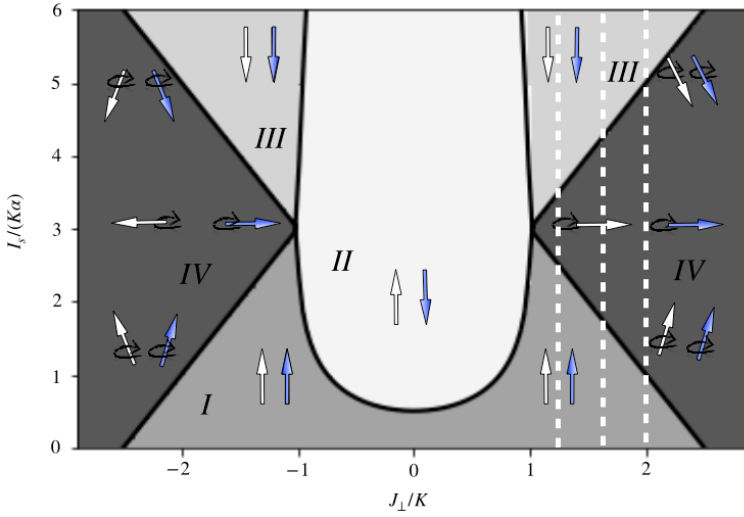


Figure 5.2: Dynamical phase diagram for $K > 0$ as a function of coupling J_{\perp} and current I_s . The analytical predictions from Eqs. (5.4) and (5.12) are plotted as the black lines. The steady-state configuration is indicated for each region. The region IV correspond to oscillations. The z -component of the magnetization in this region depends on the injected spin current. We took $B/K = 1.5$ and $J_z = 0$.

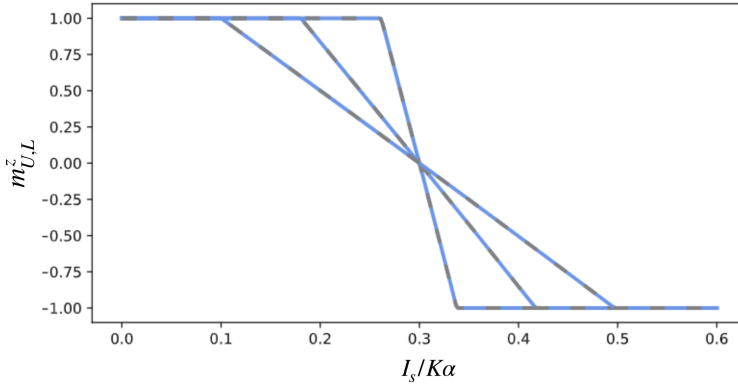


Figure 5.3: Plot of the z direction of the macrospins in both synthetic layers as a function of the current I_s . The three different lines correspond to different values in the coupling strength ($J_{\perp}/K = 1.2, 1.6, 2$), with the steeper slope corresponding to decreasing J_{\perp} . These values are depicted by the dotted lines in Fig. 5.2. Parameters taken are $B/K = 1.5$ and $J_z = 0$.

When considering the non-linear behaviour beyond the EP, region IV is of most interest. In this region the two macro-spins are oscillating, with a frequency I_s/α depending only on the current I_s and the damping α . These two macrospins exhibit nearly parallel orientations for positive values of the coupling and antiparallel orientations for negative values. In Fig. 5.3 we show the z component of the magnetization as a function of the current I_s , in which the different lines correspond to the vertical dashed lines in Fig. 5.2. The numerical simulations confirm that the current and the macrospin orientation are related in a linear way given by Eq. (5.12).

We have focused on the situation that $J_z = 0$, which is the most interesting because all the four phases (I, II, III, IV) meet at one point. In fact, starting from (Fig. 2) and increasing J_z , only the three regions I, III and IV meet at the two points, since the antiparallel region progressively shrinks and the points shift outward. If instead we consider negative values of J_z , the antiparallel region progressively enlarges and the region I decreases.

5.5 DISCUSSION AND CONCLUSIONS

We analytically and numerically explored the non-linear behaviour of a synthetic antiferromagnetic spin-torque oscillator with anisotropic RKKY coupling. We found that the EP which is found in its linearized dynamics leads to enhanced sensitivity of the power of the oscillator, in particular as a function of injected spin current. This enhanced sensitivity may be used to engineer magnetometers or sensors of spin current. Furthermore, recent work shows that it is possible to use spin torque nano-oscillators to implement different computing schemes and to classify waveforms [151]. Moreover, spin-torque oscillators may be used as tunable spin-wave emitters that excite a specific spin wave depending on the current. We expect that the enhanced sensitivity we predict is an asset for such applications.

Regarding the experimental realization of our model, an ingredient is the anisotropic interlayer coupling. This anisotropic exchange coupling is not essential but makes the phase diagram much richer. Anisotropic exchange coupling has been proposed and experimentally observed in Refs. [155, 156].

The required anisotropies may be engineered by interfaces with heavy metals and/or engineering the shape of the magnetic layers, whereas the interlayer coupling may be tuned by varying the thickness of the non-magnetic spacer. In our approach we have relied on a macrospin approximation. This is a good description and is in agreement with micromagnetic simulation and experimental results for STOs with diameters < 30 nm [157].

Future work could focus on the inclusion of thermal fluctuations. We expect that these will affect the phase but not the orientation or the amplitude of the oscillations. Finally, we hope that our work, together with that of Deng *et al.* [152], inspires the operation of STOs near EPs. In fact, while resubmitting this work a recent preprint appeared [158] which has experimentally observed EPs in STOs, albeit in a set-up that is slightly different from ours.

ACKNOWLEDGEMENTS

J.S.H. would like to thank W. Q. Boon for fruitful discussions.

5.A SECOND TYPE OF LIMIT CYCLES FOR $J_{\perp}^2 < K^2$ FOR $J_z \rightarrow 0$

For $J_{\perp}^2 < K^2$ we also need to consider $\eta^2 = 1 + \mu^2 - 2|K||\mu|/\sqrt{K^2 - J_{\perp}^2}$ as a solution to $\dot{\phi} = \dot{\eta} = 0$. Using the above ansatz we find that Eqs. (5.9a) and (5.10a) give

$$\begin{aligned} \dot{\mu}/\alpha = & \left[B + K\mu - \frac{I_s}{2\alpha} \right] \left[-2\mu^2 + \frac{2|K||\mu|}{\sqrt{K^2 - J_{\perp}^2}} \right] - \mu \frac{J_{\perp}^2}{K} \frac{2|K||\mu|}{\sqrt{K^2 - J_{\perp}^2}} \\ & - 2K\mu \left[1 + \mu^2 - \frac{2|K||\mu|}{\sqrt{K^2 - J_{\perp}^2}} \right] - \frac{I_s}{\alpha} \text{sgn}(\eta)\mu \sqrt{1 + \mu^2 - \frac{2|K||\mu|}{\sqrt{K^2 - J_{\perp}^2}}}. \end{aligned} \quad (5.14)$$

In first instance we note that $\mu = 0$ gives a static solution to the above equation. This describes the configuration in Fig. 5.1, in which two spins point in opposite direction. From Section 5.C it follows that a requirement

for stability of this phase is $\partial_{\mu}\dot{\mu} < 0$ at the fixed point. This requirement for stability, with $\text{sgn}(\eta) = 1$, becomes

$$\frac{-K - |K|B/\sqrt{K^2 - J_{\perp}^2}}{1 - |K|/\sqrt{K^2 - J_{\perp}^2}} > \frac{I_s}{2\alpha} > \frac{-K + |K|B/\sqrt{K^2 - J_{\perp}^2}}{1 + |K|/\sqrt{K^2 - J_{\perp}^2}}. \quad (5.15)$$

These are precisely the same conditions as in Eq. (5.4) for $J_z \rightarrow 0$. The fixed point with $\text{sgn}(\eta) = -1$ on the other hand is stable if

$$\frac{K + |K|B/\sqrt{K^2 - J_{\perp}^2}}{1 + |K|/\sqrt{K^2 - J_{\perp}^2}} > \frac{I_s}{2\alpha} > \frac{-K + |K|B/\sqrt{K^2 - J_{\perp}^2}}{-1 + |K|/\sqrt{K^2 - J_{\perp}^2}}. \quad (5.16)$$

we see that the configuration with $\text{sgn}(\eta) = -1$ is always unstable, since there is no interval for stability.

In order to make progress in the regime where we expect limit cycles we rewrite Eq. (5.14)

$$\begin{aligned} g(I_s, \mu) &= \dot{\mu}/\alpha|\mu| \\ &= (1 - 2\epsilon|\mu|) \times \left[2K[\mu - \text{sgn}(\mu)\epsilon] + \left(B - \frac{I_s}{2\alpha} \right) \right] - \text{sgn}(\mu)\epsilon\frac{I_s}{\alpha}\eta(\mu), \end{aligned} \quad (5.17)$$

where $\epsilon \equiv \sqrt{K^2 - J_{\perp}^2}/2|K| \in (0, 1/2)$. Let us analyse the above equation in a bit more detail. We assume that $\mu > 0$ at the fixed point, from here we find that Eq. (5.17) implies

$$\frac{I_s}{2\alpha} = \frac{B + 2K(\mu - \epsilon)}{1 + 2\epsilon\eta/(1 - 2\epsilon\mu)}. \quad (5.18)$$

From Section 5.C we find the stability requirement $\dot{\mu} \leq 0$ for limit cycles of Eq. (5.17) to be

$$\frac{I_s}{2\alpha} \frac{1 - 4\epsilon^2}{(1 - 2\epsilon\mu)^2} + 2K\eta < 0. \quad (5.19)$$

We like to find the minimal current I_s for these limit cycles to be stable, hence we like to find the current for which Eq. (5.19) is zero, in other words

$\partial_\mu \dot{\mu} = \partial_\mu g(I_s, \mu)|_{I_s(\mu)} = 0$. On the other hand we know $g(I_s(\mu), \mu) = 0$ is the limit cycle –fixed point– condition. From here we find $d_\mu g(I_s(\mu), \mu) = (\partial_{I_s} g)(\partial_\mu I_s) + \partial_\mu g = 0$, and hence $\partial_\mu I_s = 0 \leftrightarrow \partial_\mu g \equiv \partial_\mu \dot{\mu} = 0$. Thus when looking for the critical current it is sufficient to consider $\partial_\mu I_s = 0$. We proceed by writing Eq. (5.18) as

$$(1 - 2\epsilon\mu + 2\epsilon\eta)I_s/2\alpha = (1 - 2\epsilon\mu)(B + 2K(\mu - \epsilon)).$$

Furthermore, we take the derivative with respect to μ of the above and note that we are considering points which satisfy $\partial_\mu I_s = 0$. This leaves us with

$$(1 - 2\epsilon\mu + 2\epsilon\eta)I_s/2\alpha = [2\epsilon(B + 2K(\mu - \epsilon)) + 2K(1 - 2\epsilon\mu)]\eta.$$

which according to Eq. (5.18) gives us

$$(1 - 2\epsilon\mu)(B + 2K(\mu - \epsilon)) = [2\epsilon B - 2K(1 - 4\epsilon\mu + 2\epsilon^2)]\eta. \quad (5.20)$$

In order to proceed we assume $\eta^2 \ll 1$ around the critical current. A consequence of the above is that we assume $\mu_\epsilon - \delta\mu \ll 1$ with

$$\mu_\epsilon = \frac{1}{2\epsilon} \left(1 - \sqrt{1 - 4\epsilon^2} \right), \quad (5.21)$$

and from relation (5.8) we see that $\eta^2 \sim (2\epsilon)^{-1} \sqrt{1 - 4\epsilon^2} \delta\mu$ at linear order in $\delta\mu$ and η^2 . By squaring Eq. (5.20) and expanding up to linear order in $\delta\mu$ we find the solution to be

$$2\delta\mu \sim \sqrt{\frac{1}{4\epsilon^2} - 1} \frac{\left[K(1 - 2\epsilon^2 - \sqrt{1 - 4\epsilon^2}) + \epsilon B \right]^2}{\left[K(1 - 2\epsilon^2 - 2\sqrt{1 - 4\epsilon^2}) + \epsilon B \right]^2}. \quad (5.22)$$

Accordingly the critical current is well approximated by using Eq. (5.18)

$$I_{s,c} \simeq I_s(\mu_\epsilon - \delta\mu). \quad (5.23)$$

We thus have two forms of stable limit cycles for $-|J_\perp| < K < 0$ and $I_s > I_{s,c}$, namely one described in Section 5.3 where $\eta = 0$ and one with $\eta \neq 0$ which we described in this Appendix.

5.B STABILITY REQUIREMENTS FOR LIMIT CYCLES WITH $\eta = 0$

To perform the stability analyses, we first determine the fixed points in ϕ and η up to first order in dissipative terms. Including dissipative corrections Eq. (5.7d) become

$$\delta\dot{\eta} = 4|J_{\perp}|(1 - \mu^2)\delta\phi_{\text{fp}} - \frac{I_s}{2}(1 - \mu^2) = 0. \quad (5.24)$$

The above implies $\delta\phi_{\text{fp}} = I_s/8|J_{\perp}|$. We continue the stability analyses by linearizing around the fixed point $\eta = 0$, $\sin(\phi) = I_s/4J_{\perp}$ and $\mu = (B - I_s/2\alpha)/(|J_{\perp}| - K)$,

$$\begin{pmatrix} \dot{\phi} \\ \dot{\eta} \\ \dot{\mu} \end{pmatrix} = \begin{pmatrix} 0 & \gamma_{\eta}^{\phi} & 0 \\ \gamma_{\phi}^{\eta} & \epsilon_{\eta}^{\eta} & 0 \\ 0 & \epsilon_{\eta}^{\mu} & \epsilon_{\mu}^{\mu} \end{pmatrix} \begin{pmatrix} \delta\phi \\ \delta\eta \\ \delta\mu \end{pmatrix}. \quad (5.25)$$

Where γ is zeroth order in α and I_s , and ϵ is first order in dissipation. The eigenvalues λ of the above matrix are given by

$$(\epsilon_{\mu}^{\mu} - \lambda)[(\epsilon_{\eta}^{\eta} - \lambda)\lambda - \gamma_{\phi}^{\eta}\gamma_{\eta}^{\phi}] = 0. \quad (5.26)$$

Hence, one eigenvalue is given by ϵ_{μ}^{μ} and the real part of the other two eigenvalues is given by ϵ_{η}^{η} . The fixed point is stable if the real part of all eigenvalues is negative. The constraint $\epsilon_{\mu}^{\mu} < 0$ precisely gives $\partial_{\mu}\dot{\mu} < 0$ in Eq. (5.11). The requirement that $\epsilon_{\eta}^{\eta} < 0$ on the other hand gives $\epsilon_{\eta}^{\eta}/\alpha = (K - J_z)(1 - \mu^2) - |J_{\perp}|(1 + \mu^2) < 0$, which is satisfied for $K - J_z < |J_{\perp}|$.

5.C STABILITY REQUIREMENTS FOR LIMIT CYCLES WITH $\eta \neq 0$

In case $\eta \neq 0$, the angle ϕ shifts due to dissipative corrections on Eq. (5.7d). We denote this shift by $\delta\phi_{\text{fp}}$. We find that the linearized equations of motion around the fixed point give

$$\begin{pmatrix} \dot{\phi} \\ \dot{\eta} \\ \dot{\mu} \end{pmatrix} = \begin{pmatrix} \epsilon_{\phi}^{\phi} & \gamma_{\eta}^{\phi} & \gamma_{\mu}^{\phi} \\ \gamma_{\phi}^{\eta} & \epsilon_{\eta}^{\eta} & \epsilon_{\mu}^{\eta} \\ 0 & \epsilon_{\eta}^{\mu} & \epsilon_{\mu}^{\mu} \end{pmatrix} \begin{pmatrix} \delta\phi \\ \delta\eta \\ \delta\mu \end{pmatrix}. \quad (5.27)$$

With γ zeroth order in α and I_s , and ϵ first order in dissipation. The eigenvalues λ of the above matrix are given by the third order polynomial equation

$$(\epsilon_\mu^\mu - \lambda)[(\epsilon_\phi^\phi - \lambda)(\epsilon_\eta^\eta - \lambda) - \gamma_\mu^\eta \gamma_\eta^\phi] + \gamma_\mu^\eta \gamma_\mu^\phi \epsilon_\eta^\mu - \epsilon_\mu^\mu \epsilon_\mu^\eta (\epsilon_\phi^\phi - \lambda) = 0. \quad (5.28)$$

Hence, the eigenvalues – up to first order in α and I_s are given by $\lambda_1 = \epsilon_\mu^\mu - (\gamma_\mu^\phi / \gamma_\eta^\phi) \epsilon_\eta^\mu$ and $\lambda_\pm = (\epsilon_\phi^\phi + \epsilon_\eta^\eta) / 2 \pm \sqrt{\gamma_\phi^\eta \gamma_\eta^\phi} \pm \epsilon_\mu^\mu \gamma_\phi^\eta \gamma_\eta^\phi / \sqrt{\gamma_\phi^\eta \gamma_\eta^\phi}$. Since we're only interested in the real part of the eigenfrequencies for our stability analyses, we find that the limit cycle is stable if

$$\text{Re}(\lambda_1) = \epsilon_\mu^\mu - (\gamma_\mu^\phi / \gamma_\eta^\phi) \epsilon_\eta^\mu = \epsilon_\mu^\mu + (\partial_\mu \eta) \epsilon_\eta^\mu = \partial_\mu \dot{\mu} \leq 0, \quad (5.29a)$$

$$\text{Re}(\lambda_\pm) = (\epsilon_\phi^\phi + \epsilon_\eta^\eta) / 2 \leq 0. \quad (5.29b)$$

First we note that $(\epsilon_\phi^\phi + \epsilon_\eta^\eta) / 2 = (\mu - \eta) I_s / 2\alpha - \mu(B + 2K(\mu - \epsilon)) \leq 0$, which implies $\text{sgn}[B + 2K(\mu - \epsilon)]\eta > 0$. This condition is satisfied at the limit cycle. Hence we're left with the stability condition $\partial_\mu \dot{\mu} \leq 0$.

5.D PHASE DIAGRAM FOR $K < 0$ WITH $J_z \rightarrow 0$

In this appendix we describe the phase diagram in case $K < 0$, which is given in Fig. 5.4. For $J_\perp^2 > K^2$ this system once again only has limit cycles with $\eta = 0$ and the dynamics of the system is described by Eqs. (5.12) and (5.13). On the other hand, when $K^2 < J_\perp^2$, two types of limit cycles are stable if $I_s > I_{s,c}$, as we have seen in Sections 5.A, 5.C and 5.3. One of these limit cycles has $\eta = 0$ and is described by Eqs. (5.12) and (5.13). The stability requirement $|J_\perp|(1 + \mu^2) > K(1 - \mu^2)$ for $K < 0$, in this case leads to $(B - I_s/2\alpha)^2 < (K - J_\perp)^3 / (J_\perp + K)$. The second type of limit cycle has $\eta \neq 0$ is discussed in Section 5.A and only exist for current larger than Eq. (5.23). We denote the region in Fig. 5.4 in which both limit cycles exist as the hysteretic regime.

The regions of stable static configurations with $\eta = 1$ and $\mu = 0$ are given by Eqs. (5.11) and (5.15). Additionally, we find the region of stability with $\mu = \pm 1$ and $\eta = 0$ by requiring $\partial_\mu \dot{\mu} < 0$ on Eq. (5.11). This results in $B - I_s/2\alpha < \mp(K - |J_\perp|)$.

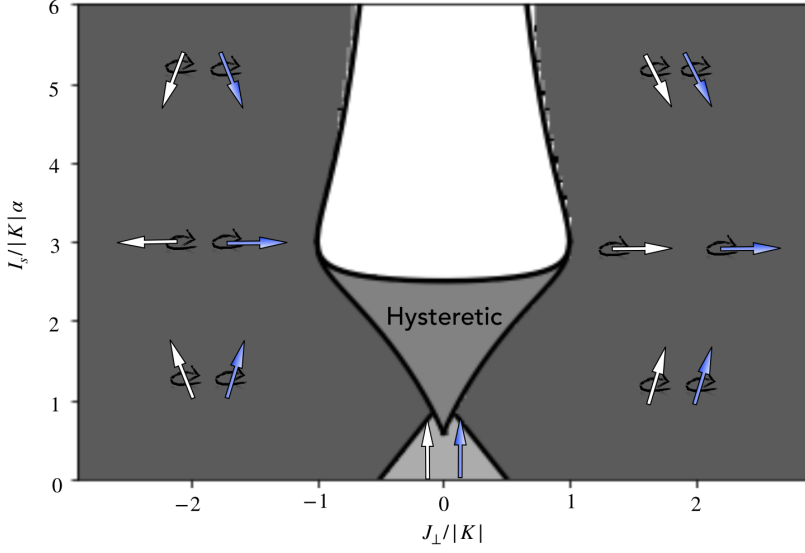


Figure 5.4: Numerical phase diagram for the case $K < 0$ as a function of coupling J_\perp and current I_s . In black the analytical predictions from Eqs. (5.4), (5.15) and (5.23) are plotted. In each region the corresponding long time configuration is indicated. The regions for large and small J_\perp correspond to oscillations. The z -component of the magnetization in this region depends on the injected spin current. The characteristic of the hysteretic region is the dependence of the long-time configuration on the initial conditions. We took $B/K = 1.5$ and $J_z = 0$.

6

SINGLE-MODE SPIN-WAVE LASER DRIVEN BY SPIN-ORBIT TORQUE

This Chapter is unpublished. R.A.D. and J.S.H. conceived the project, J.S.H. did the analytic calculations and prepared the manuscript. All authors contributed to the manuscript.

6.1 INTRODUCTION

An important topic in magnonics is the ability to inject, detect and control magnons using electrical currents. Coherent excitation of magnons typically uses alternating currents (AC)— using for instance antennas —, while direct currents (DC) are usually used to excite magnons diffusively using spin Hall effect (SHE) to create a local spin accumulation. Although excitation of coherent magnons with AC currents is relatively straightforward, excitation of coherent magnons using DC currents is usually more complex and relies on injection of angular momentum with either spin-transfer-torque (STT) or spin-orbit-torque (SOT). Since efficient excitation of magnons by electrical current is crucial to combine magnonic devices with electronic devices, the ability to inject coherent magnons with DC currents is significant towards the technological use of magnonics.

One possibility to inject coherent magnons using DC currents was put forward by Slonczewski [67] and Berger [159, 160]. In their proposals, they argued that a spin-polarized current could be used to drive magnetic precession or reorient the magnetization. To achieve this spin-polarized current, an

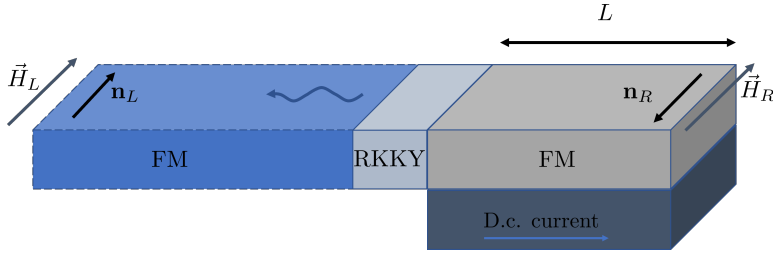


Figure 6.1: Figure of the setup we propose in this Chapter.

electric current is run through a fixed magnet layer, creating a STT on the free magnetic layer. These devices, as put forward by Slonczewski and Berger, are described in the literature as spin-torque nano oscillators (STNOs) or spin-wave amplification by stimulated emission of radiation (SWASER). The injection of angular momentum in these devices gives rise to an angular precession of the free magnetization, which in turn stimulates the emission of spin waves [161–163]. Experimentally, the macrospin precession [164], magnetization reversal [165] and spin wave emission [166–169] in STNOs or SWASERs have been observed. Although coherent spin-wave emission using an STNO should be possible, in practice it seems difficult to get single mode coherent spin-wave emission and usually a handfull of modes with a wavelength determined by the size of the STNO are excited and the frequency of excited spin waves depends on the injected current due non-linear interactions [161, 162]. Besides spin-torque oscillators (STOs) based on the injection of spin angular momentum using STT, angular momentum can also be injected into a magnet layer using the SHE, creating an SOT in the magnetic layer. The use of SOT rather than STT has the advantage that the spin current that is injected into the magnetic layer is perpendicular to the charge current. This allows for the injection of angular momentum in both insulating and conducting magnets, and gives a torque that can be exerted over a much larger area as compared to STT. SOT-based spin-wave emitters should be similar to the ones proposed by Slonczewski and Berger and hence also face the similar challenges injecting coherent spin waves [170–172].

In this Chapter, we propose a setup to excite coherent spin waves using SOT, in which spin waves are coherently excited by coupling to a confined spatial region with negative energy spin waves, see Fig. 6.1. We will show that there exist regimes in coupling strength, size of the system and injected angular momentum for which it becomes a single mode laser for spin waves in the non-linear regime. This setup should have the advantage that it is tunable and does not experience a non-linear frequency shift depended on the injection of angular momentum.

Fundamentally, the setup under consideration is quite different from a usual STO or SWASER setup [67, 159, 160] and is considered in the literature on analogue gravity as a realization of a black-hole laser [26, 41]. The main difference is the fact that a black-hole laser starts lasing in the linear regime without the need of dissipation. This instability can exist due mode coalescence between positive energy modes in the left magnet and a negative energy mode in the right magnet. In short, negative magnetic energy spin-waves form closed orbits of specific frequencies, which — for sufficiently strong coupling strengths — become self amplified and hence start lasing. On the other hand, the conventional STOs or SWASERs start lasing due to pumping of specific mode(s) and hence require dissipation for the onset of the laser. For stability of our black-hole lasing setup we, on the other hand, need to dynamically stabilize the system by injecting angular momentum into the right magnet in the form of SOT.

6.2 MODEL

We consider a set-up of two exchange coupled ferromagnetic thin insulating films subject to an external magnetic field pointing along the z direction. The right film is subject to SOTs keeping the equilibrium magnetization against the direction of the external magnetic field. We assume temperatures far below the Curie temperature for which amplitude fluctuations of the magnetization are negligible. Accordingly, the dynamics of the magnetization direction

$\mathbf{n} = \mathbf{M}/M_s$ is well described by the Landau-Lifschitz-Gilbert equation (LLG) with spin orbit torques given by

$$\partial_t \mathbf{n}_\nu - \alpha \mathbf{n} \times \partial_t \mathbf{n}_\nu = -\gamma \mathbf{n}_\nu \times \mathbf{H}_{\text{eff},\nu} + J_\nu \mathbf{n}_\nu \times (\hat{z} \times \mathbf{n}_\nu), \quad (6.1)$$

where $\nu \in \{L, R\}$ denotes the left or right ferromagnet. The LLG equation describes damped precession around the effective magnetic field strength $\mathbf{H}_{\text{eff},\nu} = -\delta E_\nu / (M_s \delta \mathbf{n})$. Here, we consider the magnetic energy functional $E_\nu[\mathbf{n}]$ in both magnets to be of the form

$$E_\nu = M_s \int dV \left\{ \frac{J}{2} (\nabla_i \mathbf{n}_\nu)^2 - \mu_0 H_\nu n_{\nu,z} \right\}, \quad (6.2)$$

with J the exchange constant and H_e the external magnetic field strength. In the above α is the dimensionless Gilbert damping constant and J_ν characterizes the SOTs — which is only non-vanishing in the right ferromagnet. In principle, anisotropies can relatively straightforwardly be included in the above energy functional, but we don't expect them to change the qualitative physics and omit them here for brevity.

We proceed by defining the canonical coordinate Ψ to be $\sqrt{2 - |\Psi|^2} \Psi = (\hat{x} \mp i\hat{y}) \cdot \mathbf{n}$ and notice that $n_z = \pm(1 - |\Psi|^2)$ — since the magnetization lives on the sphere. In these coordinates the energy functional (6.2), up to fourth order in Ψ and Ψ^* , becomes

$$E_\nu \simeq M_s \int dV \left\{ J (1 - |\Psi_\nu|^2/2) (\partial_x \Psi_\nu^*) (\partial_x \Psi_\nu) + \frac{J}{4} (\partial_x |\Psi_\nu|^2)^2 \mp \mu_0 H_e (1 - |\Psi_\nu|^2) \right\}. \quad (6.3)$$

To incorporate the effect of dissipation, that is, Gilbert damping and SOT, in these canonical coordinates we introduce the Rayleigh dissipation functional

$$\begin{aligned} \mathcal{W}_\nu &= \frac{M_s}{\gamma} \int dV \left\{ \frac{\alpha}{2} (\partial_t \mathbf{n}_\nu)^2 - J_\nu \hat{z} \cdot (\mathbf{n}_\nu \times \partial_t \mathbf{n}_\nu) \right\} \\ &= \frac{M_s}{\gamma} \int dV \left\{ \alpha [1 - |\Psi_\nu|^2/2] (\partial_t \Psi_\nu^*) (\partial_t \Psi_\nu) + \frac{\alpha}{4} (\partial_t |\Psi_\nu|^2)^2 \right. \\ &\quad \left. \pm i J_\nu [1 - |\Psi_\nu|^2/2] (\Psi_\nu \partial_t \Psi_\nu^* - \Psi_\nu^* \partial_t \Psi_\nu) \right\}. \end{aligned} \quad (6.4)$$

We stress that the Rayleigh dissipation functional is also expanded up to fourth order in the fields Ψ_ν and Ψ_ν^* . The Euler-Lagrange equations with Rayleigh dissipation yields the two equations of motion describing the non-linear magnetization dynamics

$$\begin{aligned} i\partial_t\Psi_\nu &\simeq -\Lambda^2(1 - |\Psi_\nu|^2/2)\partial_x^2\Psi_\nu - \Lambda^2(\partial_x^2|\Psi_\nu|^2)\Psi_\nu/2 \\ &\quad -\Lambda^2(\partial_x\Psi_\nu^*)(\partial_x\Psi_\nu)\Psi_\nu/2 \pm h\Psi_\nu \\ &\quad +\alpha [1 - |\Psi_\nu|^2/2] (\partial_t\Psi_\nu) + \alpha(\partial_t|\Psi_\nu|^2)\Psi_\nu/2 \\ &\quad \pm iI_\nu [1 - |\Psi_\nu|^2/2] \Psi_\nu, \end{aligned} \tag{6.5}$$

where the second equation of motion is given by the complex conjugate of the above. In the above we defined the dimensionless time $t \rightarrow t/\gamma\mu_0 M_s$, the exchange length $\Lambda = \sqrt{J/\gamma\mu_0 M_s}$, the dimensionless SOT $I_\nu = J_\nu/\gamma\mu_0 M_s$ and the dimensionless magnetic field $h = H_e/M_s$.

We find the linear spin-wave excitations in the left and right magnet using a plane wave ansatz and linearizing the equation of motion. This gives the following dispersion relation for spin waves

$$\omega_L = \Lambda^2(k^L)^2 + h_L - i\alpha\text{Re}\omega_L, \tag{6.6a}$$

$$\omega_R = \Lambda^2(k^R)^2 - h_R - i(I_R + \alpha\text{Re}\omega_R), \tag{6.6b}$$

where $\omega_{L/R}$ gives the dispersion in the left and right magnet respectively with $k^L \in \mathbb{R}$ and $k^R = \pi m/L$ with $m \in \mathbb{N}$ — since the right ferromagnet has finite size. Dynamical stability of the right ferromagnet, at the linear level, in the absence of coupling between the left and right magnet, requires $\text{Im}\omega_R < 0$. We thus find that the SOT should satisfy $-I_R > \alpha h_R$ for the right magnet to be dynamically stable. From this point onward we ignore Gilbert damping in the left magnet and, for future purposes, note that the wavenumber of the left moving mode in the left magnet at the precessional frequency ω is given by $\Lambda k_l^L = -\sqrt{\omega - h_L}$.

Next, we determine the boundary conditions between the continuum of magnons in the left ferromagnet and the discrete states in the energetically unstable right ferromagnet. The RKKY interaction energy of the magnets is

$$E_{\text{int}} = -J_c \mathbf{n}_L \cdot \mathbf{n}_R|_{x=0} = J_c \left[(1 - |\Psi_L|^2)(1 - |\Psi_R|^2) - \sqrt{(1 - |\Psi_L|^2/2)(1 - |\Psi_R|^2/2)}(\Psi_L \Psi_R + \Psi_L^* \Psi_R^*) \right] |_{x=0}. \quad (6.7)$$

From here we find the boundary conditions by employing the variational derivative at the boundaries. This yields the boundary condition at the left RKKY interface

$$J(1 - |\Psi_L|^2/2)\partial_x \Psi_L + J\Psi_L \partial_x |\Psi_L|^2/2 = J_c \left[\sqrt{(1 - |\Psi_L|^2/2)(1 - |\Psi_R|^2/2)}\Psi_R^* + (1 - |\Psi_R|^2)\Psi_L - \sqrt{(2 - |\Psi_R|^2)/(2 - |\Psi_L|^2)}(\Psi_L \Psi_R + \Psi_L^* \Psi_R^*)\Psi_L/4 \right]. \quad (6.8)$$

The boundary condition at the right RKKY interface is similar with $\Psi_L \leftrightarrow \Psi_R$ and $\partial_x \rightarrow -\partial_x$.

We proceed by treating the spin wave fluctuations in the left ferromagnet to be much smaller in amplitude than the amplitude of the standing wave in the right ferromagnet. This assumption follows from energy conservation at the weakly coupled interface and by noting that we only allow for outgoing modes in the left magnet. As a result we treat the continuum in the left ferromagnet using linear spin-wave theory, while treating the right ferromagnet non-linearly. We furthermore assume $-\Lambda k_l^L \gg \Lambda_c$, which corresponds to weak coupling. The boundary condition in Eq. (6.8), for weak coupling strengths, becomes $J\partial_x \Psi_L|_{x=0} \simeq J_c \sqrt{1 - |\Psi_R|^2/2} \Psi_R^*|_{x=0}$. This leaves us with

$$i\Lambda k_l^L \Psi_L|_{x=0} \simeq \Lambda_c \sqrt{1 - |\Psi_R|^2/2} \Psi_R^*|_{x=0}, \quad (6.9)$$

with $\Lambda_c = J_c/\Lambda\gamma\mu_0 M_s$.

Rather than incorporating the RKKY interaction at the right interface as a boundary condition, we include this interaction as a boundary term in the equation of motion of the right ferromagnet after which we substitute Eq. (6.9).

The contribution of the RKKY interaction to the equation of motion of Ψ_R , in this instance, gives

$$\delta E_{\text{int}}/\delta\Psi^* = [\Lambda_c\Lambda\Psi_R - i(\Lambda_c^2/k_l^L)(1 - |\Psi_R|^2/2)\Psi_R]\delta(x), \quad (6.10)$$

which should be added to the equation of motion in Eq. (6.5). The first term in the above describes an energetic boundary contribution, while the second term gives the flow of energy from the right ferromagnetic to the left ferromagnet.

6.3 NON-LINEAR ANALYSES OF THE SPIN-WAVE LASING MODE

Because the RKKY coupling between the left and right magnet is small compared to their exchange coupling, it is natural to consider a mode expansion which satisfies the exchange boundary conditions, $\partial_x\Psi|_{x\in\{0,L\}} = 0$, at the boundaries in the right magnet

$$\Psi_R = \sum_m A_m(t)e^{i\phi_m(t)}e^{-i\omega_m t}\sqrt{\frac{2 - \delta_{n,0}}{L}}\cos[k_m x]. \quad (6.11)$$

with $k_m = \pi m/L$ for $m \in \mathbb{N}$ and $\omega_m = \Lambda^2 k_m^2 + h_R$ the precessional frequency of the right magnet. We note that the energetic boundary contribution of the RKKY interaction could in principle be included using the Sturm-Liouville expansion. We however disregard this. Since we consider α , I_R and Λ_c^2 to be small, there is no need to include this correction up to first order in these parameters. In the above expansion, we explicitly expect the timescale in which A_n and ϕ_n changes to be much larger than the timescale set by ω_n^{-1} .

We are ultimately interested in the possibility of limit cycles at finite amplitude because they will correspond, as we shall see, to lasing or coherent emission of spin waves. We start with the approximation in which only one

non-uniform mode is present. For a non-uniform mode, $n \neq 0$, the equations of motion in Eq. (6.5) become

$$\partial_t \phi_n \simeq -\alpha(\partial_T A_n)(1 + 3A_n^2/4L) + 2\Lambda_c \Lambda/L, \quad (6.12a)$$

$$\begin{aligned} \partial_t A_n \simeq & -(2\Lambda_c^2/k_l^L L)(1 - A_n^2/L)A_n \\ & - (\alpha\omega_n - \alpha\partial_t \phi_n + I_R)(1 - 3A_n^2/4L)A_n. \end{aligned} \quad (6.12b)$$

The first equation gives corrections to the precessional frequency due to amplitude fluctuations and the RKKY interaction. The second equation describes the dissipative dynamics of the amplitude of the n -th spin-wave mode. As we have seen before, the linear equation of motion in Eq. (6.6b) predicts that $I_R > \alpha h_R$ for the spin waves in the right ferromagnetic to be stable to start with. Furthermore, Eq. (6.12b) predicts the onset of a linear instability for coupling strengths Λ_c exceeding $-2\Lambda_c^2/k_{l,n}^L L > I_R + \alpha\omega_n$, where we used the shorthand notation $k_{l,n}^L \equiv k_l^L(\omega_n) = -\sqrt{\omega_n - h_L}$. Hence, the closed orbits of negative energy spin waves become self amplified for sufficiently strong coupling strengths. This instability is due to mode coalescence between spin waves in the left ferromagnet and the negative energy standing waves in the right magnet [43]. The mechanism behind this is similar to the formation of an exceptional point [44]. Including the non-linear contributions in Eq. (6.12b), we find the amplitude of the self amplified mode to be stabilized by the non-linear interactions and to be given by

$$\frac{A_n^2}{L} \simeq \frac{x_n - 1}{x_n - 3/4}, \quad (6.13)$$

with $x_n = -2\Lambda_c^2/(\alpha\omega_n + I_R)k_{l,n}^L L > 1$.

We may express the emitted spin current in terms of the above spin wave amplitude. This can be done since the amplitude of emitted spin waves is related to the amplitude of the spin wave mode in the right magnetic via Eq. (6.9). We further define the dimensionless spin-current in the left ferromagnet by $iJ_{\text{spin}} = \Psi_L \partial_x \Psi_L^* - \Psi_L^* \partial_x \Psi_L$. This yields that the coherent spin current carried by spin waves of frequency ω_n emitted by this lasing setup is given by

$$J_{\text{spin}} = |A_L|^2 \Lambda k_{l,n}^L, \quad (6.14)$$

with $|A_L|^2 = 2(\Lambda_c/\Lambda k_{l,n}^L)^2(1 - A_n^2/L)A_n^2/L$. In the proceeding section we consider the current interval for which this one-mode laser remains stable.

6.4 CURRENT INTERVAL FOR A STABLE ONE-MODE LASER

From this point onwards we consider the n -th mode to be the linearly most unstable mode and the interaction between this lasing mode and the other modes close to the resonant condition $\omega_{n'} = \omega_{n_1} - \omega_{n_2}^* + \omega_{n_3}$, with n_1, n_2 and n_3 arbitrary for the moment. Since by assumption the n -th mode is the only mode with non-vanishing amplitude, we consider $n_2 = n$ and either $n_1 = n$ and $n_3 = n'$ or $n_1 = n'$ and $n_3 = n$. We therefore consider only modes that appear twice in Eq. (6.5). To recap, we are interested in the stability of the situation in which the n -th mode is lasing and the other modes remain stable, in the sense that their amplitude remains vanishing. The equation for the amplitude of these other modes is follows from Eqs. (6.5) and (6.9) as

$$\begin{aligned} \frac{\partial_t A_{n'}}{A_{n'}} &\simeq -\alpha\omega_{n'} - I_R + \frac{(2 - \delta_{n'})\Lambda_c^2}{k_{l,n'}^L L} \\ &+ \left[\alpha\omega_n + I_R + \frac{\Lambda^2 k_n^2}{2} - \frac{2(2 - \delta_{n'})\Lambda_c^2}{k_{l,n'}^L L} \right] \frac{A_n^2}{L} < 0, \end{aligned} \quad (6.15)$$

where the last equality is the stability requirement. This condition, for the n' -th mode, thus gives a constraint on the amplitude of the lasing mode

$$\frac{A_n^2}{L} < \frac{I_R - \alpha h + \alpha\Lambda^2 k_{n'}^2 - (2 - \delta_{n'})\Lambda_c^2/k_{l,n'}^L L}{I_R - \alpha h + 3\alpha\Lambda^2 k_n^2/2 - 2(2 - \delta_{n'})\Lambda_c^2/k_{l,n'}^L L}. \quad (6.16)$$

Hence, the one mode laser is stable if the amplitude in Eq. (6.13) satisfies the above constraint for arbitrary n' . We expect the uniform mode or the first non-uniform be the most susceptible to the instability, but foremost the uniform mode. Therefore we consider $n' \rightarrow 0$ in the following. With use of Eq. (6.13), the constraint in Eq. (6.16) can be written as a quadratic equation in $I_R - \alpha h + \alpha\Lambda^2 k_n^2$. Namely, $(I_R - \alpha h + \alpha\Lambda^2 k_n^2)^2 + (I_R - \alpha h + \alpha\Lambda^2 k_n^2)[5\alpha\Lambda^2 k_n^2 + 5\Lambda_c^2/k_{l,0}^L L] + (4\Lambda_c^2/k_{l,n}^L L)[2\Lambda_c^2/k_{l,0}^L L + 3\alpha\Lambda^2 k_n^2] \gtrsim 0$. From the fact that this equation is quadratic we find that all currents within the

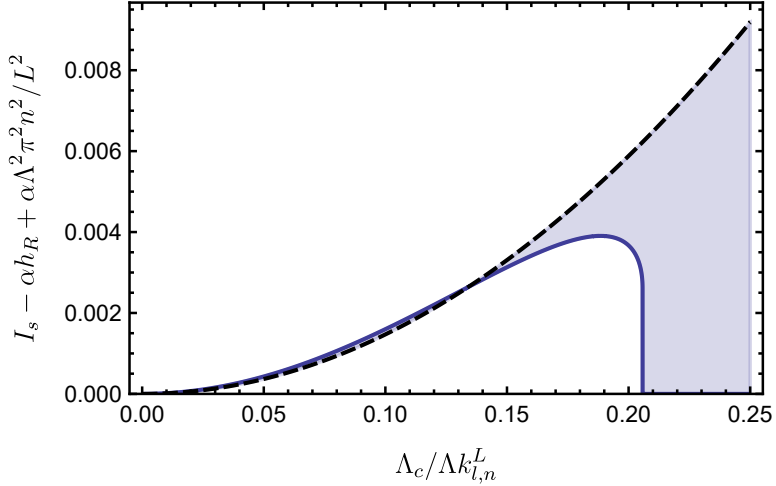


Figure 6.2: Figure of the current interval presented in Eq. (6.18), for $h_R - h_L = 1/2$, $L/\Lambda = 8$ and $\alpha = 10^{-2}$. The solid curve describes the lower bound, while the dashed curve describes the upper bound. We furthermore notice a sudden drop in the required current I_R for coupling strengths $\Lambda_c > \Lambda_{c,\text{critical}}$.

linearly unstable range $-2\Lambda_c^2/k_{l,n}^L L > I_R + \alpha\omega_n > 0$ are in principle allowed if the discriminant is negative. By assuming $1/k_{l,n}^L L$ to be small compared to $1/k_{l,n}^L L$ we find the critical coupling strength to be approximately

$$\Lambda_{c,\text{critical}}^2 \gtrsim 3\alpha\Lambda^2 k_n^2 |k_{l,0}^L| L/2. \quad (6.17)$$

If Λ_c , on the other hand, is smaller than this critical value, the current interval in which there exists a stable one mode laser becomes

$$\begin{aligned} -2\Lambda_c^2/k_{l,n}^L L \geq I_R - \alpha h + \alpha\Lambda^2 k_n^2 &\gtrsim 5 (\alpha\Lambda^2 k_n^2 + \Lambda_c^2/k_{l,0}^L L) \\ \times \frac{1}{2} \left[\sqrt{1 - \frac{48\Lambda_c^2 k_{l,0}^L}{25 k_{l,n}^L} \frac{\alpha\Lambda^2 k_n^2 k_{l,0}^L L + 2\Lambda_c^2/3}{(\alpha\Lambda^2 k_n^2 k_{l,0}^L L + \Lambda_c^2)^2}} - 1 \right]. \end{aligned} \quad (6.18)$$

The upper bound in the injected current comes from the lasing condition $-2\Lambda_c^2/k_{l,n}^L L \geq I_R - \alpha h + \alpha\Lambda^2 k_n^2$ which makes the $A_n = 0$ an unstable fixed point in Eq. (6.12b). In Fig. 6.2, we plot the current interval as a function of the coupling strength Λ_c . From this figure, we notice that the lower boundary

in the current I_R for $\Lambda_c > \Lambda_{c,\text{critical}}$ becomes the requirement of spin waves with frequency ω_n to be dynamically stable, i.e., $I_R > \alpha(h_R - \Lambda^2 k_n^2)$.

Lastly, the upper bound in the current — above which there is no self amplification of the n -th mode — and the quadratic constraint equation which follows from Eqs. (6.13) and (6.16), predicts a lower bound in the coupling strength below which a stable one mode laser can not exist. We find this lower bound in the coupling strength to be

$$2\Lambda_{c,\text{lower bound}}^2 \gtrsim \alpha\Lambda^2 k_n^2 |k_{l,n}^L| L. \quad (6.19)$$

Let us finish by checking the self-consistency of the assumption $-\Lambda k_{l,n}^L \gg \Lambda_c$, which allows us to treat the spin waves in the left domain linearly. This assumption implies $1 \gg \Lambda_c^2 / (\Lambda k_{l,n}^L)^2 \gtrsim \alpha k_n^2 L / 2 |k_{l,n}^L|$, which is equivalent to $(2L/\Lambda) \sqrt{h_R - h_L - n^2 \pi^2 \Lambda^2 / L^2} \gg \alpha n^2 \pi^2$. Hence, a one mode laser is stable if only a few — and most likely only two or three — energetically unstable modes are present.

6.5 CONCLUSION, DISCUSSION AND OUTLOOK

In this Chapter, we proposed a way to inject spin-waves of a specific frequencies, thereby constituting what is called a black-hole laser [41]. This realization depended crucially on the coupling of magnonic excitations to negative energy magnon excitations in a confined region. Via the coupling of magnons to these negative energy magnons, the system can form closed orbits, thereby dynamically destabilizing the system. The formation of the dynamical unstable modes is similar to that of the mode coalescence forming an exceptional point. Since the finitely many modes start lasing, i.e., exponentially growing, the non-linear theory is quickly important in this model. Hence, we investigated the non-linear regime for which the one-mode laser would be stable. More specifically, we considered the case in which one mode dominates and analyzed its stability towards instabilities in other modes. We found there to be a region in parameter space for which this one-mode black-hole laser is stable and hence emits a beam of coherent magnons. The results in this Chapter have been found using the approximation that $-\Lambda k_l^L \gg \Lambda_c$, which

allows us to treat spin waves in the left magnet linearly. This approximation becomes less exact when the resonant frequencies in the right magnet are close to the Kittel frequency of the left magnet or when exploring stronger coupling strengths. Developing a theory beyond this limit is in principle of interest, since $\Lambda_c/\Lambda k_l^L$ is responsible for the onset of the lasing mode. In future work, one could develop a theory that treats the left magnet non-linearly, possible by inserting a static soliton profile in the left magnet. Furthermore, it could be useful to consider this set-up with two interfaces in the quantum regime. This is due to the fact that this setup is likely to produce entangled pairs of magnons. Another direction would be to consider the coupling between positive and standing wave negative energy magnons in antiferromagnets to create a one-mode laser in this class of materials to.

CONCLUSION AND OUTLOOK

In this Thesis, we developed new ideas to inject and amplify spin waves in ferromagnetic materials. The key concept behind the proposals is that the coupling of positive energy excitations to long lived negative energy excitations can lead to novel phenomena. This Thesis consisted of two parts. We discussed dipole-exchange spin waves in Part i, while we considered applications of the coupling between positive and negative energy spin waves in Part ii.

In the first chapter of Part i, namely Chapter 2, we discussed how spin-transfer torques (STTs) can be used to create negative magnetic energy excitations that are dynamically stable. The effect of STTs on the dynamics of metallic ferromagnets is twofold. One effect is due to the adiabatic torque which Doppler shifts the spin-wave dispersion and thus intuitively drags spin waves along with the charge current. The spin-wave dispersion can now become negative for sufficiently strong injected currents, which yields an energetic instability. The other effect of driving a charge current through a magnetic conductor is that a non-adiabatic STT is also exerted onto the magnetization. This is a dissipative torque that competes with Gilbert damping. Usually, if a system becomes energetically unstable it also becomes dynamically unstable due to dissipation. In metallic ferromagnets however, the dissipation of energy can be counteracted by the injection of angular momentum in the form of non-adiabatic STT. In this work, we determined the critical current for spin waves to become energetically unstable due to adiabatic STT and determined the dynamical stability of these spin waves. To be concrete, we included

the effects of magnetostatic interactions, Dzyaloshinskii-Moriya interactions (DMI) and crystalline and surface anisotropies. For typical magnetic fields and system parameters found in experiments, we found the critical current to be of the order $j_c \sim (1 - D/D_c)10^{13}\text{A/m}^2$, with D_c the critical DMI constant above which the ferromagnet becomes unstable towards the formation of spirals or skyrmions. In principle 10^{13}A/m^2 is a rather large current, at the limit of what is experimentally possible. By fine tuning the magnetic parameters such that the ferromagnetic state is close to a phase transition, however, one can make the critical current arbitrarily small.

In Chapter 3 we developed an analytic theory to describe the dipole-exchange spin wave dispersion of ferromagnetic films, in the Damon-Eshbach configuration. We focused on this configuration, since it is most typically used in experiments. Currently, the spin wave spectrum that follows from the diagonal approximation in the widely used analytic theory by Kalinikos and Slavin [84, 111] becomes inaccurate in relative thick ferromagnetic films — as they also noted in their article. Rather than solving an integrodifferential equation, as done by Kalinikos and Slavin, we derived the dipole-exchange spin wave dispersion by applying the magnetostatic and exchange boundary conditions on bulk spin wave solutions. This boundary problem turned out to have an accurate analytic solution, which agreed well with the numerically obtained dispersion relations. The main result of this chapter is the analytic spin wave dispersion in Eq. (3.35), which is quantitatively different from the spin wave spectrum in Kalinikos and Slavin [84, 111]. At last, the spin wave dispersion in Eq. (3.35) can be further simplified in the thin and thick film limits of the ferromagnet as shown in Eqs. (3.41) and (3.47).

The first chapter of Part ii is Chapter 4. Here, we discussed how spin currents can be amplified of an interface with an energetically unstable ferromagnet. The mechanism behind this amplification is superradiant scattering of magnons with antimagnons at this interface. This is analogous to the mechanism which causes superradiant scattering in the bosonic Klein paradox. We considered a setup of two coupled ferromagnets, in which the magnetization in the left magnet is pointing along the external magnetic field and the magnetization in the right magnet is pointing against the external magnetic

field and is stabilized by SOT. Thus, in the left magnet only magnons exist, while in the right magnet both antimagnons and magnons exist since the steady state magnetization direction is inverted with respect to the external field. In order to achieve a coupling between magnons in the left magnet and antimagnons in the right magnet the steady state directions of both magnets should be opposite. This can be made intuitive by remembering that magnons and antimagnons have opposite handedness. In conclusion, we found that conservation of energy at the interface implies superradiant reflection magnons of the interface with antimagnons — $|R|^2 > 1$ —, within the range of frequencies in which magnons and antimagnons couple. Hence, this setup can be used as an amplifier for spin waves and quite possibly emits entangled pairs of magnons.

In Chapter 5, we discussed the non-linear dynamics of a spin-torque oscillator (STO) consisting of two anisotropic exchange coupled macrospins. We considered the initial situation in which the bottom spin is directed against the external magnetic field and is driven by SOT, while the upper spin is aligned with the external magnet. Here both of the magnets experience dissipation in the form of Gilbert damping. We found there to be a point in the coupling strength between the magnets beyond which the STO becomes unstable. To be precise, the linearised dynamics exhibits an exceptional point (EP), which is characterised by the mode coalescence of the eigenvectors and eigenvalues and a square root dependence of the imaginary part of the eigenvalues. While the details of the EP are not really of concern here, we like to highlight that the coupling of a dynamically stable magnon with a dynamically stable antimagnon can lead to an instability, for sufficiently strong coupling strengths. Since the unstable modes blow up exponentially in time, a non-linear theory is necessary to describe the dynamics. In this work, we developed an analytic theory that described the non-linear limit cycles of the STO. We found a relative simple description of the STO dynamics near the EP. Furthermore, we have shown that the power of the STO depends extremely sensitively on the injected spin-current for vanishing out of plane couplings. For non-vanishing out of plane coupling strengths, we found that the point in phase-space at which the extreme sensitivity in the power occurs

shifts slightly away from the EP. Moreover, we found excellent agreement between the analytic theory and numerically performed spin simulations which gives a complete understanding of the steady-state behaviour of the STO.

In the final chapter, namely Chapter 6, we investigated the non-linear dynamics in a system consisting of two coupled ferromagnets, in which a linear instability is initiated by coupling continuum spin wave excitations in the left magnet to a discrete amount of negative energy spin waves in the right magnet. The antimagnonic excitations in the right magnet are realized by considering the magnetization to be opposite to the external magnetic field and are again stabilized by SOT. In the literature of analogue gravity, such a setup is called a black-hole laser [41, 43], and in this Chapter, we determined the range in currents and parameter space for which this setup becomes a stable one-mode laser. Such a one-mode laser would be quite useful within the field of magnonics, since it gives the ability to inject magnons using DC currents. This setup is quite different from the conventional lasing setup in which a specific mode(s) start lasing due to driving of the mode(s). Here, the onset of the lasing mode is initiated by the coupling between positive and negative energy excitations and is stabilized by injection of SOT and non-linearities.

OUTLOOK

As we move towards the end of this Thesis, we like to give an outlook into possible paths for future research. First and most foremost, experimental realization of antimagnons will be an important building block. While this work, until thus far, has been solely theoretical, its eventual usefulness will depend on experimental realizations of these proposals. Since the models presented in Part ii contain the bare essentials for the desired effects to occur, more accurate modelling of realistic experimental situations might be necessary. One way to proceed is described in Chapter 2, in which we determined experimentally realistic situations driven by STT. We found there that the order of magnitude of the critical current is typically rather

large and close to the limit what is experimentally realizable. But we also found that this critical current can be made arbitrarily small by considering ferromagnetic metals that are close to a structural phase transition, induced by either anisotropies or Dzyaloshinskii-Moriya interaction. In this case it might be worthwhile — in an experimental collaboration — to optimize the choice of ferromagnetic metals, such that the critical current is significantly reduced. The proposals discussed in Part ii, on the other hand, rely on SOTs to stabilize antimagnons. At the moment of writing, the electric currents needed to stabilize a reversed magnetization are still large for experimentally realistic parameters, but may still be within experimental reach. If materials with a larger SH angles are discovered both the efficiency and the realizability of our proposals drastically increases.

A continuation of the work presented in Chapter 3 would be to generalize the analytic dipole-exchange spin wave dispersion derived to arbitrary angles between the spin wave propagation direction and an in-plane external magnetic field. Also, the magnetization profile of the spin waves could be derived analytically in continuations of this work. As a broader theme, further theoretical efforts can be put in the study of the quantum regime of the models presented in Part ii of this Thesis. The reason this would be interesting is the fact that most of the set-ups we consider are expected to spontaneously generate entangled pairs of magnons. This might become useful for quantum computational operations. It would also be interesting to consider the initial time behaviour of the model presented in Chapter 4 in the absence of SOT. Thus, to consider two coupled magnets, in which the initial magnetization direction of one of these magnets is directed against the external magnetic field. In this case the initial time behaviour is expected to be characterized by spontaneously emitted pairs of magnons at the interface between the magnets and a generic timescale at which fluctuations grow exponentially, set by the coupling between the magnets and the Gilbert damping. Still, within this timescale for instance the amplification of spin waves and the spontaneously emitted pairs of magnons and antimagnons will occur. Another direction to continue is to model the non-linear dynamics of the spin wave laser presented in [65]. From the standpoint of analogue gravity this would also be called a

black-hole laser. In this model however, the antimagnonic states are created and stabilized by STT. The description of the non-linear dynamics in this model will be a bit more involved than the one presented in Chapter 6, since the amplitude of emitted spin waves is not expected to be small. A possible approach to model this, is to consider spin wave soliton profiles near the interface between magnonic and antimagnonic excitations. Finally, while the proposals in this Thesis are realized in ferromagnets, in future work these models could be generalized to antiferromagnets.

BIBLIOGRAPHY

- [1] J. S. Harms, H. Y. Yuan, and R. A. Duine, “Antimagnonics,” arXiv:2210.16698 (2022).
- [2] J. S. Harms, A. Rückriegel, and R. A. Duine, “Dynamically stable negative-energy states induced by spin-transfer torques,” *Physical Review B* **103**, 144408 (2021).
- [3] J. S. Harms and R. A. Duine, “Theory of the dipole-exchange spin wave spectrum in ferromagnetic films with in-plane magnetization revisited,” *Journal of Magnetism and Magnetic Materials* **557**, 169426 (2022).
- [4] J. S. Harms, H. Y. Yuan, and R. A. Duine, “Enhanced magnon spin current using the bosonic Klein paradox,” *Physical Review Applied* **18**, 064026 (2022).
- [5] R. A. Duine, V. Errani, and J. S. Harms, “Nonlinear dynamics near exceptional points of synthetic antiferromagnetic spin-torque oscillators,” *Phys. Rev. B* **108**, 054428 (2023).
- [6] P. M. Gunnink, J. S. Harms, R. A. Duine, and A. Mook, “Zero-frequency chiral magnonic edge states protected by nonequilibrium topology,” *Phys. Rev. Lett.* **131**, 126601 (2023).
- [7] C. Freitag, M. Berners-Lee, K. Widdicks, B. Knowles, G. S. Blair, and A. Friday, “The real climate and transformative impact of ICT: a critique of estimates, trends, and regulations,” *Patterns* **2**, 100340 (2021).
- [8] A. S. G. Andrae and T. Edler, “On global electricity usage of communication technology: trends to 2030,” *Challenges* **6**, 117–157 (2015).

- [9] A. S. G. Andrae, “Projecting the chiaroscuro of the electricity use of communication and computing from 2018 to 2030,” *10.13140/RG.2.2.25103.02724* (2019).
- [10] L. Belkhir and A. Elmeligi, “Assessing ICT global emissions footprint: trends to 2040 & recommendations,” *Journal of Cleaner Production* **177**, 448–463 (2018).
- [11] T. N. Theis and H.-S. P. Wong, “The end of moore’s law: a new beginning for information technology,” *Computing in Science & Engineering* **19**, 41–50 (2017).
- [12] S. A. Wolf, D. D. Awschalom, R. A. Buhrman, J. M. Daughton, S. Von Molnár, M. L. Roukes, A. Y. Chtchelkanova, and D. M. Treger, “Spintronics: a spin-based electronics vision for the future,” *Science* **294**, 1488–1495 (2001).
- [13] A. V. Chumak, V. I. Vasyuchka, A. A. Serga, and B. Hillebrands, “Magnon spintronics,” *Nature physics* **11**, 453–461 (2015).
- [14] M. Kostylev, A. Serga, T Schneider, B Leven, and B Hillebrands, “Spin-wave logical gates,” *Applied Physics Letters* **87**, 153501 (2005).
- [15] K. Ganzhorn, S. Klingler, T. Wimmer, S. Geprägs, R. Gross, H. Huebl, and S. T. Goennenwein, “Magnon-based logic in a multi-terminal yig/pt nanostructure,” *Applied Physics Letters* **109**, 022405 (2016).
- [16] A. V. Chumak, A. A. Serga, and B. Hillebrands, “Magnon transistor for all-magnon data processing,” *Nature communications* **5**, 1–8 (2014).
- [17] H Wu, L Huang, C Fang, B. Yang, C. Wan, G. Yu, J. Feng, H. Wei, and X. Han, “Magnon valve effect between two magnetic insulators,” *Physical review letters* **120**, 097205 (2018).
- [18] L. Cornelissen, J Liu, B. Van Wees, and R. Duine, “Spin-current-controlled modulation of the magnon spin conductance in a three-terminal magnon transistor,” *Physical review letters* **120**, 097702 (2018).

- [19] J. Cramer, F. Fuhrmann, U. Ritzmann, V. Gall, T. Niizeki, R. Ramos, Z. Qiu, D. Hou, T. Kikkawa, J. Sinova, et al., “Magnon detection using a ferroic collinear multilayer spin valve,” *Nature communications* **9**, 1–7 (2018).
- [20] J. Lan, W. Yu, R. Wu, J. Xiao, et al., “Spin-wave diode,” *Physical Review X* **5**, 041049 (2015).
- [21] H. Yuan, P. Yan, S. Zheng, Q. He, K. Xia, and M.-H. Yung, “Steady bell state generation via magnon-photon coupling,” *Physical Review Letters* **124**, 053602 (2020).
- [22] H. Yuan and R. A. Duine, “Magnon antibunching in a nanomagnet,” *Physical Review B* **102**, 100402 (2020).
- [23] H. Yuan, S. Zheng, Z. Ficek, Q. He, and M.-H. Yung, “Enhancement of magnon-magnon entanglement inside a cavity,” *Physical Review B* **101**, 014419 (2020).
- [24] D. Lachance-Quirion, S. P. Wolski, Y. Tabuchi, S. Kono, K. Usami, and Y. Nakamura, “Entanglement-based single-shot detection of a single magnon with a superconducting qubit,” *Science* **367**, 425–428 (2020).
- [25] H. Yuan, Y. Cao, A. Kamra, R. A. Duine, and P. Yan, “Quantum magnonics: when magnon spintronics meets quantum information science,” *Physics Reports* **965**, 1–74 (2022).
- [26] W. G. Unruh, “Experimental Black-Hole Evaporation?” *Physical Review Letters* **46**, 10.1103/PhysRevLett.46.1351 (1981).
- [27] C. Barcelo, S. Liberati, and M. Visser, “Analogue Gravity,” *Living Reviews in Relativity* **8**, 10.12942/lrr-2005-12 (2005).
- [28] M. Novello, M. Visser, and G. Volovik, *Artificial Black Holes* (WORLD SCIENTIFIC, Oct. 2002).
- [29] D. Faccio, F. Belgiorno, S. Cacciatori, V. Gorini, S. Liberati, and U. Moschella, editors, *Analogue Gravity Phenomenology*, Vol. 870, Lecture Notes in Physics (Springer International Publishing, 2013).

- [30] L. Susskind, “Black holes and the information paradox,” *Scientific American* (1997).
- [31] A. Roldán-Molina, A. S. Nunez, and R. A. Duine, “Magnonic Black Holes,” en, *Physical Review Letters* **118**, 061301 (2017).
- [32] J. R. Muñoz de Nova, K. Golubkov, V. I. Kolobov, and J. Steinhauer, “Observation of thermal Hawking radiation and its temperature in an analogue black hole,” en, *Nature* **569**, 10.1038/s41586-019-1241-0 (2019).
- [33] L. J. Garay, J. R. Anglin, J. I. Cirac, and P. Zoller, “Sonic analog of gravitational black holes in Bose-Einstein condensates,” en, *Physical Review Letters* **85**, 10.1103/PhysRevLett.85.4643 (2000).
- [34] U. Leonhardt, “Space-time geometry of quantum dielectrics,” *Physical Review A* **62**, 10.1103/PhysRevA.62.012111 (2000).
- [35] U. Leonhardt and P. Piwnicki, “Relativistic Effects of Light in Moving Media with Extremely Low Group Velocity,” *Physical Review Letters* **84**, 10.1103/PhysRevLett.84.822 (2000).
- [36] B. Horstmann, B. Reznik, S. Fagnocchi, and J. I. Cirac, “Hawking Radiation from an Acoustic Black Hole on an Ion Ring,” *Physical Review Letters* **104**, 10.1103/PhysRevLett.104.250403 (2010).
- [37] R. Schützhold, M. Uhlmann, L. Petersen, H. Schmitz, A. Friedenauer, and T. Schätz, “Analogue of cosmological particle creation in an ion trap,” *Physical Review Letters* **99**, 10.1103/PhysRevLett.99.201301 (2007).
- [38] G. E. Volovik, “Black hole and hawking radiation by type-II Weyl fermions,” en, *JETP Letters* **104**, 645–648 (2016).
- [39] S. W. Hawking, “Black hole explosions?” en, *Nature* **248**, 10.1038/248030a0 (1974).
- [40] A. Bachelot, “Superradiance and scattering of the charged Klein–Gordon field by a step-like electrostatic potential,” en, *Journal de Mathématiques Pures et Appliquées* **83**, 1179–1239 (2004).

- [41] S. Corley and T. Jacobson, “Black hole lasers,” *Physical Review D* **59**, 10.1103/PhysRevD.59.124011 (1999).
- [42] S. Corley and T. Jacobson, “Hawking Spectrum and High Frequency Dispersion,” en, *Physical Review D* **54**, 10.1103/PhysRevD.54.1568 (1996).
- [43] A. Coutant and R. Parentani, “Black hole lasers, a mode analysis,” en, *Physical Review D* **81**, 084042 (2010).
- [44] A. Coutant, F. Michel, and R. Parentani, “Dynamical instabilities and quasi-normal modes, a spectral analysis with applications to black-hole physics,” en, *Classical and Quantum Gravity* **33**, 125032 (2016).
- [45] L. D. Landau and E. M. Lifshitz, editors, *Electrodynamics of continuous media (second edition)*, Vol. 8, Course of Theoretical Physics (Pergamon, Amsterdam, Jan. 1, 1984).
- [46] D. I. Khomskii, *Basic Aspects of The Quantum Theory of Solids: Order and Elementary Excitations*, en (Cambridge University Press, Cambridge, 2010).
- [47] P. Hohenberg and A. Krekhov, “An introduction to the ginzburg–landau theory of phase transitions and nonequilibrium patterns,” *Physics Reports* **572**, 1–42 (2015).
- [48] H. T. C. Stoof, K. B. Gubbels, and D. B. M. Dickerscheid, *Ultracold quantum fields*, en, Theoretical and mathematical physics (Springer, Dordrecht ; New York, 2009).
- [49] J. D. Jackson, *Classical Electrodynamics* (Wiley, 1998).
- [50] E. M. Lifshitz and L. P. Pitaevskii, *Statistical physics: theory of the condensed state*, Vol. 9 (Elsevier, 2013).
- [51] T. Gilbert, “A phenomenological theory of damping in ferromagnetic materials,” *IEEE Transactions on Magnetics* **40**, 3443–3449 (2004).
- [52] P. A. M. Dirac, “Quantum mechanics of many-electron systems,” *Proceedings of the Royal Society of London. Series A, Containing Papers of a Mathematical and Physical Character* **123**, 714–733 (1929).

- [53] J. H. Van Vleck, “The dirac vector model in complex spectra,” *Phys. Rev.* **45**, 405–419 (1934).
- [54] J. VAN KRANENDONK and J. H. VAN VLECK, “Spin waves,” *Rev. Mod. Phys.* **30**, 1–23 (1958).
- [55] W. Heisenberg, *Zur theorie des ferromagnetismus* (Springer, 1985).
- [56] F. Bloch, “Zur theorie des ferromagnetismus,” *Zeitschrift für Physik* **61**, 206–219 (1930).
- [57] A. Brataas, A. D. Kent, and H. Ohno, “Current-induced torques in magnetic materials,” en, *Nature Materials* **11**, 372–381 (2012).
- [58] Y. Tserkovnyak, H. J. Skadsem, A. Brataas, and G. E. W. Bauer, “Current-induced magnetization dynamics in disordered itinerant ferromagnets,” *Phys. Rev. B* **74**, 144405 (2006).
- [59] Y. Tserkovnyak, A. Brataas, and G. E. Bauer, “Theory of current-driven magnetization dynamics in inhomogeneous ferromagnets,” *Journal of Magnetism and Magnetic Materials* **320**, 1282–1292 (2008).
- [60] A. Manchon, J. Železný, I. M. Miron, T. Jungwirth, J. Sinova, A. Thiaville, K. Garello, and P. Gambardella, “Current-induced spin-orbit torques in ferromagnetic and antiferromagnetic systems,” *Reviews of Modern Physics* **91**, 035004 (2019).
- [61] Y. Tserkovnyak and S. A. Bender, “Spin hall phenomenology of magnetic dynamics,” *Physical Review B* **90**, 014428 (2014).
- [62] W. Heiss, “The physics of exceptional points,” *Journal of Physics A: Mathematical and Theoretical* **45**, 444016 (2012).
- [63] T. Holstein and H. Primakoff, “Field dependence of the intrinsic domain magnetization of a ferromagnet,” *Phys. Rev.* **58**, 1098–1113 (1940).
- [64] S. Weinfurtnner, E. W. Tedford, M. C. J. Penrice, W. G. Unruh, and G. A. Lawrence, “Measurement of stimulated Hawking emission in an analogue system,” en, *Physical Review Letters* **106**, 10.1103/PhysRevLett.106.021302 (2011).

- [65] R. J. Doornenbal, A. Roldán-Molina, A. S. Nunez, and R. A. Duine, “Spin-wave amplification and lasing driven by inhomogeneous spin transfer torques,” en, *Physical Review Letters* **122**, 10.1103/PhysRevLett.122.037203 (2019).
- [66] D. C. Ralph and M. D. Stiles, “Spin transfer torques,” en, *Journal of Magnetism and Magnetic Materials* **320**, 1190–1216 (2008).
- [67] J. C. Slonczewski, “Current-driven excitation of magnetic multilayers,” en, *Journal of Magnetism and Magnetic Materials* **159**, L1–L7 (1996).
- [68] J. Fernández-Rossier, M. Braun, A. S. Núñez, and A. H. MacDonald, “Influence of a uniform current on collective magnetization dynamics in a ferromagnetic metal,” *Physical Review B* **69**, 10.1103/PhysRevB.69.174412 (2004).
- [69] R. A. Duine, A. S. Núñez, J. Sinova, and A. H. MacDonald, “Functional Keldysh theory of spin torques,” *Physical Review B* **75**, 10.1103/PhysRevB.75.214420 (2007).
- [70] G. Tatara and H. Kohno, “Theory of Current-Driven Domain Wall Motion: Spin Transfer versus Momentum Transfer,” *Physical Review Letters* **92**, 10.1103/PhysRevLett.92.086601 (2004).
- [71] Y. B. Bazaliy, B. A. Jones, and S.-C. Zhang, “Modification of the Landau-Lifshitz equation in the presence of a spin-polarized current in colossal- and giant-magnetoresistive materials,” en, *Physical Review B* **57**, R3213–R3216 (1998).
- [72] V. Vlaminck and M. Bailleul, “Current-Induced Spin-Wave Doppler Shift,” en, *Science* **322**, 410–413 (2008).
- [73] J. Shibata, G. Tatara, and H. Kohno, “Effect of spin current on uniform ferromagnetism: domain nucleation,” *Phys. Rev. Lett.* **94**, 076601 (2005).
- [74] J. Chaline, G. Jannes, P. Maïssa, and G. Rousseaux, “Some aspects of dispersive horizons: lessons from surface waves,” en, arXiv:1203.2492 [gr-qc, physics:physics] **870**, 10.1007/978-3-319-00266-8_7 (2013).

- [75] J. Lucassen, C. F. Schippers, M. A. Verheijen, P. Fritsch, E. J. Geluk, B. Barcones, R. A. Duine, S. Wurmehl, H. J. M. Swagten, B. Koopmans, and R. Lavrijsen, “Extraction of Dzyaloshinskii-Moriya interaction from propagating spin waves validated,” *Physical Review B* **101**, 10.1103/PhysRevB.101.064432 (2020).
- [76] R. Damon and J. Eshbach, “Magnetostatic modes of a ferromagnet slab,” en, *Journal of Physics and Chemistry of Solids* **19**, 308–320 (1961).
- [77] A. Kreisel, F. Sauli, L. Bartosch, and P. Kopietz, “Microscopic spin-wave theory for yttrium-iron garnet films,” en, *The European Physical Journal B* **71**, 59 (2009).
- [78] S. M. Rezende, “Theory of coherence in Bose-Einstein condensation phenomena in a microwave-driven interacting magnon gas,” en, *Physical Review B* **79**, 174411 (2009).
- [79] M. Kostylev, “Non-reciprocity of dipole-exchange spin waves in thin ferromagnetic films,” en, *Journal of Applied Physics* **113**, 053907 (2013).
- [80] O. Gladii, M. Haidar, Y. Henry, M. Kostylev, and M. Bailleul, “Frequency nonreciprocity of surface spin wave in permalloy thin films,” en, *Physical Review B* **93**, 054430 (2016).
- [81] R. E. De Wames and T. Wolfram, “Dipole-Exchange Spin Waves in Ferromagnetic Films,” en, *Journal of Applied Physics* **41**, 987–993 (1970).
- [82] T. Wolfram and R. DeWames, “Surface dynamics of magnetic materials,” en, *Progress in Surface Science* **2**, 233–330 (1972).
- [83] B. A. Kalinikos, “Spectrum and linear excitation of spin waves in ferromagnetic films,” en, *Soviet Physics Journal* **24**, 718–731 (1981).
- [84] B. A. Kalinikos and A. N. Slavin, “Theory of dipole-exchange spin wave spectrum for ferromagnetic films with mixed exchange boundary conditions,” en, *Journal of Physics C: Solid State Physics* **19**, 7013–7033 (1986).

- [85] R. F. Soohoo, “General Exchange Boundary Condition and Surface Anisotropy Energy of a Ferromagnet,” en, *Physical Review* **131**, 594–601 (1963).
- [86] J.-Y. Chauleau, H. G. Bauer, H. S. Körner, J. Stigloher, M. Härtinger, G. Woltersdorf, and C. H. Back, “Self-consistent determination of the key spin-transfer torque parameters from spin-wave doppler experiments,” *Phys. Rev. B* **89**, 020403 (2014).
- [87] M. Belmeguenai, J.-P. Adam, Y. Roussigné, S. Eimer, T. Devolder, J.-V. Kim, S. M. Cherif, A. Stashkevich, and A. Thiaville, “Interfacial dzyaloshinskii-moriya interaction in perpendicularly magnetized pt/co/alo x ultrathin films measured by brillouin light spectroscopy,” *Physical Review B* **91**, 180405 (2015).
- [88] A. A. Stashkevich, M. Belmeguenai, Y. Roussigné, S. M. Cherif, M. Kostylev, M. Gabor, D. Lacour, C. Tiusan, and M. Hehn, “Experimental study of spin-wave dispersion in Py/Pt film structures in the presence of an interface Dzyaloshinskii-Moriya interaction,” *Physical Review B* **91**, 10.1103/PhysRevB.91.214409 (2015).
- [89] K. Y. Guslienko and A. N. Slavin, “Magnetostatic Green’s functions for the description of spin waves in finite rectangular magnetic dots and stripes,” en, *Journal of Magnetism and Magnetic Materials* **323**, 2418–2424 (2011).
- [90] A. V. Chumak, V. I. Vasyuchka, A. A. Serga, and B. Hillebrands, “Magnon spintronics,” en, *Nature Physics* **11**, 453–461 (2015).
- [91] E. B. Sonin, “Is spin superfluidity possible in YIG films?” *Physical Review B* **95**, 10.1103/PhysRevB.95.144432 (2017).
- [92] R. E. Arias, “Spin-wave modes of ferromagnetic films,” en, *Physical Review B* **94**, 134408 (2016).
- [93] G. T. Rado and J. R. Weertman, “Spin-wave resonance in a ferromagnetic metal,” *Journal of Physics and Chemistry of Solids* **11**, 315–333 (1959).

- [94] M. Vaňatka, K. Szulc, O. Wojewoda, C. Dubs, A. V. Chumak, M. Krawczyk, O. V. Dobrovolskiy, J. W. Kłos, and M. Urbánek, “Spin-Wave Dispersion Measurement by Variable-Gap Propagating Spin-Wave Spectroscopy,” *Physical Review Applied* **16**, 054033 (2021).
- [95] I. M. Miron, K. Garello, G. Gaudin, P.-J. Zermatten, M. V. Costache, S. Auffret, S. Bandiera, B. Rodmacq, A. Schuhl, and P. Gambardella, “Perpendicular switching of a single ferromagnetic layer induced by in-plane current injection,” *Nature* **476**, 189–193 (2011).
- [96] L. Liu, O. Lee, T. Gudmundsen, D. Ralph, and R. Buhrman, “Current-induced switching of perpendicularly magnetized magnetic layers using spin torque from the spin hall effect,” *Physical review letters* **109**, 096602 (2012).
- [97] K. Garello, I. M. Miron, C. O. Avci, F. Freimuth, Y. Mokrousov, S. Blügel, S. Auffret, O. Boule, G. Gaudin, and P. Gambardella, “Symmetry and magnitude of spin–orbit torques in ferromagnetic heterostructures,” *Nature nanotechnology* **8**, 587–593 (2013).
- [98] A. Manchon, H. C. Koo, J. Nitta, S. Frolov, and R. Duine, “New perspectives for rashba spin–orbit coupling,” *Nature materials* **14**, 871–882 (2015).
- [99] O. Klein, “Die reflexion von elektronen an einem potentialsprung nach der relativistischen dynamik von dirac,” *Zeitschrift für Physik* **53**, 157–165 (1929).
- [100] N. Dombey and A Calogeracos, “Seventy years of the klein paradox,” *Physics Reports* **315**, 41–58 (1999).
- [101] A. Hansen and F. Ravndal, “Klein’s paradox and its resolution,” *Physica Scripta* **23**, 1036 (1981).
- [102] A. Nikishov, “Barrier scattering in field theory removal of klein paradox,” *Nuclear Physics B* **21**, 346–358 (1970).
- [103] S. Gavrilov and D. Gitman, “Quantization of charged fields in the presence of critical potential steps,” *Physical Review D* **93**, 045002 (2016).

- [104] R. Brito, V. Cardoso, and P. Pani, *Superradiance* (Springer, 2020).
- [105] J. D. Bjorken and S. D. Drell, *Relativistic quantum mechanics* (Mcgraw-Hill College, 1964).
- [106] M. Katsnelson, K. Novoselov, and A. Geim, “Chiral tunnelling and the klein paradox in graphene,” *Nature physics* **2**, 620–625 (2006).
- [107] N Stander, B Huard, and D Goldhaber-Gordon, “Evidence for klein tunneling in graphene p- n junctions,” *Physical review letters* **102**, 026807 (2009).
- [108] C. Gutiérrez, L. Brown, C.-J. Kim, J. Park, and A. N. Pasupathy, “Klein tunnelling and electron trapping in nanometre-scale graphene quantum dots,” *Nature Physics* **12**, 1069–1075 (2016).
- [109] C. Kittel, “On the theory of ferromagnetic resonance absorption,” *Physical review* **73**, 155 (1948).
- [110] M Sparks, “Ferromagnetic resonance in thin films. iii. theory of mode intensities,” *Physical Review B* **1**, 3869 (1970).
- [111] B. Kalinikos and A. Slavin, “Theory of dipole-exchange spin wave spectrum for ferromagnetic films with mixed exchange boundary conditions,” *Journal of Physics C: Solid State Physics* **19**, 7013 (1986).
- [112] E. Lundh and H. M. Nilsen, “Dynamic stability of a doubly quantized vortex in a three-dimensional condensate,” *Physical Review A* **74**, 063620 (2006).
- [113] R. Verba, V. Tiberkevich, and A. Slavin, “Spin-wave transmission through an internal boundary: beyond the scalar approximation,” *Physical Review B* **101**, 144430 (2020).
- [114] H. Wang, J. Chen, T. Liu, J. Zhang, K. Baumgaertl, C. Guo, Y. Li, C. Liu, P. Che, S. Tu, et al., “Chiral spin-wave velocities induced by all-garnet interfacial dzyaloshinskii-moriya interaction in ultrathin yttrium iron garnet films,” *Physical Review Letters* **124**, 027203 (2020).

- [115] J. Wegrowe, M.-C. Ciornei, and H. Drouhin, “Spin transfer in an open ferromagnetic layer: from negative damping to effective temperature,” *Journal of Physics: Condensed Matter* **19**, 165213 (2007).
- [116] Y. Cao and P. Yan, “Negative gilbert damping,” *Physical Review B* **105**, 064418 (2022).
- [117] T. Sebastian, K. Schultheiss, B. Obry, B. Hillebrands, and H. Schultheiss, “Micro-focused brillouin light scattering: imaging spin waves at the nanoscale,” *Frontiers in Physics* **3**, 35 (2015).
- [118] V Vlamincck and M Bailleul, “Spin-wave transduction at the submicrometer scale: experiment and modeling,” *Physical Review B* **81**, 014425 (2010).
- [119] L. Cornelissen, J Liu, R. Duine, J. B. Youssef, and B. Van Wees, “Long-distance transport of magnon spin information in a magnetic insulator at room temperature,” *Nature Physics* **11**, 1022–1026 (2015).
- [120] H. Wang, C. Du, Y Pu, R Adur, P. C. Hammel, and F. Yang, “Scaling of spin hall angle in 3d, 4d, and 5d metals from y 3 fe 5 o 12/metal spin pumping,” *Physical review letters* **112**, 197201 (2014).
- [121] A. Vansteenkiste, J. Leliaert, M. Dvornik, M. Helsen, F. Garcia-Sanchez, and B. Van Waeyenberge, “The design and verification of mumax3,” *AIP advances* **4**, 107133 (2014).
- [122] W. Chen, Ş. Kaya Özdemir, G. Zhao, J. Wiersig, and L. Yang, “Exceptional points enhance sensing in an optical microcavity,” *Nature* **548**, 192–196 (2017).
- [123] J. Wiersig, “Enhancing the sensitivity of frequency and energy splitting detection by using exceptional points: application to microcavity sensors for single-particle detection,” *Physical review letters* **112**, 203901 (2014).
- [124] M.-A. Miri and A. Alu, “Exceptional points in optics and photonics,” *Science* **363**, eaar7709 (2019).

- [125] C Dembowski, H.-D. Gräf, H. Harney, A Heine, W. Heiss, H Rehfeld, and A Richter, “Experimental observation of the topological structure of exceptional points,” *Physical review letters* **86**, 787 (2001).
- [126] L. Feng, Z. J. Wong, R.-M. Ma, Y. Wang, and X. Zhang, “Single-mode laser by parity-time symmetry breaking,” *Science* **346**, 972–975 (2014).
- [127] Z. Lin, A. Pick, M. Lončar, and A. W. Rodriguez, “Enhanced spontaneous emission at third-order dirac exceptional points in inverse-designed photonic crystals,” *Physical review letters* **117**, 107402 (2016).
- [128] C Dembowski, B Dietz, H.-D. Gräf, H. Harney, A Heine, W. Heiss, and A Richter, “Encircling an exceptional point,” *Physical Review E* **69**, 056216 (2004).
- [129] D. Chowdhury, A. Banerjee, and A. Narayan, “Exceptional hexagonal warping effect in multi-weyl semimetals,” *Physical Review B* **105**, 075133 (2022).
- [130] Ş. K. Özdemir, S. Rotter, F. Nori, and L Yang, “Parity–time symmetry and exceptional points in photonics,” *Nature materials* **18**, 783–798 (2019).
- [131] S. Longhi and G. Della Valle, “Optical lattices with exceptional points in the continuum,” *Physical Review A* **89**, 052132 (2014).
- [132] P Renault, H Yamaguchi, and I Mahboob, “Virtual exceptional points in an electromechanical system,” *Physical Review Applied* **11**, 024007 (2019).
- [133] M. Partanen, J. Goetz, K. Y. Tan, K. Kohvakka, V. Sevriuk, R. E. Lake, R. Kokkonen, J. Ikonen, D. Hazra, A. Mäkinen, et al., “Exceptional points in tunable superconducting resonators,” *Physical Review B* **100**, 134505 (2019).
- [134] J González and R. A. Molina, “Topological protection from exceptional points in weyl and nodal-line semimetals,” *Physical Review B* **96**, 045437 (2017).

- [135] R. A. Molina and J. González, “Surface and 3d quantum hall effects from engineering of exceptional points in nodal-line semimetals,” *Physical review letters* **120**, 146601 (2018).
- [136] J. Lee, T. Kottos, and B Shapiro, “Macroscopic magnetic structures with balanced gain and loss,” *Physical Review B* **91**, 094416 (2015).
- [137] H. Yang, C Wang, T. Yu, Y. Cao, and P. Yan, “Antiferromagnetism emerging in a ferromagnet with gain,” *Physical Review Letters* **121**, 197201 (2018).
- [138] T. Yu, H. Yang, L. Song, P. Yan, and Y. Cao, “Higher-order exceptional points in ferromagnetic trilayers,” *Physical Review B* **101**, 144414 (2020).
- [139] X.-g. Wang, G.-h. Guo, and J. Berakdar, “Enhanced sensitivity at magnetic high-order exceptional points and topological energy transfer in magnonic planar waveguides,” *Physical Review Applied* **15**, 034050 (2021).
- [140] T Jeffrey, W Zhang, and J Sklenar, “Effect of dipolar interaction on exceptional points in synthetic layered magnets,” *Applied Physics Letters* **118**, 202401 (2021).
- [141] H. Liu, D. Sun, C. Zhang, M. Groesbeck, R. Mclaughlin, and Z. V. Vardeny, “Observation of exceptional points in magnonic parity-time symmetry devices,” *Science advances* **5**, eaax9144 (2019).
- [142] Y. Tserkovnyak, “Exceptional points in dissipatively coupled spin dynamics,” *Physical Review Research* **2**, 013031 (2020).
- [143] K. Deng, X. Li, and B. Flebus, “Exceptional points as a route to magnetic nano-oscillators,” *arXiv preprint arXiv:2205.02308* (2022).
- [144] A. Brataas, A. D. Kent, and H. Ohno, “Current-induced torques in magnetic materials,” *Nature materials* **11**, 372–381 (2012).
- [145] J.-V. Kim, “Spin-torque oscillators,” in *Solid state physics*, Vol. 63 (Elsevier, 2012), pages 217–294.

- [146] I Firastrau, L. Buda-Prejbeanu, B Dieny, and U Ebels, “Spin-torque nano-oscillator based on a synthetic antiferromagnet free layer and perpendicular to plane polarizer,” *Journal of Applied Physics* **113**, 113908 (2013).
- [147] D Houssameddine, U Ebels, B Delaët, B Rodmacq, I Firastrau, F Ponthenier, M Brunet, C Thirion, J.-P. Michel, L Prejbeanu-Buda, et al., “Spin-torque oscillator using a perpendicular polarizer and a planar free layer,” *Nature materials* **6**, 447–453 (2007).
- [148] V. Tiberkevich, A. Slavin, and J.-V. Kim, “Microwave power generated by a spin-torque oscillator in the presence of noise,” *Applied Physics Letters* **91**, 192506 (2007).
- [149] J.-R. Chen, A. Smith, E. A. Montoya, J. G. Lu, and I. N. Krivorotov, “Spin-orbit torque nano-oscillator with giant magnetoresistance readout,” *Communications Physics* **3**, 1–8 (2020).
- [150] T. Chen, R. K. Dumas, A. Eklund, P. K. Muduli, A. Houshang, A. A. Awad, P. Dürrenfeld, B. G. Malm, A. Rusu, and J. Åkerman, “Spin-torque and spin-hall nano-oscillators,” *Proceedings of the IEEE* **104**, 1919–1945 (2016).
- [151] D. Marković, N. Leroux, M. Riou, F. Abreu Araujo, J. Torrejon, D. Querlioz, A. Fukushima, S. Yuasa, J. Trastoy, P. Bortolotti, et al., “Reservoir computing with the frequency, phase, and amplitude of spin-torque nano-oscillators,” *Applied Physics Letters* **114**, 012409 (2019).
- [152] K. Deng, X. Li, and B. Flebus, “Exceptional points as signatures of dynamical magnetic phase transitions,” *Phys. Rev. B* **107**, L100402 (2023).
- [153] S. Komineas, *Non-hermitian dynamics of a two-spin system with pt symmetry*, 2022.
- [154] N. R. Bernier, L. D. Tóth, A. K. Feofanov, and T. J. Kippenberg, “Level attraction in a microwave optomechanical circuit,” *Phys. Rev. A* **98**, 023841 (2018).

- [155] K. Xia, W. Zhang, M. Lu, and H. Zhai, “Noncollinear interlayer exchange coupling caused by interface spin-orbit interaction,” *Physical Review B* **55**, 12561 (1997).
- [156] X.-X. Li, J. Bao, L.-Y. Lu, X.-G. Xu, and Y. Jiang, “Oscillatory antiferromagnetic interlayer coupling in co/pt multilayer with perpendicular anisotropy,” *Solid state communications* **148**, 209–212 (2008).
- [157] G. Csaba, M. Pufall, W. Rippard, and W. Porod, “Modeling of coupled spin torque oscillators for applications in associative memories,” in 2012 12th IEEE International Conference on Nanotechnology (IEEE-NANO) (2012), pages 1–4.
- [158] S. Wittrock, S. Perna, R. Lebrun, K. Ho, R. Dutra, R. Ferreira, P. Bortolotti, C. Serpico, and V. Cros, “Non-hermiticity in spintronics: oscillation death in coupled spintronic nano-oscillators through emerging exceptional points,” (2023).
- [159] L. Berger, “Emission of spin waves by a magnetic multilayer traversed by a current,” *Physical Review B* **54**, 10.1103/PhysRevB.54.9353 (1996).
- [160] L. Berger, “Spin-wave emitting diodes and spin diffusion in magnetic multilayers,” *IEEE Transactions on Magnetics* **34**, 3837–3841 (1998).
- [161] M. A. Hofer, M. J. Ablowitz, B. Ilan, M. R. Pufall, and T. J. Silva, “Theory of magnetodynamics induced by spin torque in perpendicularly magnetized thin films,” *Physical Review Letters* **95**, 267206 (2005).
- [162] A. Slavin and V. Tiberkevich, “Spin Wave Mode Excited by Spin-Polarized Current in a Magnetic Nanocontact is a Standing Self-Localized Wave Bullet,” *Physical Review Letters* **95**, 237201 (2005).
- [163] A. Slavin and V. Tiberkevich, “Nonlinear Auto-Oscillator Theory of Microwave Generation by Spin-Polarized Current,” *IEEE Transactions on Magnetics* **45**, 1875–1918 (2009).
- [164] M. Tsoi, A. G. M. Jansen, J. Bass, W.-C. Chiang, M. Seck, V. Tsoi, and P. Wyder, “Excitation of a magnetic multilayer by an electric current,” *Physical Review Letters* **80**, 4281–4284 (1998).

- [165] B. Özyilmaz, A. D. Kent, D. Monsma, J. Z. Sun, M. J. Rooks, and R. H. Koch, “Current-induced magnetization reversal in high magnetic fields in c o / c u / c o nanopillars,” *Physical Review Letters* **91**, 067203 (2003).
- [166] W. Rippard, M. Pufall, S. Kaka, S. Russek, and T. Silva, “Direct-current induced dynamics in c o 90 f e 10 / n i 80 f e 20 point contacts,” *Physical Review Letters* **92**, 027201 (2004).
- [167] V. E. Demidov, S. Urazhdin, and S. O. Demokritov, “Direct observation and mapping of spin waves emitted by spin-torque nano-oscillators,” *Nature Materials* **9**, 984–988 (2010).
- [168] V. E. Demidov, S. Urazhdin, R. Liu, B. Divinskiy, A. Telegin, and S. O. Demokritov, “Excitation of coherent propagating spin waves by pure spin currents,” *Nature Communications* **7**, 10446 (2016).
- [169] M. Madami, S. Bonetti, G. Consolo, S. Tacchi, G. Carlotti, G. Gubbiotti, F. B. Mancoff, M. A. Yar, and J. Åkerman, “Direct observation of a propagating spin wave induced by spin-transfer torque,” en, *Nature Nanotechnology* **6**, 635–638 (2011).
- [170] B. Divinskiy, V. E. Demidov, S. Urazhdin, R. Freeman, A. B. Rinkevich, and S. O. Demokritov, “Excitation and amplification of spin waves by spin–orbit torque,” *Advanced Materials* **30**, 1802837 (2018).
- [171] V. E. Demidov, S. Urazhdin, A. Anane, V. Cros, and S. O. Demokritov, “Spin–orbit-torque magnonics,” *Journal of Applied Physics* **127**, 170901 (2020).
- [172] M. Collet, X. De Milly, O. d’Allivy Kelly, V. V. Naletov, R. Bernard, P. Bortolotti, J Ben Youssef, V. Demidov, S. Demokritov, J. L. Prieto, et al., “Generation of coherent spin-wave modes in yttrium iron garnet microdiscs by spin–orbit torque,” *Nature communications* **7**, 10377 (2016).

NEDERLANDSE SAMENVATTING

Tegenwoordig gebruikt elektronica een significant deel van de wereldwijde energieconsumptie. Niet alleen het energieverbruik van onze persoonlijke apparaten draagt hieraan bij, maar onze apparaten vragen ook veel data op uit data centra die veel energie verbruiken. Verder wordt verwacht dat de vraag naar rekenkracht, zonder politiek ingrijpen, alleen maar zal stijgen in de komende jaren. Met een klimaatcrisis voor de deur, is het belangrijk dat alle sectoren, dus ook de ICT sector hun uitstoot proberen te verminderen of op zijn minst niet verder doen stijgen. Gegeven dat de vraag naar rekenkracht zal stijgen, zullen we moeten proberen efficiëntere technologieën te ontwikkelen.

Ondanks dat er op dit moment veel tijd en geld in de innovatie van geïntegreerde schakelingen wordt gestopt, raakt de energieconsumptie van deze geïntegreerde schakelingen een plateau. Dit komt doordat historisch gezien hogere efficiënties werden behaald door het verkleinen van deze geïntegreerde schakelingen. Dit gaat helaas niet langer meer, omdat de ontwikkeling van deze geïntegreerde schakelingen tegen fundamentele limieten aanloopt. Een mogelijke oplossing is om nieuwe technologie te ontwikkelen die fundamenteel verschillend is van huidige elektronica en dus geen hinder heeft van dezelfde fundamentele limieten.

Een zo'n kandidaat is spintronica. Hierin worden spin golven in plaats van elektronen gebruikt om informatie over te dragen. Deze spingolven, en hun quanta magnonen, zijn excitaties die voorkomen in geordende magneten. Als dragers van informatie hebben ze het voordeel dat ze energie efficiënt zijn en omdat er geen verplaatsing van lading hoeft plaats te vinden. Hierdoor hebben spintronische systemen geen last van dezelfde fundamentele limieten als elektronische systemen.

Een obstakel binnen de spintronica is het verval van spin golven door interacties met zijn omgeving, zoals, vrije elektronen, roostertrillingen en

onzuiverheden. Dit zorgt ervoor dat de amplitude en coherentie van spin golven uitdempt over tijd, wat onpraktisch is voor spintronische toepassingen. Een andere te overkomen hindernis is de mogelijkheid om coherent spin golven te injecteren met gelijkstromen. Om spintronische toepassingen compatibel te maken huidige elektronica is een efficiënte injectie van spin golven met gelijkstroom noodzakelijk. Op dit moment is het exciteren van coherente spin golven met wisselstroom relatief eenvoudig, maar het injecteren van magnonen met gelijkstroom blijkt een stuk complexer.

In dit proefschrift hebben we naar manieren gekeken om de levensduur spin golven te verlengen en om spin golven te injecteren met een gelijkstroom. Het gros van de ideeën die we hebben ontwikkeld ontleen hun oorsprong uit analogieën tussen de natuurkunde van de gecondenseerde materie en de hoge energie fysica. De essentie voor de toepassingen die wij voorstellen zit in de koppeling tussen positieve energie excitaties en negatieve energie excitaties. Dit is een concept dat natuurlijk is in de hoge energie fysica en komt bijvoorbeeld voor rond de horizon van een zwart gat, maar ook als je elektronen wilt beschrijven die verstrooien tegen een zeer sterk elektrisch veld. In het kort, in de toepassingen beschreven in dit proefschrift kan deze koppeling gebruikt worden om de amplitude van spin golven te versterken dan wel om coherent spin golven te injecteren met een gelijkstroom.

In Hoofdstuk 1 introduceren we magnetisme, spin golven en hoe we negatieve energie spin golven kunnen creëren die desondanks toch stabiel zijn. Het vervolg van dit proefschrift is opgedeeld in twee delen. In het eerste deel beschrijven we voornamelijk de invloed die dipool-dipool interacties op spin golven hebben. Terwijl we in het tweede deel vooral concrete voorstellen bespreken om spin golven te versterken en te injecteren met gelijkstroom.

Hoofdstuk 2 beschrijft een opstelling waarin spin golven negatieve energie kunnen krijgen door een elektrische stroom door een ferromagneet te laten lopen. Verder zorgt deze stroom tevens dat deze spin golven stabiel kunnen blijven. Dit is uniek voor magnetische systemen, normaal gesproken zorgt het bestaan van negatieve energie excitaties dat een systeem onstabiel is en vervalt naar de grondtoestand. In magnetische systemen pompt de elektrische stroom impulsmoment in de magneet wat er toe kan leiden dat de toestand

van magneet stabiel is omdat die zijn energie niet voldoende kwijt kan. In dit hoofdstuk bepaalden we wanneer deze negatieve energie spin golven stabiel zijn, en nemen hierbij de interacties, zoals dipool-dipool interactie, in ogenschouw die relevant zijn in experimenteel realistische situaties.

In Hoofdstuk 3 beschrijven we de dispersie van spin golven in dunne films als zowel dipool-dipool interactie als de exchange interactie belangrijk zijn. Tot op heden is de diagonale benadering gedaan door Kalinikos en Slavin (1986) de theorie die veel wordt gebruikt om dipole-exchange spin golven te beschrijven. Deze theorie werkt echter niet even goed voor alle diktes en wordt vooral inaccuraat voor dikkere films. In dit hoofdstuk beschrijven we een analytische theorie die zeer goed overeen komt met numerieke oplossingen van de dipole-exchange spin golf dispersie voor alle diktes.

Het tweede deel van dit proefschrift ging over de toepassing van negatieve energie spin golven. In Hoofdstuk 4 behandelen we hoe een spin golf versterkt kan worden door te kaatsen van een interface waarachter negatieve energie spin golven bestaan. De inspiratie voor dit hoofdstuk komt uit de hoge energie fysica en wordt daar de Klein paradox genoemd.

Hoofdstuk 5 geeft een niet lineaire analyse van een model met twee gekoppelde macrospins waarvan de onderste macrospin wordt aangedreven met SOT. In het specifiek bekijken we een geval waarin deze opstelling instabiel wordt door de koppeling tussen beide magneten, waarbij de twee spin blijven oscilleren voor sterkere interacties. We vonden de niet-lineaire dynamica zowel analytisch als numeriek en beiden bleken zeer goed overeen te komen. Verder lieten we zien dat de sterkte van oscillaties zeer sterk afhangt van de parameters en dat deze opstelling dus nuttig kan blijken als sensor.

In het laatste hoofdstuk van dit proefschrift, namelijk Hoofdstuk 6, kijken we naar de niet-lineaire dynamica van een opstellingen die coherente spin golven uitzendt door een gelijkstroom. Om preciezer te zijn, we bekijken twee gekoppelde magneten, waarvan één magneet eindig en energetisch onstabiel is maar stabiel wordt gehouden door injectie van impulsmoment met een gelijkstroom. Inspiratie voor dit hoofdstuk komt uit het vakgebied van analoge zwaartekracht en een vergelijkbare opstelling wordt daar een zwarte gat laser genoemd.

DANKWOORD

Als eerst wil ik mijn begeleider Rembert heel erg bedanken. Ik overdrijf niet als ik zeg dat ik me geen betere begeleider had kunnen voorstellen. Je gaf me het vertrouwen en de vrijheid om uit te zoeken wat ik interessant vind en je bent altijd heel ondersteunend geweest. Mede door de ontspannen sfeer in onze groep heb ik de afgelopen vier jaar als zeer plezierig ervaren. Net zoals het geval lijkt bij iedere AiO in jouw groep, heb ook ik een racefiets gekocht. Hier fiets ik regelmatig op, al is het me nog geen enkele week gelukt om in de buurt te komen van meters die jij maakt op de fiets.

Pieter, wij hebben veel tijd samen doorgebracht in koffiepauzes en op conferenties waar we geregeld samen een kamer deelde. Ik heb je door de jaren beter leren kennen en heb je gezelschap altijd zeer gewaardeerd. Ik wens je het beste toe in Mainz en alles wat erna komt. Meike, het was me een genoegen om vanaf ons tweede jaar een kantoor te delen. Vaak was jij al aanwezig op kantoor en kwam ik vervolgens aan om je van je werk af te leiden. Ik heb met veel plezier over van alles en nog wat gekletst met jou, wat mijn dag vaak een stukje luchtiger maakte. Ik wens je succes met de afronding van je promotie en je loopbaan daarna. Artim, in mijn laatste half jaar heb ik het genoegen gehad om met jou samen te mogen werken. Naast het feit dat ik veel plezier in onze samenwerking heb gehad, hebben we het ook gezellig gehad tijdens verschillende uitjes en de workshop in Trondheim — waar we merkten dat grote spierballen toch onpraktisch zijn als je een berg op wilt lopen. Succes met de rest van de promotie. Huaiyang, I would like to thank you for the many fruitful collaborations we had. As a matter of fact, most of my collaborations were together with you, as can also be seen from the contents of this Thesis. I wish you the best of luck with your further scientific career.

Verder wil ik Cas en Mexx bedanken dat jullie je masterscriptie onder mijn (co-)supervisie wilden doen.

Daarnaast wil ik mijn familie bedanken. Mijn ouders Edwin en Angela en mijn drie zusjes Jessie, Elin en Marin. Jessie, ik wil jou nog specifiek bedanken voor je hulp aan de omslag en de introductie van dit Proefschrift. Ook mijn vrienden bij wie ik afleiding kon vinden wil ik graag bedanken Steyn, Niek, Pim, Paul, Simon, Thijs, Joost, Nils, Stijn, Lotte, Ruud, Rik, Tim, Renske, Emmy, Menno, Marijke, Eline, Levi, Lotte, Colin, Larissa, Vera. I would also like to thank the group I have been a part of for the relaxed atmosphere they provided. So thank you Tim, Ali, Lukasz, Huaiyang, Valentina, Pieter, Thomas and Artim. And finally, Sandro (Alexander), Emanuelle, Willem, Meike, Jeroen, Iris, Nico, Anouar, Lumen I enjoyed your company at university and outside it. You made the past four years fun.

CURRICULUM VITAE

I, Joren Stan Harms, was born on the 14th of August 1994 in Groningen, the Netherlands. I got my pre-university education at het Christelijk Lyceum Zeist and additionally received education in the science subjects at Junior College Utrecht in the final two years of secondary school. I finished both programs in 2013. After secondary school I enrolled in the Bachelors programmes of Physics and Astronomy and Mathematics at Utrecht University. In 2017 I wrote my Bachelors Thesis on “quantum dynamics of skyrmions and vortices in antiferromagnets” under supervision of Prof. Rembert Duine, for which I got awarded the EMMEPH prize for best Bachelors Thesis. In the same year I completed both Bachelors cum laude together with an honours programme in Physics. I continued my studies in the masters programme of Theoretical Physic at Utrecht University. In 2019 I wrote my Masters Thesis under the supervision of Prof. Henk Stoof on “thermoelectric transport in strange metals” and graduated cum laude the same year. From 2019 onwards I started my PhD under the supervision of Prof. Rembert A. Duine, of which the main results are enclosed in this Thesis.